Physics – Uspekhi **57** (9) 839 – 876 (2014)

REVIEWS OF TOPICAL PROBLEMS

PACS numbers: **61.43.–j**, 61.50.Ah, 61.50.Ks, 61.66.Fn, 61.72.jd, 61.72.jj

Nonstoichiometry and superstructures

A I Gusev

DOI: 10.3367/UFNe.0184.201409a.0905

Contents

1. Introduction **839**
2. Disorder–order transition channel and the distribution function **841**
3. M_2X superstructures **843**
3.1 Trigonal M_2X superstructure; 3.2 Cubic M_2X superstructure; 3.3 Tetragonal M_2X superstructures; 3.4 Superstructures of lithium nickelite $Li_{1-x-z}Ni_{1+x}O_2$; 3.5 Sequence of M_2X superstructure formation
4. M_3X_2 superstructures **849**
4.1 Monoclinic M_3X_2 superstructure; 4.2 Orthorhombic M_3X_2 superstructures; 4.3 Trigonal M_3X_2 superstructure; 4.4 Sequence of M_3X_2 superstructure formation
5. M_4X_3 superstructures **853**
5.1 Cubic and tetragonal superstructures of type M_4X_3; 5.2 Ordering in the trigonal ζ-Ta_4C_{3-x} phase
6. M_6X_5 superstructures **855**
6.1 Trigonal M_6X_5 superstructure; 6.2 Monoclinic M_6X_5 superstructure: $C2/c$ or $C2$ space group? 6.3 Monoclinic (space group $C2/m$) M_6X_5 superstructure; 6.4 Sequence of M_6X_5 superstructure formation
7. M_8X_7 cubic superstructures **861**
8. Superstructures of lower hexagonal M_2C_y carbides **863**
8.1 Rhombohedral β''-W_2C superstructure; 8.2 Trigonal ε-W_2C superstructure; 8.3 Orthorhombic β'-W_2C superstructure; 8.4 Sequence of disorder–order and order–order transformations in W_2C_y
9. Superstructures of nonstoichiometric Ti_xO_z and V_xO_z oxides with double defectiveness **866**
9.1 Monoclinic Ti_5O_5 superstructure; 9.2 Cubic Ti_5O_5 superstructure; 9.3 Relation between monoclinic and cubic Ti_5O_5 superstructures; 9.4 Rhombic Ti_3O_2 and Ti_2O_3 superstructures; 9.5 Tetragonal Ti_4O_5 superstructure; 9.6 Tetragonal $V_{52}O_{64}$ superstructure; 9.7 Monoclinic $V_{14}O_6$ superstructure
10. Conclusion **874**
References **875**

Abstract. **The way in which nonstoichiometry and order and disorder interrelate in solid phase compounds is discussed. Nonstoichiometry due to the presence of structural vacancies is widely found in such solid phase compounds as transition metal carbides, nitrides, and oxides, and in related ternary interstitial compounds. It is shown that it is nonstoichiometry that determines the disordered or ordered distribution of atoms and vacancies. A review is given of the current status of research into structural order–disorder phase transitions in nonstoichiometric compounds with basal cubic and hexagonal crystal lattices. Symmetry analysis results for disorder–order and order–order phase transformations are considered in detail. Key superstructure types that form in nonstoichiometric compounds with vacancies in one or two sublattices are also described.**

A I Gusev Institute of Solid State Chemistry,
Ural Branch of the Russian Academy of Sciences,
ul. Pervomaiskaya 91, 620990 Ekaterinburg, Russian Federation
Tel. +7 (343) 374 73 06. Fax +7 (343) 374 44 95
E-mail: gusev@ihim.uran.ru

Received 24 October 2013, revised 26 November 2013
Uspekhi Fizicheskikh Nauk **184** (9) 905 – 945 (2014)
DOI: 10.3367/UFNr.0184.201409a.0905
Translated by Yu V Morozov; edited by A Radzig

1. Introduction

Nonstoichiometry reflects the mismatch between the chemical composition of a compound and the number of sites in crystal sublattices occupied by the atoms of its different components [1, 2]. Nonstoichiometry is only possible in two- and multicomponent crystalline compounds. The elemental composition of nonstoichiometric compounds cannot be expressed as a ratio of small integers.

The nonstoichiometry of a solid is due to the presence of structural vacancies and interstitial atoms. The concentration of these point defects in the majority of double and more complex crystalline compounds is rather low and does not exceed 0.01 at.% at 300 K, allowing deviations from stoichiometry to be often neglected for such compounds. Strongly nonstoichiometric compounds are those containing structural vacancies and homogeneity intervals in which vacancy concentration is such that it ensures interaction between them [1–6]. The group of strongly nonstoichiometric compounds includes oxides, sulfides, selenides, carbides, nitrides, borides, metal hydrides, and related ternary compounds possessing homogeneity intervals [1–7]. Such intervals comprise a concentration region in which the type of crystalline structure of a nonstoichiometric compound remains unaltered despite a change in its composition [1–6].

The location of the upper and lower boundaries of the homogeneity interval depends on temperature.

The best known nonstoichiometric compound, wustite (FeO), always contains excess oxygen due to the presence of vacancies in the iron sublattice: the homogeneity interval of wustite extends at high temperatures from $Fe_{0.84}O$ to $Fe_{0.96}O$ and does not include the stoichiometric composition of FeO. Large deviations from stoichiometry with vacancies in the metal sublattice occur in the $Fe_{0.85}S$ and $Cu_{1.73}S$ sulfides. Nonstoichiometry with vacancies in the oxygen sublattice is characteristic of the TiO_{2-x}, V_2O_{5-x}, CeO_{2-x}, UO_{2-x}, MoO_{3-x}, and WO_{3-x} oxides. Cubic titanium (Ti_xO_z) and vanadium (V_xO_z) monoxides contain up to 15 at.% of vacancies in both metal and oxygen sublattices; their composition within the homogeneity interval varies from $TiO_{0.65-0.80}$ to $TiO_{1.25-1.33}$ and from $VO_{0.55-0.60}$ to $VO_{1.25-1.30}$, respectively. The highest degree of nonstoichiometry is found in cubic MX_y carbides and nitrides ($M =$ Ti, Zr, Hf, V, Nb, Ta; $X =$ C, N; $0.50 \leqslant y \leqslant 1.0$); under normal conditions, they may contain up to approximately 30–50 at.% of structural vacancies in the nonmetal sublattice. Hexagonal carbides and nitrides $M_2X_{y'} \equiv MX_{y'/2}$ $(0.40 \leqslant y'/2 \leqslant 0.50)$ have a narrower homogeneity interval.

In 1799–1806, the French researcher J L Proust formulated the law of definite proportions, stating that each chemically pure substance always contains exactly the same proportion of elements by mass. In 1803, the English chemist J Dalton discovered the law of multiple proportions, according to which the elemental composition of a compound can be expressed as the ratio of small integers, i.e., it is stoichiometric. The notion of stoichiometry was introduced by Jeremias Benjamin Richter (1762–1807) in his book *Anfansgrunden der Stochiometrie oder Messkunst chemischer Elemente* [8]. Proust's ideas were opposed by C L Berthollet, who studied alloys and arrived at the conclusion that the composition of compounds may change steadily, and some of them may have a varying composition. The controversy between Proust and Berthollet lasted from 1800 till 1808 and ended in a temporary defeat of the latter. On the one hand, the law of definite proportions and the law of multiple proportions significantly contributed to many achievements in chemistry and metallurgy but, on the other hand, they hampered the development of the solid state theory. Nonstoichiometry had been regarded as a curiosity till the early 20th century, when N S Kurnakov [9] demonstrated the practical utility of Berthollet's ideas. Since the 1930s, the notion of nonstoichiometry has been used, based on Kurnakov's works, in a sense opposite to stoichiometry.

The conception of the crystal as a periodic three-dimensional ordered ensemble of particles is a physical model of an ideal solid. Real crystals always have various defects. In fact, crystals totally free of defects for $T > 0$ K are nonexistent; therefore, the presence of defects is not in itself a sign of nonstoichiometry. Its essential feature is the mismatch observed between the chemical composition of a compound and the number of sites in the crystal lattice occupied by its components.

Nonstoichiometry of a solid is due to the presence of such point defects as structural vacancies. The introduction of structural vacancies into a solid changes the number of atoms in the crystal and its composition. Therefore, they differ from Frenkel, Schottky, and anti-Schottky defects that are point-like, too, but do not affect the crystal composition. From the crystallographic standpoint, the presence of structural vacancies is a consequence of the discrepancy between the chemical composition of a compound, i.e., the relative number of atoms of various kinds, and the relative number of sites in different crystal sublattices occupied by these atoms. Physically, the cause of producing structural vacancies is the mismatch between the composition of a compound and its crystalline structure, owing to which the atoms of one sublattice cannot occupy the sites of another. It makes impossible the formation of antistructural defects and gives rise to structural vacancies in the crystal.

Structural vacancies, i.e., vacant sites of a crystal lattice, behave as atoms occupying the sites of the same lattice. Therefore, they are considered to be an analog of atoms rather than mere 'holes' in the lattice. Deviation from stoichiometry and the resulting homogeneity interval can be described as a substitution solid solution, the components of which are atoms and structural vacancies located in a sole sublattice. Thus, vacancies and atoms of a nonstoichiometric compound make up a substitution solution that can be either disordered or ordered.

Under certain conditions, interstitional atoms and vacancies undergo redistribution over lattice sites and give rise to a variety of ordered structures. The ordered distribution is most probable at low temperatures, whereas disordered distribution occurs at high temperatures, when the entropic contribution to the free energy of a nonstoichiometric compound is large enough [1–6]. Indeed, the thermodynamically equilibrium state of strongly nonstoichiometric compounds at temperatures below 1000 K is an ordered state, whereas the disordered state in the same temperature range is metastable.

Totally ordered and totally disordered distributions are the limiting states of a nonstoichiometric compound. Ordering is responsible for the formation of one or several ordered phases in the homogeneity interval of a nonstoichiometric compound. Nonstoichiometry is a prerequisite for promoting disorder or order in atom and vacancy distributions in the structure of a nonstoichiometric compound.

Nonstoichiometry occupies a highly important place in solid state research and materials science, especially in semiconductor electronics. Nonstoichiometry accounts for the dependence of all properties of nonstoichiometric substances on their composition and the possibility of a targeted modification of these properties by varying the composition of a nonstoichiometric compound within its homogeneity interval or by ordering such a compound at fixed chemical composition.

Investigations in recent decades have shown that changes in the properties of a nonstoichiometric compound undergoing ordering are comparable in terms of magnitude with those resulting from the alteration of its composition within the homogeneity interval of the ordered phase. This means that variation of the composition of strongly nonstoichiometric compounds and redistribution of atoms and vacancies in their crystal lattices represent two equally acceptable modes of controling their properties.

The notion of atomic or atomic-vacancy ordering is a synonym of the disorder–order structural phase transition. The interchanging components of a substitutional solid solution in the disordered state are randomly distributed over crystal lattice sites, with the probability of filling any site by an atom of a given type corresponding to its concentration in the solution. A drop in temperature induces a disorder–order phase transition that, in turn, causes the lattice sites of a disordered solution to break up into a few sublattices. Sublattices of an ordered solid solution differ from one another in probabilities of site occupation by atoms of a given type. The ordered phases resulting from lattice breakup into several sublattices in a disordered crystal are called superstructures.

Ordering processes occur not only in solid substitution solutions (alloys) but also in interstitial solid solutions, given the number of interstitial positions is greater than the number of atoms occupying them. In ordering of interstitial solid solutions, the unoccupied positions and interstitial atoms act as components of a substitution solid solution, while solvent atoms form an immobile atomic core in which interstitial atoms and vacancies undergo redistribution.

Thus, the presence of structural vacancies in nonstoichiometric interstitial compounds leads in certain conditions to ordering. In the description of ordering in nonstoichiometric compounds, interstitial atoms and structural vacancies are regarded as interchanging components of a binary substitution solution in the nonmetal sublattice. Due to this, in the simplest case of a nonmetal sublattice of nonstoichiometric compounds having a type $B1$ or $L'3$ structure, ordering is reduced to the breakup of the site system formed by octahedral interstices of the metal sublattice into two new sublattices. All sites of the first superstructural sublattice are filled up with interstitial atoms, while the sites of the other sublattice remain vacant. Clearly, it is quite admissible to speak about the existence of a vacancy sublattice in the case of ordering in nonstoichiometric compounds.

Ordering of nonstoichiometric compounds is accompanied by symmetry reduction. Indeed, part of symmetry transformations in a disordered nonmetal or metal sublattice combining occupied and unoccupied sites do not belong to the group of symmetry elements of an ordered crystal, since these sites become crystallographically nonequivalent.

Atomic-vacancy ordering is widespread in nonstoichiometric compounds and observed in most ongoing experiments with nonstoichiometric carbides, nitrides, and oxides.

However, the available experimental data on the structure of ordered phases of nonstoichiometric compounds are far from complete and not infrequently contradictory.

Crystallographic considerations in Ref. [10] suggest the formation of type M_2C, M_3C$_2$, M_8C$_5$, M_4C$_3$, M_5C$_3$, M_5C$_4$, M_6C$_5$, and M_8C$_7$ ordered structures in carbides. Calculations of ordering processes in strongly nonstoichiometric cubic MX_y compounds by the order parameter functional method [1–6, 11–17] showed that only M_2X, M_3X_2, and M_6X_5 superstructures can form, taking into account thermodynamic limitations. In the case of a specific position of the upper boundary of the homogeneity interval (as in cubic vanadium carbide VC$_y$), the M_8X_7 phase can appear as a result of the disorder–order transition.

The first review of ordered structures of carbides and nitrides of transition metals was presented in Ref. [18]. Atomic ordering of nonstoichiometric compounds was discussed in later studies [19–23]. A sufficiently detailed comprehensive analysis of ordering processes in nonstoichiometric compounds, based on the results obtained before 2000, can be found in several reviews and monographs [1–6, 12–14, 24–29]. New data on the superstructures of nonstoichiometric compounds were reported at the beginning of the 21st century; also, the sequence of disorder–order and order–disorder phase transformations became for the first time a matter of discussion. The present work is an attempt to summarize the available data on superstructures of nonstoichiometric compounds and additionally attract the attention of experimentalists to such interesting objects as strongly nonstoichiometric compounds.

2. Disorder–order transition channel and the distribution function

It is convenient to describe the structure of ordered phases using the distribution function $n(\mathbf{r})$, i.e., the probability of discovering an atom of a given kind at site $\mathbf{r} = (x_{\mathrm{I}}, y_{\mathrm{I}}, z_{\mathrm{I}})$ of the Ising lattice undergoing ordering transformations. To perform the symmetry analysis and to calculate the distribution functions of interstitial atoms in various superstructures, it is necessary to move to the reciprocal lattice of these superstructures and to find the channel of the disorder–order structural phase transition. The basis vectors $\mathbf{b}_i^*$ of the reciprocal lattice are defined via translation vectors $\mathbf{a}_i$ of the unit cell by the ordinary formula

$$\mathbf{b}_i^* = 2\pi\,\frac{\mathbf{a}_j \times \mathbf{a}_k}{\mathbf{a}_1(\mathbf{a}_2 \times \mathbf{a}_3)}\,, \tag{1}$$

where $i, j, k = 1, 2, 3$.

In the case of nonstoichiometric MX_y compounds with the basic structure $B1$, the Ising lattice undergoing atomic-vacancy ordering is the nonmetal face-centered cubic (fcc) sublattice. Translation vectors determining the positions of $\mathbf{r}$ sites in this sublattice have the form: $\mathbf{r} = x_{\mathrm{I}}\mathbf{a}_1 + y_{\mathrm{I}}\mathbf{a}_2 + z_{\mathrm{I}}\mathbf{a}_3$, where $\mathbf{a}_1$, $\mathbf{a}_2$, $\mathbf{a}_3$ are the fundamental translations of the fcc lattice in the $[100]_{B1}$, $[010]_{B1}$, and $[001]_{B1}$ ($|\mathbf{a}_1| = |\mathbf{a}_2| = |\mathbf{a}_3| = a$) directions, and x_{I}, y_{I}, z_{I} are the site coordinates (integers or half-integers) in the nonmetal fcc sublattice. The basis vectors of the reciprocal lattice corresponding to the direct fcc lattice are equal to $\mathbf{b}_1 = \langle\bar{1}11\rangle$, $\mathbf{b}_2 = \langle 1\bar{1}1\rangle$, and $\mathbf{b}_3 = \langle 11\bar{1}\rangle$ in $2\pi/a_{B1}$ units. From here on, the numbering and description of $\{\mathbf{k}_s\}$ stars of the wave vectors of the fcc lattice and their $\mathbf{k}_s^{(j)}$ rays are given in accordance with monographs [1, 2, 30, 31].

Combining the above superstructure vectors $\mathbf{b}_1^*$, $\mathbf{b}_2^*$, and $\mathbf{b}_3^*$ of the reciprocal lattice and translating them by the vector $\mathbf{r} = n_1\mathbf{b}_1^* + n_2\mathbf{b}_2^* + n_3\mathbf{b}_3^*$ permit us to determine which nonequivalent vectors enter the first Brillouin zone of the disordered nonmetal fcc sublattice and to which $\{\mathbf{k}_s\}$ stars these nonequivalent vectors belong. In this way, we find the channel of disorder–order structural phase transition, i.e., the set of all nonequivalent superstructure vectors $\mathbf{k}_s^{(j)}$ of the reciprocal lattice measured from the nearest structural site of this lattice and entering the first Brillouin zone of the disordered lattice constructed around this site; these vectors are the rays of $\{\mathbf{k}_s\}$ stars associated with this phase transformation. Such a definition of the phase transition channel was formulated in paper [26] based on previous studies [12, 13, 32–34]. The term ‘transition channel’ was proposed in Ref. [35] with respect to second-order phase transitions. Today, it is used when describing second- and first-order structural phase transitions. Since the transition channel is known, it is possible to calculate the distribution function $n(\mathbf{r})$ of atoms in an ordered lattice.

Deviation of the probability $n(\mathbf{r})$ from its magnitude in the case of disordered (statistical) distribution can be represented as the superposition of several plane concentration waves [36]. Their wave vectors are superstructure vectors making up a disorder–order transition channel [1, 2]. In the static concentration wave method [36], the distribution function

$n(\mathbf{r})$ has the form

$$n(\mathbf{r}) = y + \frac{1}{2}\sum_{s}\sum_{j\in s}\eta_s\gamma_s\big[\exp(\mathrm{i}\varphi_s^{(j)})\exp(\mathrm{i}\mathbf{k}_s^{(j)}\mathbf{r}) + \exp(-\mathrm{i}\varphi_s^{(j)})\exp(-\mathrm{i}\mathbf{k}_s^{(j)}\mathbf{r})\big]\,, \qquad (2)$$

where y is the fraction of sites occupied by the atoms of a given kind in the lattice undergoing ordering; the quantity

$$\frac{1}{2}\,\eta_s\gamma_s\big[\exp(\mathrm{i}\varphi_s^{(j)})\exp(\mathrm{i}\mathbf{k}_s^{(j)}\mathbf{r}) + \exp(-\mathrm{i}\varphi_s^{(j)})\exp(-\mathrm{i}\mathbf{k}_s^{(j)}\mathbf{r})\big] \equiv \Delta(\mathbf{k}_s^{(j)},\mathbf{r})$$

is the plane standing static concentration wave generated by the $\mathbf{k}_s^{(j)}$ superstructure vector of the $\{\mathbf{k}_s\}$ star; η_s is the long-range order parameter corresponding to the $\{\mathbf{k}_s\}$ star, and $\eta_s\gamma_s$ and $\varphi_s^{(j)}$ are the amplitude and the phase shift of the concentration wave, respectively. It follows from Eqn (2) that each star of the wave vector $\{\mathbf{k}_s\}$ corresponds to a long-range order parameter η_s. The distribution function at sites $\mathbf{r}$ located in crystallographically equivalent positions assumes one and the same value, because it is invariant with respect to rotation and reflection transformations entering the symmetry point group of the ordered crystal. The total number of values taken by the distribution function is greater by unity than the number of long-range order parameters. Summation in formula (2) should only be taken over nonequivalent superstructure vectors of the first Brillouin zone.

The notion of the phase transition channel is of importance for the construction of the diffraction pattern of an ordered crystal; it ensures correct and unambiguous determination of parameters γ_s and $\varphi_s^{(j)}$ of the distribution function $n(\mathbf{r})$.

Given ordering in the Bravais lattice, each superstructure vector $\mathbf{k}_s^{(j)}$ in the first Brillouin zone corresponds to the opposite superstructure vector $-\mathbf{k}_s^{(j)}$. Vector $-\mathbf{k}_s^{(j)}$ enters the phase transition channel if it is not equivalent to vector $\mathbf{k}_s^{(j)}$, i.e., if $[\mathbf{k}_s^{(j)} - (-\mathbf{k}_s^{(j)})] = 2\mathbf{k}_s^{(j)} \neq \mathbf{H}$. The concentration wave with the opposite wave vector $-\mathbf{k}_s^{(j)}$ undergoes a phase shift with the opposite sign equaling $-\varphi_s^{(j)}$. Thus, the opposite superstructure vector $-\mathbf{k}_s^{(j)}$ does not enter the phase transition channel in that and only in that case where the doubled superstructure vector $2\mathbf{k}_s^{(j)}$ equals the structural vector $\mathbf{H}$ of the reciprocal lattice. In the case of ordering in the fcc lattice, such vectors are the rays of $\{\mathbf{k}_9\}$ and $\{\mathbf{k}_{10}\}$ stars.

Nonequivalent superstructure vectors $\mathbf{k}_s^{(j)}$ and $-\mathbf{k}_s^{(j)}$ give two similar concentration waves; due to this, the corresponding terms of Eqn (2) can be combined. As a result (see paper [26]), function $n(\mathbf{r})$ takes the form

$$n(\mathbf{r}) = y + \frac{1}{2}\sum_{s}\eta_s\sum_{j\in s}\Big[2 - \sum_{\mathbf{H}}\delta(2\mathbf{k}_s^{(j)} - \mathbf{H})\Big] \times \big[\gamma(\mathbf{k}_s^{(j)})\exp(\mathrm{i}\mathbf{k}_s^{(j)}\mathbf{r}) + \gamma^*(\mathbf{k}_s^{(j)})\exp(-\mathrm{i}\mathbf{k}_s^{(j)}\mathbf{r})\big]\,, \qquad (3)$$

where $\gamma(\mathbf{k}_s^{(j)}) = \gamma_s\exp(\mathrm{i}\varphi_s^{(j)})$ and $\gamma^*(\mathbf{k}_s^{(j)}) = \gamma_s\exp(-\mathrm{i}\varphi_s^{(j)})$ are complex-conjugate quantities, and

$$\delta(2\mathbf{k}_s^{(j)} - \mathbf{H}) = \begin{cases} 1\,, & \text{if } \ 2\mathbf{k}_s^{(j)} = \mathbf{H}\,,\\ 0\,, & \text{if } \ 2\mathbf{k}_s^{(j)} \neq \mathbf{H}\,. \end{cases}$$

The delta function $\delta(2\mathbf{k}_s^{(j)} - \mathbf{H})$ allows taking account of the case when the opposite superstructure vector $-\mathbf{k}_s^{(j)}$ is equivalent and does not enter the phase transition channel. The sum $\sum_{\mathbf{H}}\delta(2\mathbf{k}_s^{(j)} - \mathbf{H})$ over the entire set of sites $\{\mathbf{H}\}$ of the reciprocal lattice equals either unity (in an fcc lattice, such vectors are the rays of Lifshitz $\{\mathbf{k}_9\}$ and $\{\mathbf{k}_{10}\}$ stars alone) or zero. Summation over s and j in Eqn (3) means summation taken over all vectors of the phase transition channel, barring the opposite vectors $-\mathbf{k}_s^{(j)}$, i.e., summation over the truncated phase transition channel.

Bearing in mind the known relations $\exp(\mathrm{i}\alpha) = \cos\alpha + \mathrm{i}\sin\alpha$ and $\exp(-\mathrm{i}\alpha) = \cos\alpha - \mathrm{i}\sin\alpha$, the authors of Ref. [26] transformed the distribution function (3) into the trigonometric form used in practice to describe concrete superstructures:

$$n(\mathbf{r}) = y + \sum_{s}\eta_s\sum_{j\in s}\big[A_{sj}\cos(\mathbf{k}_s^{(j)}\mathbf{r}) + B_{sj}\sin(\mathbf{k}_s^{(j)}\mathbf{r})\big]\,, \qquad (4)$$

where

$$A_{sj} = \Big[2 - \sum_{\mathbf{H}}\delta(2\mathbf{k}_s^{(j)} - \mathbf{H})\Big]\,\gamma_s\cos\varphi_s^{(j)}\,,$$

$$B_{sj} = -\Big[2 - \sum_{\mathbf{H}}\delta(2\mathbf{k}_s^{(j)} - \mathbf{H})\Big]\,\gamma_s\sin\varphi_s^{(j)}\,.$$

The numerical values of A_{sj} and B_{sj} coefficients [i.e., the explicit form of the distribution function $n(\mathbf{r})$] being known, it is possible to find parameters γ_s and $\varphi_s^{(j)}$ of this function:

$$\gamma_s = \Big[2 - \sum_{\mathbf{H}}\delta(2\mathbf{k}_s^{(j)} - \mathbf{H})\Big]^{-1}\big|(A_{sj}^2 + B_{sj}^2)^{1/2}\big|\,, \qquad (5)$$

$$\varphi_s^{(j)} = -\arctan\left(\frac{B_{sj}}{A_{sj}}\right) + \frac{\pi}{2}\left(1 - \frac{A_{sj}}{|A_{sj}|}\right) + \frac{\pi}{2}\left(1 + \frac{A_{sj}}{|A_{sj}|}\right)\left(1 + \frac{B_{sj}}{|B_{sj}|}\right). \qquad (6)$$

For the Lifshitz $\{\mathbf{k}_9\}$ and $\{\mathbf{k}_{10}\}$ stars in an fcc lattice, coefficient $B_{sj} \equiv 0$ and $\gamma_s = |A_{sj}|$. As follows from formula (6), the phase shift $\varphi_s^{(j)} = 2\pi \equiv 0$ in this case for $A_{sj} > 0$, and $\varphi_s^{(j)} = \pi$ for $A_{sj} < 0$. If certain coefficients B_{sj} corresponding to Lifshitz stars from $\{\mathbf{k}_8\}$ to $\{\mathbf{k}_0\}$ vanish in the distribution function, i.e., $B_{sj} = 0$, the phase shift $\varphi_s^{(j)} = 0$, too, for $A_{sj} > 0$, and is $\varphi_s^{(j)} = \pi$ for $A_{sj} < 0$.

In calculating the distribution function, coefficients γ_s are defined so that the long-range order parameters η_s equaling unity correspond to the fully ordered state of the crystal. Under this condition, the distribution function of nonmetal atoms assumes only two different values at the totality of sites of the nonmetal fcc sublattice undergoing ordering: $n_1 = 0$ at vacant sites, and $n_2 = 1$ at the sites occupied by nonmetal atoms. Thus, knowledge of the transition channel and the use of the static concentration wave method allow us to obtain the general form of the distribution function for any structure without specifying the values of the long-range order parameters η_s.

It was shown both experimentally and theoretically that superstructures $M_{2t}X_{2t-1}$ ($M_{2t}X_{2t-1}\square$), where $t = 1$, 1.5, 2, 3, and 4, are produced in strongly nonstoichiometric compounds together with some other superstructures (Ti_5O_5, Ti_2O_3, Ti_4O_5, $V_{14}O_6$, $V_{52}O_{64}$). A few new superstructures have recently been described and the data on the known ones substantially corrected and improved.

With this in mind, we shall consider below transition channels and distribution functions corresponding to superstructures of nonstoichiometric compounds. For uniformity and convenience, the unit cells of superstructures will be constructed whenever possible so that vacant sites are located at their vertices.

3. M_2X superstructures

3.1 Trigonal M_2X superstructure

The unit cell of a trigonal (space group $R\bar{3}m$) M_2X superstructure is shown in Fig. 1. The major axis of such a unit cell has direction $[1\bar{1}1]_{B1}$. Its translation vectors, as well as the coordinates of atoms and vacancies in an ideal trigonal M_2X structure, are presented in Table 1. The trigonal (space group $R\bar{3}m$) M_2X type ordered phase was observed experimentally in titanium carbide [37].

Calculations of superstructure vectors and their translation showed that the trigonal M_2X superstructure forms in a nonstoichiometric MX_y compound in the phase transition channel involving a single ray $\mathbf{k}_9^{(3)} = \mathbf{b}_2/2$ of the Lifshitz star $\{\mathbf{k}_9\}$ (Table 2). For other orientations of the unit cell ($[111]_{B1}$, $[\bar{1}11]_{B1}$, and $[11\bar{1}]_{B1}$), the transition channel contains rays $\mathbf{k}_9^{(1)}$, $\mathbf{k}_9^{(2)}$, or $\mathbf{k}_9^{(4)}$, respectively. The subscript of the wave vector corresponds to the star number, and the superscript to its ray number. The distribution function describing a trigonal (space group $R\bar{3}m$) M_2X superstructure has the form

$$n(x_{\mathrm{I}}, y_{\mathrm{I}}, z_{\mathrm{I}}) = y - \frac{\eta_9}{2} \cos\left[\pi(x_{\mathrm{I}} - y_{\mathrm{I}} + z_{\mathrm{I}})\right]. \tag{7}$$

In this superstructure, coordinates $(x_{\mathrm{I}}, y_{\mathrm{I}}, z_{\mathrm{I}})$ of the sites of the fcc Ising lattice correspond to those in Fig. 1 and are related to the trigonal coordinates in Table 1 by the following expressions: $x_{\mathrm{I}} = x_{\mathrm{tr}}/2 + y_{\mathrm{tr}} + z_{\mathrm{tr}}/2$, $y_{\mathrm{I}} = -x_{\mathrm{tr}} - y_{\mathrm{tr}}/2 - z_{\mathrm{tr}}/2$, and $z_{\mathrm{I}} = x_{\mathrm{tr}}/2 + y_{\mathrm{tr}}/2 + z_{\mathrm{tr}}$. Function (7) also describes the trigonal (space group $R\bar{3}m$) substitution superstructure AB (of the CuPt type).

The completely ordered state of a nonstoichiometric MX_y compound is reached when the long-range order parameter $\eta_9(y)$ equals unity, and the relative concentration of interstitial atoms in the nonmetal sublattice is $y_{\mathrm{st}} = 1/2$. In the nonmetal sublattice of a fully ordered trigonal (space group $R\bar{3}m$) M_2X structure, the complete atomic plane $(1\bar{1}1)_{B1}$, in which all sites are occupied by interstitial atoms, and the defective plane $(1\bar{1}1)_{B1}$, all sites of which are vacant, successively alternate in the $[1\bar{1}1[_{B1}$ direction. In such a superstructure, distortions of the metal sublattice must be apparent.

Distribution function (7) at all sites of the fcc nonmetal sublattice takes two values, n_1 and n_2, that are the probabilities of detecting interstitial atoms at these sites (see Table 1). Parameters γ_s and $\varphi_s^{(j)}$ of distribution function (7) are presented in Table 2.

A trigonal (space group $R\bar{3}m$) M_2X superstructure can also be represented in the hexagonal arrangement (see Fig. 1). Translation vectors of the hexagonal unit cell of this superstructure and magnitudes of the distribution function at its sites are listed in Table 1.

3.2 Cubic M_2X superstructure

The unit cell of the cubic (space group $Fd\bar{3}m$) M_2X superstructure is illustrated in Fig. 2. Translation vectors of this unit cell, together with atom and vacancy coordinates, are given in Table 1. The cubic (space group $Fd\bar{3}m$) M_2X ordered phase was observed experimentally in titanium and zirconium carbides [37–39]. In Ref. [26], the position of the unit cell of this superstructure in the lattice with structure $B1$ is shown incorrectly (without the shift of the origin of its coordinates by the vector $-(1/4)\langle 111\rangle_{B1}$); as a result, the coordinates of atoms and vacancies in the unit cell of the cubic (space group $Fd\bar{3}m$) superstructure were given incorrectly, too.

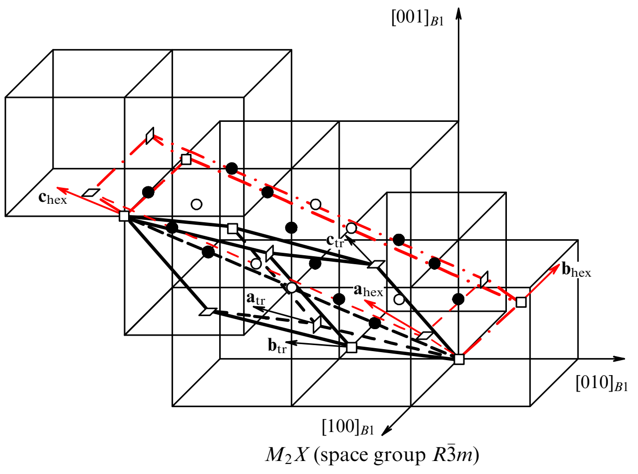

Figure 1. Positions of trigonal and hexagonal unit cells of the trigonal (space group $R\bar{3}m$) M_2X superstructure in a lattice with the basic structure $B1$: (○) interstitial atom, (●) metal atom, and (□) vacancy. The hexagonal unit cell is shown by dashed-dotted lines.

The disorder–order $MX_y - M_2X$ (space group $Fd\bar{3}m$) phase transition channel includes all four rays of the $\{\mathbf{k}_9\}$ star (see Table 2). The cubic M_2X superstructure under consideration is described by the distribution function

$$\begin{aligned} n(x_{\mathrm{I}}, y_{\mathrm{I}}, z_{\mathrm{I}}) = y - \frac{\eta_9}{4}\Big\{ &-\cos\left[\pi(x_{\mathrm{I}} + y_{\mathrm{I}} + z_{\mathrm{I}})\right] \\ &+ \cos\left[\pi(-x_{\mathrm{I}} + y_{\mathrm{I}} + z_{\mathrm{I}})\right] + \cos\left[\pi(x_{\mathrm{I}} - y_{\mathrm{I}} + z_{\mathrm{I}})\right] \\ &+ \cos\left[\pi(x_{\mathrm{I}} + y_{\mathrm{I}} - z_{\mathrm{I}})\right]\Big\}, \end{aligned} \tag{8}$$

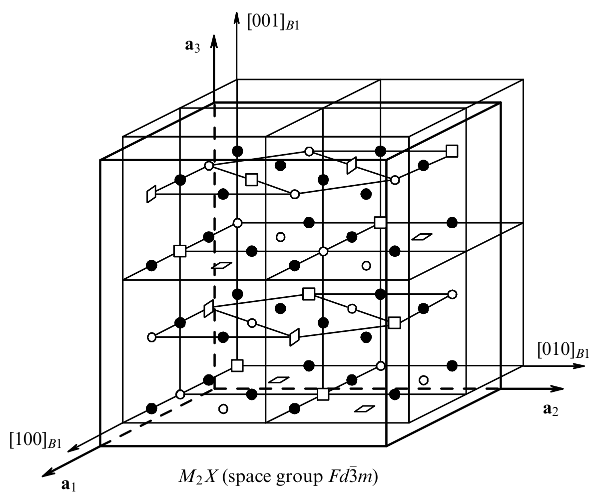

Figure 2. Position of the cubic (space group $Fd\bar{3}m$) unit cell of the M_2X superstructure in a lattice with structure $B1$: (○) interstitial atom, (●) metal atom, and (□) vacancy. The origin of coordinates of the cubic M_2X superstructure has coordinates $(-1/4\ -1/4\ -1/4)_{B1}$ of the lattice with the basic structure $B1$.

Table 1. Superstructures of type M_2X.

Symmetry	Space group	Translation vectors of unit cell	V^*	Atom	Position and multi-plicity	Atomic coordinates in ideal ordered structure			Values of distribution function $n(x_{\mathrm{I}}, y_{\mathrm{I}}, z_{\mathrm{I}})$
						x/a_{tr}	y/b_{tr}	z/c_{tr}	
Trigonal	No. 166 $R\bar{3}m$ (D_{3d}^5)	$\mathbf{a}_{\mathrm{tr}} = \frac{1}{2}\langle 1\bar{2}1\rangle_{B1}$, $\mathbf{b}_{\mathrm{tr}} = \frac{1}{2}\langle 2\bar{1}1\rangle_{B1}$, $\mathbf{c}_{\mathrm{tr}} = \frac{1}{2}\langle 1\bar{1}2\rangle_{B1}$	$a_{B1}^3/2$	$X1$ (vacancy)	$1(a)$	0	0	0	$n_1 = y - \eta_9/2$
				$X2$	$1(b)$	1/2	1/2	1/2	$n_2 = y + \eta_9/2$
				$M1$	$2(c)$	1/4	1/4	1/4	
						x/a_{hex}	y/b_{hex}	z/c_{hex}	
Hexagonal	No. 166 $R\bar{3}m$ (D_{3d}^5)	$\mathbf{a}_{\mathrm{hex}} = \frac{1}{2}\langle \bar{1}01\rangle_{B1}$, $\mathbf{b}_{\mathrm{hex}} = \frac{1}{2}\langle 011\rangle_{B1}$, $\mathbf{c}_{\mathrm{hex}} = 2\langle 1\bar{1}1\rangle_{B1}$	$3a_{B1}^3/2$	$X1$ (vacancy)	$3(a)$	0	0	0	$n_1 = y - \eta_9/2$
				$X2$	$3(b)$	0	0	1/2	$n_2 = y + \eta_9/2$
				$M1$	$6(e)$	0	0	1/4	
						x/a_{cub}	y/b_{cub}	z/c_{cub}	
Cubic	No. 227 $Fd\bar{3}m$ (O_h^7)	$\mathbf{a}_{\mathrm{cub}} = \langle 200\rangle_{B1}$, $\mathbf{b}_{\mathrm{cub}} = \langle 020\rangle_{B1}$, $\mathbf{c}_{\mathrm{cub}} = \langle 002\rangle_{B1}$	$8a_{B1}^3$	$X1$ (vacancy)	$16(c)$	1/8	1/8	1/8	$n_1 = y - \eta_9/2$
				$X2$	$16(d)$	5/8	5/8	5/8	$n_2 = y + \eta_9/2$
				$M1$	$32(e)$	3/8	3/8	3/8	
						x/a_{t}	y/b_{t}	z/c_{t}	
Tetragonal	No. 123 $P4/mmm$ (D_{4h}^1)	$\mathbf{a}_{\mathrm{t}} = \frac{1}{2}\langle 1\bar{1}0\rangle_{B1}$, $\mathbf{b}_{\mathrm{t}} = \frac{1}{2}\langle 110\rangle_{B1}$, $\mathbf{c}_{\mathrm{t}} = \langle 001\rangle_{B1}$	$a_{B1}^3/2$	$X1$ (vacancy)	$1(a)$	0	0	0	$n_1 = y - \eta_{10}/2$
				$X2$	$1(d)$	1/2	1/2	1/2	$n_2 = y + \eta_{10}/2$
				$M1$	$1(b)$	0	0	1/2	
				$M2$	$1(c)$	1/2	1/2	0	
						x/a_{t}	y/b_{t}	z/c_{t}	
Tetragonal	No. 141 $I4_1/amd$ (D_{4h}^{19})	$\mathbf{a}_{\mathrm{t}} = \langle 100\rangle_{B1}$, $\mathbf{b}_{\mathrm{t}} = \langle 010\rangle_{B1}$, $\mathbf{c}_{\mathrm{t}} = \langle 002\rangle_{B1}$	$2a_{B1}^3$	$X1$ (vacancy)	$4(a)$	0	0	0	$n_1 = y - \eta_8/2$
				$X2$	$4(b)$	0	0	1/2	$n_2 = y + \eta_8/2$
				$M1$	$8(e)$	0	0	1/4	

* The volume of the unit cell of a superstructure expressed through parameter a_{B1} of the unit cell of the basic disordered structure of type $B1$.

Table 2. Disorder–order phase transition channels $MX_y - M_2X$ and parameters of the distribution functions $n(x_{\mathrm{I}}, y_{\mathrm{I}}, z_{\mathrm{I}})$ describing M_2X superstructures.

Symmetry	Space group	Disorder–order transition channel		Parameters of the distribution function	
		Star $\{\mathbf{k}_s\}$	Rays $\mathbf{k}_s^{(j)}$ of the $\{\mathbf{k}_s\}$ star	γ_s	$\varphi_s^{(j)}$
Trigonal	No. 166 $R\bar{3}m$ (D_{3d}^5)	$\{\mathbf{k}_9\}$	$\mathbf{k}_9^{(3)} = \mathbf{b}_2/2$	$\gamma_9 = 1/2$	$\varphi_9^{(3)} = \pi$
Cubic	No. 227 $Fd\bar{3}m$ (O_h^7)	$\{\mathbf{k}_9\}$ $\{\mathbf{k}_9\}$ $\{\mathbf{k}_9\}$ $\{\mathbf{k}_9\}$	$\mathbf{k}_9^{(1)} = (\mathbf{b}_1 + \mathbf{b}_2 + \mathbf{b}_3)/2$, $\mathbf{k}_9^{(2)} = \mathbf{b}_1/2$, $\mathbf{k}_9^{(3)} = \mathbf{b}_2/2$, $\mathbf{k}_9^{(4)} = \mathbf{b}_3/2$	$\gamma_9 = 1/4$ $\gamma_9 = 1/4$ $\gamma_9 = 1/4$ $\gamma_9 = 1/4$	$\varphi_9^{(1)} = 0$ $\varphi_9^{(2)} = \pi$ $\varphi_9^{(3)} = \pi$ $\varphi_9^{(4)} = \pi$
Tetragonal	No. 123 $P4/mmm$ (D_{4h}^1)	$\{\mathbf{k}_{10}\}$	$\mathbf{k}_{10}^{(1)} = (\mathbf{b}_1 + \mathbf{b}_2)/2$	$\gamma_{10} = 1/2$	$\varphi_{10}^{(1)} = \pi$
Tetragonal	No. 141 $I4_1/amd$ (D_{4h}^{19})	$\{\mathbf{k}_8\}$ $\{\mathbf{k}_8\}$	$\mathbf{k}_8^{(1)} = (\mathbf{b}_1 + 3\mathbf{b}_2 + 2\mathbf{b}_3)/4$, $\mathbf{k}_8^{(2)} = -\mathbf{k}_8^{(1)}$	$\gamma_8 = \sqrt{2}/4$ $\gamma_8 = \sqrt{2}/4$	$\varphi_8^{(1)} = 3\pi/4$ $\varphi_8^{(2)} = -3\pi/4$

with parameters γ_9 and $\varphi_9^{(j)}$ presented in Table 2. For a fully ordered crystal, the relative stoichiometric concentration of interstitial atoms is $y_{\mathrm{st}} = 1/2$. As Fig. 2 depicts, coordinates $(x_{\mathrm{I}}, y_{\mathrm{I}}, z_{\mathrm{I}})$ are related to the coordinates of this superstructure, given in Table 1, by expressions $x_{\mathrm{I}} = 2x_{\mathrm{cub}} - 1/4$, $y_{\mathrm{I}} = 2y_{\mathrm{cub}} - 1/4$, and $z_{\mathrm{I}} = 2z_{\mathrm{cub}} - 1/4$.

Function (8) at the sites of the fcc nonmetal sublattice takes the same values n_1 and n_2 (see Table 1) as function (7) describing the trigonal M_2X superstructure.

3.3 Tetragonal M_2X superstructures

The literature mentions two tetragonal (space groups $P4/mmm$ and $I4_1/amd$) M_2X superstructures. Their unit

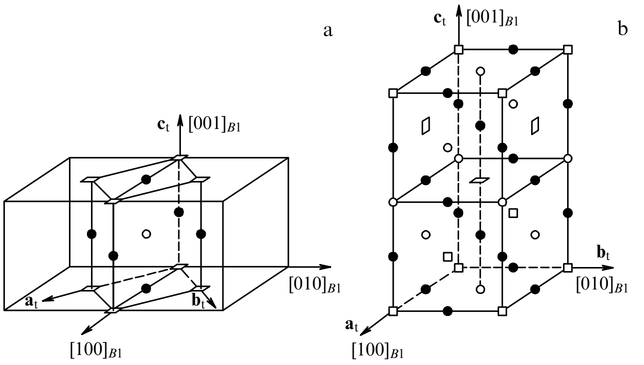

M_2X (space group $P4/mmm$) M_2X (space group $I4_1/amd$)

Figure 3. Position of tetragonal unit cells of M_2X superstructures in a lattice with the basic structure $B1$: (a) space group $P4/mmm$, and (b) space group $I4_1/amd$; (○) interstitial atom, (●) metal atom, and (□) vacancy.

cells are demonstrated in Fig. 3 (a different arrangement of the unit cell, with the origin of coordinates displaced with respect to that of the basic lattice $B1$, is possible for a superstructure with the space group $I4_1/amd$). Translation vectors of tetragonal unit cells of the M_2X phases and coordinates of atoms and vacancies in them are presented in Table 1.

The phase transition channel associated with the formation of a tetragonal (space group $P4/mmm$) superstructure contains one ray $\mathbf{k}_{10}^{(1)}$ of the $\{\mathbf{k}_{10}\}$ star (see Table 2). The distribution function of interstitial atoms in the tetragonal (space group $P4/mmm$) M_2X superstructure has the form

$$n(x_{\mathrm{I}}, y_{\mathrm{I}}, z_{\mathrm{I}}) = y - \frac{\eta_{10}}{2}\cos(2\pi z_{\mathrm{I}})\,. \tag{9}$$

A similar distribution function describes the tetragonal (space group $P4/mmm$) substitution superstructure AB (of the CuAu type). The values of distribution function (9) at sites related to different positions of the nonmetal sublattice of the superstructure of interest are given in Table 1. According to Fig. 3a, coordinates $(x_{\mathrm{I}}, y_{\mathrm{I}}, z_{\mathrm{I}})$ are linked by the expressions $x_{\mathrm{I}} = x_{\mathrm{t}}/2 + y_{\mathrm{t}}/2$, $y_{\mathrm{I}} = -x_{\mathrm{t}}/2 + y_{\mathrm{t}}/2$, and $z_{\mathrm{I}} = z_{\mathrm{t}}$ to the tetragonal coordinates of this superstructure, listed in Table 1.

In the nonmetal sublattice of the perfectly ordered tetragonal (space group $P4/mmm$) M_2X phase, the complete and fully defective (containing only vacancies) $(001)_{B1}$ planes successively alternate. In such superstructures, the metal sublattice is grossly distorted, which makes unlikely the existence of a tetragonal (space group $P4/mmm$) M_2X superstructure in nonstoichiometric compounds; it should be regarded as a model as far as nonstoichiometric compounds are concerned.

The ordered tetragonal (space group $I4_1/amd$) M_2X phase (Fig. 3b) was experimentally examined in titanium nitride [40, 41]. Its disorder–order phase transition channel contains rays $\mathbf{k}_8^{(1)}$ and $\mathbf{k}_8^{(2)}$ of the $\{\mathbf{k}_8\}$ star (see Table 2). The distribution function describing this M_2X superstructure depends on a single long-range order parameter:

$$n(x_{\mathrm{I}}, y_{\mathrm{I}}, z_{\mathrm{I}}) = y - \frac{\eta_8}{2}\left\{\cos\left[\pi(2x_{\mathrm{I}} + z_{\mathrm{I}})\right] + \sin\left[\pi(2x_{\mathrm{I}} + z_{\mathrm{I}})\right]\right\}. \tag{10}$$

Function (10) assumes two values at the sites found to belong to different positions of the nonmetal sublattice under consideration (see Table 1). Parameters of the distribution function (10) are listed in Table 2. According to Fig. 3b, coordinates $(x_{\mathrm{I}}, y_{\mathrm{I}}, z_{\mathrm{I}})$ are related to the tetragonal coordinates of this superstructure by expressions $x_{\mathrm{I}} = x_{\mathrm{t}}$, $y_{\mathrm{I}} = y_{\mathrm{t}}$, and $z_{\mathrm{I}} = 2z_{\mathrm{t}}$.

In fully ordered tetragonal M_2X phases, where the respective long-range order parameter (η_{10} or η_8) equals unity, the relative stoichiometric concentration y_{st} of interstitial atoms is 1/2.

3.4 Superstructures of lithium nickelite $\mathrm{Li}_{1-x-z}\mathrm{Ni}_{1+x}\mathrm{O}_2$

Marked deviations from stoichiometry in the metal sublattice are characteristic of lithium nickelite, related $\mathrm{Li}M\mathrm{O}_2$ oxides, and their solid solutions. The crystalline structures of complex $\mathrm{Li}M\mathrm{O}_2$ (M = Ni, Co) oxides are derivatives of the basic structure $B1$ and differ in the mode of ordering of lithium and transition metal (M) cations in $(111)_{B1}$ planes or in equivalent $(\bar{1}11)_{B1}$, $(1\bar{1}1)_{B1}$, and $(11\bar{1})_{B1}$ planes of the fcc sublattice. When ions of lithium and metal M separately fill the alternating metal $(111)_{B1}$ planes of the basic cubic lattice, layered structures are formed.

A few ways of writing out the chemical formula of lithium nickelite are applied in the literature: $\mathrm{Li}_x\mathrm{NiO}_2$ [42–44], $\mathrm{Li}_{1-x}\mathrm{Ni}_{1+x}\mathrm{O}_2$ [43, 45], and $\mathrm{Li}_{x'}\mathrm{Ni}_{2-x'}\mathrm{O}_2$ (or $\mathrm{Li}_y\mathrm{Ni}_{1-y}\mathrm{O}$, where $y = x'/2$) [46, 47]. This discrepancy in formulas is due to different views of its structure. The triple Li–Ni–O system gives rise to a solid solution $\mathrm{Li}_y\mathrm{Ni}_{1-y}\mathrm{O}$ ($0 \leqslant y \leqslant 0.5$), the end members of which are cubic nickel monoxide NiO (at $y = 0$) and trigonal (rhombohedral) stoichiometric lithium nickelite LiNiO_2 (at $y = 0.5$, i.e., $\mathrm{Li}_{0.5}\mathrm{Ni}_{0.5}\mathrm{O}$). The structure of stoichiometric nickelite LiNiO_2 can be regarded as a result of ordering the Li and Ni atoms (ions) in the basic cubic structure of the $B1$ type. Formulas $\mathrm{Li}_{1-x}\mathrm{Ni}_{1+x}\mathrm{O}_2$ and $\mathrm{Li}_{x'}\mathrm{Ni}_{2-x'}\mathrm{O}_2$ are virtually identical ($x' = 1 - x$) and reflect substitution of lithium by nickel in the solid solution, even if they do not take into account possible vacancies in the lithium sublattice. Indeed, deviation of the nickelite composition from that of stoichiometric LiNiO_2 is associated with the appearance of structural vacancies in the lithium sublattice, the concentration of which can be rather high. Formula $\mathrm{Li}_x\mathrm{NiO}_2$ (or $\mathrm{Li}_x\blacksquare_{1-x}\mathrm{NiO}_2$, where ■ is the structural vacancy in the lithium sublattice) takes account of the presence of vacancies [42–44], but disregards Ni substitution for Li. Reference [48] shows that the formula of lithium nickelite should be presented as $\mathrm{Li}_{1-x-z}\mathrm{Ni}_{1+x}\mathrm{O}_2$ ($\mathrm{Li}_{1-x-z}\blacksquare_z\mathrm{Ni}_{1+x}\mathrm{O}_2$) if Li substitution by Ni during formation of $\mathrm{NiO/LiNiO}_2$ solid solution and the presence of structural vacancies ■ in the metal sublattice are to be taken into consideration. This formula takes account of peculiarities of the lithium nickelite structure and permits us to analyze its ordering by making use of the atomic distribution function.

The symmetry analysis of experimental and theoretical nickelite superstructures $\mathrm{Li}_{1-x-z}\blacksquare_z\mathrm{Ni}_{1+x}\mathrm{O}_2$, from determining the disorder–order transition channel to calculating distribution functions of the atoms undergoing ordering, was performed for the first time in paper [48].

The unit cell of the trigonal (rhombohedral) ordered LiNiO_2 phase of the nickelite $\mathrm{Li}_{1-x-z}\mathrm{Ni}_{1+x}\mathrm{O}_2$) is demonstrated in Fig. 4. Translation vectors of the unit cell and coordinates of atoms and vacancies in it are presented in Table 3. The trigonal cell is primitive as regards Li atoms; it contains a single Li atom, one Ni atom, and two oxygen (O) atoms. The nonprimitive cell is hexagonal, has a volume that is three times larger, and contains three atoms of Li and Ni together with six O atoms in positions $3(a)(000)$,

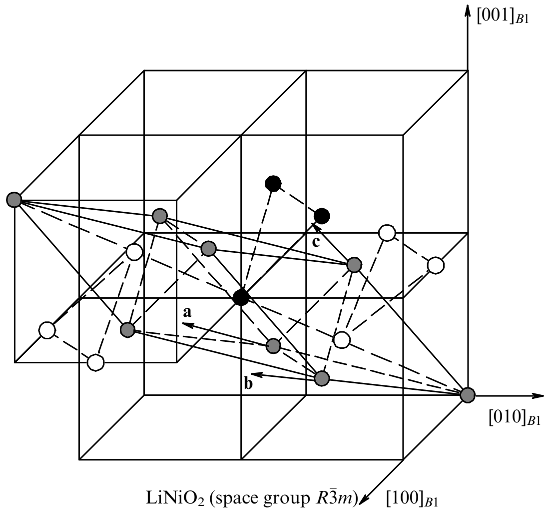

Figure 4. Position of the rhombohedral (space group $R\bar{3}m$) unit cell of lithium nickelite $LiNiO_2$ in the lattice with the basic structure $B1$ [59]: (●) Li, (●) Ni, and (○) O. The figure shows successive alternation of atomic planes filled only with Li atoms, O atoms, or Ni atoms in the direction $[1\bar{1}1]_{B1}$.

$3(b)(0\,0\,1/2)$, and $6(c)(0\,0\,1/4)$, respectively. The hexagonal cell has the translation vectors $\mathbf{a}_{\mathrm{hex}} = (1/2)\langle\bar{1}01\rangle_{B1}$, $\mathbf{b}_{\mathrm{hex}} = (1/2)\langle 011\rangle_{B1}$, $\mathbf{c}_{\mathrm{hex}} = 2\langle 1\bar{1}1\rangle_{B1}$ or $\mathbf{a}_{\mathrm{hex}} = (1/2)\langle 011\rangle_{B1}$, $\mathbf{b}_{\mathrm{hex}} = (1/2)\langle 110\rangle_{B1}$, and $\mathbf{c}_{\mathrm{hex}} = 2\langle\bar{1}\bar{1}1\rangle_{B1}$.

Unlike the trigonal M_2X ($M_2X\square$) superstructure with $\square$ vacancies in the nonmetal sublattice, the trigonal (space group $R\bar{3}m$) superstructure of lithium nickelite contains $\blacksquare$ vacancies in the metal sublattice and is referred to as of type MX_2 ($M\blacksquare X_2$). The trigonal lithium nickelite superstructure forms via the same phase transition channel as the trigonal M_2X superstructure. The transition channel includes a single $\mathbf{k}_9^{(3)}$ ray of the Lifshitz $\{\mathbf{k}_9\}$ star to which the long-range order parameter $\eta_9^{(M)}$ corresponds in the metal fcc sublattice of lithium nickelite. In disordered $Li_{1-x-z}Ni_{1+x}O_2$ ($Li_{1-x-z}\blacksquare_z Ni_{1+x}O_2$), probabilities $n^{(\mathrm{Li})}(\mathbf{r})$, $n^{(\mathrm{Ni})}(\mathbf{r})$, and $n^{(\square)}(\mathbf{r})$ coincide with the fraction of metal sublattice sites occupied by Li or Ni atoms or with the fraction of vacant sites, respectively, i.e., $n^{(\mathrm{Li})}(\mathbf{r}) = (1-x-z)/2$, $n^{(\mathrm{Ni})}(\mathbf{r}) = (1+x)/2$, and $n^{(\blacksquare)}(\mathbf{r}) = z/2$. The metal fcc sublattice takes the part of the Ising lattice in which ordering involves Ni atoms, on the one hand, and Li atoms and structural vacancies $\blacksquare$, on the other hand. According to paper [48], the distribution function of Ni atoms in the trigonal (space group $R\bar{3}m$) $Li_{1-x-z}Ni_{1+x}O_2$ superstructure has the form

$$n^{(\mathrm{Ni})}(x_{\mathrm{I}}, y_{\mathrm{I}}, z_{\mathrm{I}}) = \frac{1+x}{2} - \frac{\eta_9^{(M)}}{2}\cos\left[\pi(x_{\mathrm{I}} - y_{\mathrm{I}} + z_{\mathrm{I}})\right] \qquad (11)$$

and depends on the long-range order parameter $\eta_9^{(M)}$. Function (11) at sites of the metal fcc sublattice takes two values: $n_{\mathrm{Ni}}^{(\mathrm{Ni})} = (1+x)/2 + \eta_9^{(M)}/2$, and $n_{\mathrm{Li}}^{(\mathrm{Ni})} = (1+x)/2 - \eta_9^{(M)}/2$ (see Table 3). One ($n_{\mathrm{Ni}}^{(\mathrm{Ni})}$) is the probability of detecting Ni atoms at the sites of the nickel sublattice, and the other ($n_{\mathrm{Li}}^{(\mathrm{Ni})}$) is the probability of detecting Ni atoms at the sites of the lithium sublattice (from here on, the subscript in the notations of probabilities n and concentrations c stands for the sublattice of interest, while the superscript denotes the sort of atoms located at the sites of this sublattice). During rhombohedral ordering, Li atoms and vacancies $\square$ are statistically distributed over the sites of the common lithium sublattice; therefore, the distribution function of the sites of the sole Li-sublattice in the basic cubic lattice can be written out as

$$n^{(\mathrm{Li},\blacksquare)}(x_{\mathrm{I}}, y_{\mathrm{I}}, z_{\mathrm{I}}) = \frac{1-x}{2} + \frac{\eta_9^{(M)}}{2}\cos\left[\pi(x_{\mathrm{I}} - y_{\mathrm{I}} + z_{\mathrm{I}})\right]. \qquad (12)$$

Distribution function (12) at sites of the metal fcc sublattice takes two values: $n_{\mathrm{Li}}^{(\mathrm{Li})} = (1-x)/2 + \eta_9^{(M)}/2$, and $n_{\mathrm{Ni}}^{(\mathrm{Li})} = (1-x)/2 - \eta_9^{(M)}/2$ (see Table 3).

The fully ordered state of lithium nickelite is reached for the stoichiometric $LiNiO_2$ composition when the long-range order parameter $\eta_9^{(M)}(x) = 1$, the relative concentrations of Li and Ni atoms in the metal sublattice are identical, and structural vacancies are absent, i.e., $x_{\mathrm{st}} = 0$ and $z_{\mathrm{st}} = 0$. In the metal sublattice of the fully ordered rhombohedral (space group $R\bar{3}m$) $LiNiO_2$ structure, hexagonal atomic planes $(1\bar{1}1)_{B1}$, all sites of which are occupied by Li atoms, successively alternate in direction $[1\bar{1}1]_{B1}$ with planes $(1\bar{1}1)_{B1}$, the sites of which are occupied by Ni atoms.

Symmetry analysis [48] unambiguously indicates that the structure of rhombohedral lithium nickelite is described by a single order parameter, $\eta_9^{(M)}$, although certain authors (see, for instance, paper [46]) believe erroneously that two parameters are needed for the purpose: one for the order description in the Li sublattice, and the other for the order description in the Ni sublattice. But the long-range order parameter in these sublattices is totally determined by parameter $\eta_9^{(M)}$. Indeed, the degree of ordering in Li and Ni sublattices can be estimated using the parameter $\eta_9^{(M)}$ and the obtained values of the distribution function. The degree of ordering in the Ni sublattice is given by

$$\eta_{\mathrm{Ni}} = \frac{c_{\mathrm{Ni}}^{(\mathrm{Ni})} - c_{\mathrm{Ni}}^{(\mathrm{Li})}}{c_{\mathrm{Ni}}^{(\mathrm{Ni})\,\max}} \equiv \frac{n_{\mathrm{Ni}}^{(\mathrm{Ni})} - n_{\mathrm{Ni}}^{(\mathrm{Li})}}{c_{\mathrm{Ni}}^{(\mathrm{Ni})\,\max}}\,.$$

The highest possible concentration of nickel in the Ni-sublattice is $c_{\mathrm{Ni}}^{(\mathrm{Ni})\,\max} = 1$. Taking this into account and knowing the values $n_{\mathrm{Ni}}^{(\mathrm{Ni})}$ and $n_{\mathrm{Ni}}^{(\mathrm{Li})}$ of functions (11) and (12), the degree of ordering in the Ni-sublattice is $\eta_{\mathrm{Ni}} = \eta_9^{(M)} + x$.

Table 3. Trigonal (rhombohedral) [space group No. 166 — $R\bar{3}m$ (D_{3d}^5)] $LiNiO_2$ superstructure of lithium nickelite $Li_{1-x-z}Ni_{1+x}O_2$: $\mathbf{a}_{\mathrm{tr}} = (1/2)\langle 1\bar{2}1\rangle_{B1}$, $\mathbf{b}_{\mathrm{tr}} = (1/2)\langle 2\bar{1}1\rangle_{B1}$, and $\mathbf{c}_{\mathrm{tr}} = (1/2)\langle 1\bar{1}2\rangle_{B1}$.

Atom	Position and multiplicity	Atomic coordinates in perfectly ordered structure			Values of distribution function	
		x/a_{tr}	y/b_{tr}	z/c_{tr}	$n^{(\mathrm{Li},\blacksquare)}(x_{\mathrm{I}}, y_{\mathrm{I}}, z_{\mathrm{I}})$	$n^{(\mathrm{Ni})}(x_{\mathrm{I}}, y_{\mathrm{I}}, z_{\mathrm{I}})$
Li	$1(a)$	0	0	0	$n_{\mathrm{Li}}^{(\mathrm{Li})} = (1-x)/2 + \eta_9^{(M)}/2$	$n_{\mathrm{Li}}^{(\mathrm{Ni})} = (1+x)/2 - \eta_9^{(M)}/2$
Ni	$1(b)$	1/2	1/2	1/2	$n_{\mathrm{Ni}}^{(\mathrm{Li})} = (1-x)/2 - \eta_9^{(M)}/2$	$n_{\mathrm{Ni}}^{(\mathrm{Ni})} = (1+x)/2 + \eta_9^{(M)}/2$
O	$2(c)$	1/4	1/4	1/4		

By analogy, the degree of ordering in the Li-sublattice is $\eta_{\mathrm{Li}} = (c_{\mathrm{Li}}^{(\mathrm{Li})} - c_{\mathrm{Li}}^{(\mathrm{Ni})})/c_{\mathrm{Li}}^{(\mathrm{Li})\max}$, where $c_{\mathrm{Li}}^{(\mathrm{Li})} \equiv n_{\mathrm{Li}}^{(\mathrm{Li})}$ and $c_{\mathrm{Li}}^{(\mathrm{Ni})} \equiv n_{\mathrm{Li}}^{(\mathrm{Ni})}$ are concentrations of Li and Ni atoms in the Li-sublattice, i.e., in the Li layers. The value of $c_{\mathrm{Li}}^{(\mathrm{Li})\max} = 1 - x$ is the highest possible concentration of lithium in the Li-sublattice. Taking this into account and knowing the values $n_{\mathrm{Li}}^{(\mathrm{Ni})}$ and $n_{\mathrm{Li}}^{(\mathrm{Li})}$ of functions (11) and (12), the degree of ordering in the Li-sublattice is found to be $\eta_{\mathrm{Li}} = (\eta_9^{(M)} - x)/(1 - x)$.

The dependence of the maximum value of the long-range order parameter $\eta_9^{(M)}$ on the $\mathrm{Li}_{1-x-z}\mathrm{Ni}_{1+x}\mathrm{O}_2$ composition during formation of the rhombohedral LiNiO_2 phase for the values of $0 \leqslant x \leqslant 1$ and $0 \leqslant z < 1 - x$ has the form $\eta_9^{(M)\max}(x, z) = 1 - x$. Therefore, $\eta_{\mathrm{Li}}^{\max} = (1 - 2x)/(1 - x)$ and $\eta_{\mathrm{Ni}}^{\max} = 1$. In the case of a maximum long-range order parameter in $\mathrm{Li}_{1-x-z}\mathrm{Ni}_{1+x}\mathrm{O}_2$, when $x = 0$ and $z = 0$, the degree of ordering in the Ni- and Li-sublattices equals 1. For $x > 0$, the degree of ordering in the Ni-sublattice remains equal to 1, since all its sites are occupied only by Ni atoms. Alternatively, the degree of ordering in the Li-sublattice does not exceed $\eta_{\mathrm{Li}}^{\max} = (1 - 2x)/(1 - x)$, because its sites are occupied not only by Li atoms but also by xN_{A} nickel atoms. The degree of ordering cannot be negative; therefore, it follows from the relation $\eta_{\mathrm{Li}}^{\max} = (1 - 2x)/(1 - x)$ that a rhombohedral (space group $R\bar{3}m$) superstructure cannot exist for $x > 0.5$. Indeed, a high vacancy concentration ($z \geqslant 1/6$) leads to disordering up to the cubic phase or to a reduction in symmetry with the retention of Ni atomic planes and with ordering of Li atoms and vacancies in $(1\bar{1}1)_{B1}$ planes of the common Li-sublattice. In lithium nickelite with an excess of Ni ($x \geqslant 1/6$), the reduction of symmetry may proceed with the redistribution of Li and Ni atoms over all $(1\bar{1}1)_{B1}$ planes in the metal sublattice and their ordering in these planes. Such orderings may occur as first-order phase transformations via transition channels containing the rays of the $\{\mathbf{k}_4\}$ and $\{\mathbf{k}_3\}$ stars, besides the rays of the $\{\mathbf{k}_9\}$ star. As a result, superstructures of type $\mathrm{Li}_5\blacksquare\mathrm{Ni}_6\mathrm{O}_{12}$ with monoclinic and trigonal symmetries may arise. For $z \geqslant 0.25$, $\mathrm{Li}_3\blacksquare\mathrm{Ni}_4\mathrm{O}_8$ and $\mathrm{Li}_2\blacksquare\mathrm{Ni}_3\mathrm{O}_6$ superstructures may be formed. Indeed, Refs [42, 49] report the detection of a monoclinic $\mathrm{Li}_3\blacksquare\mathrm{Ni}_4\mathrm{O}_8$ superstructure in nickelite $\mathrm{Li}_{0.50-0.75}\mathrm{NiO}_2$. A symmetry analysis of $\mathrm{Li}_3\blacksquare\mathrm{Ni}_4\mathrm{O}_8$ ($M_7\blacksquare\mathrm{O}_8$) and $\mathrm{Li}_2\blacksquare\mathrm{Ni}_3\mathrm{O}_6$ ($M_5\blacksquare\mathrm{O}_6$) superstructures was performed in paper [48].

3.5 Sequence of M_2X superstructure formation

The thermodynamic computation of phase equilibria in Ti–C, Zr–C, and Ti–N systems by the order parameter functional method [1–5] confirms the formation of M_2X type ordered phases but does not allow the determination of their symmetry or space group. It remains to be elucidated if superstructures of type M_2X are mutually exclusive or can arise one after the other in a certain sequence as temperature drops.

References [50, 51] report the results of the symmetry analysis of the M_2X phase structure with a view to determining the possible sequence of phase transformations during the formation of M_2X type superstructures in the nonstoichiometric carbides $M\mathrm{C}_y$ and nitrides $M\mathrm{N}_y$.

Disorder–order or order–order phase transformations occurring as the temperature decreases are transitions from a higher free energy state to a lower energy one. The state of a substance undergoing atomic or atomic-vacancy ordering can be characterized by the Landau thermodynamic potential—that is, in this case, the functional of probabilities of detecting atoms of a certain kind at lattice sites, site coordinates, and temperature. The probabilities, in turn, are the functions of long-range order parameters. The Landau potential passes a few minima corresponding to high-symmetry disordered and low-symmetry ordered phases. As temperature drops, disorder–order and order–order phase transitions occur with the reduction of symmetry. The symmetry analysis permits us to quantitatively evaluate the degree of symmetry reduction during superstructure formation and to determine the physically admissible sequence in which these superstructures can arise.

The ordering of X atoms and $\square$ structural vacancies occurs in the basic nonmetal fcc sublattice of the disordered cubic (space group $Fm\bar{3}m$) MX_y phase and is associated with the splitting of highly symmetric $4(b)$ positions into two or more positions of the low-symmetry ordered phase. The disordered cubic (space group $Fm\bar{3}m$) MX_y phase has a point symmetry group $m\bar{3}m$ (O_h) including 48 symmetry elements $h_1 - h_{48}$ [1, 2, 31]. The symmetry point groups of the four M_2X superstructures under consideration belong to subgroups of the $m\bar{3}m$ (O_h) point group. Therefore, the transition from the disordered cubic MX_y phase to any of these superstructures constitutes a disorder–order phase transformation.

According to the Landau phenomenological theory of phase transitions [52], a necessary condition for the second-order phase transition is an identical equality to zero of the coefficient of the cubic term in a power series expansion of the free energy in the long-range order parameter. If a second-order phase transformation occurs with a change in translational symmetry, the group-theoretical Landau criterion is equivalent to the following necessary condition for realizing the second-order phase transition [36]: a second-order phase transformation is feasible only when it is impossible to choose from the star vectors associated with this transformation three (not necessarily different) vectors, the sum of which would be equal to zero or to the structural vector $\mathbf{H}$ of the reciprocal lattice in a disordered crystal. In other words, the following inequalities hold during a second-order phase transformation:

$$\left.\begin{array}{r}\mathbf{k}_s^{(j_1)} + \mathbf{k}_s^{(j_2)} + \mathbf{k}_s^{(j_3)} \\ 3\mathbf{k}_s^{(j)}\end{array}\right\} \neq 0 \quad \text{or} \quad \mathbf{H}\,. \tag{13}$$

Determination of $MX_y - M_2X$ phase transition channels revealed that the formation of any M_2X type superstructure is associated with one of the Lifshitz stars $\{\mathbf{k}_{10}\}$, $\{\mathbf{k}_9\}$, or $\{\mathbf{k}_8\}$. For the vectors of $\{\mathbf{k}_9\}$ and $\{\mathbf{k}_8\}$ stars entering the transition channel, condition (13) is fulfilled. This means that disorder–order transitions with the formation of M_2X superstructures (space groups $R\bar{3}m$, $Fm\bar{3}m$, $I4_1/amd$) satisfy the Landau criterion for second-order phase transitions. The formation of a tetragonal (space group $P4/mmm$) M_2X superstructure can only be a first-order phase transformation, since condition (13) is not fulfilled for the $\{\mathbf{k}_{10}\}$ star.

The trigonal (space group $R\bar{3}m$) M_2X superstructure has the point symmetry group $\bar{3}m$ (D_{3d}) including 12 symmetry elements, whereas the $m\bar{3}m$ (O_h) point group of the basic cubic disordered phase contains 48 elements; for this reason, the reduction in rotational symmetry equals 4. The reduction in translational symmetry is described by the ratio of unit cell volumes of low- and high-symmetry phases; it equals 1.5 in the case of transition from the high-symmetry disordered

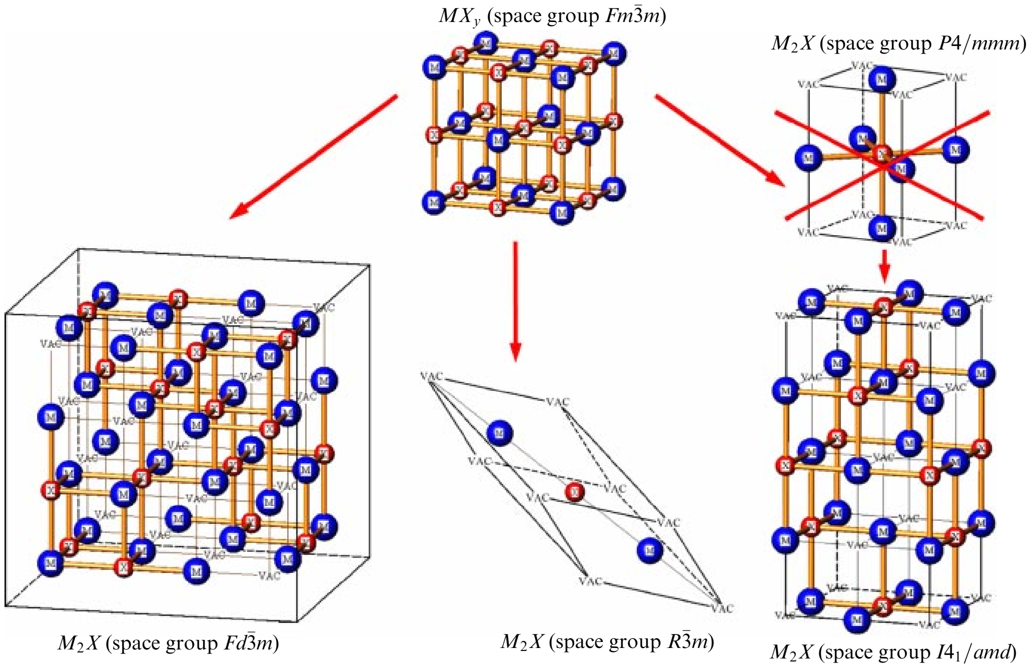

Figure 5. (Color online.) The possible sequences of disorder–order and order–order phase transformations occurring with decreasing temperature and associated with the formation of type M_2X superstructures in strongly nonstoichiometric MX_y compounds with the basic structure $B1$. The topmost unit cell of a nonstoichiometric MX_y compound has a basic cubic (space group $Fm\bar{3}m$) structure; the sites of the nonmetal sublattice in this cell are statistically occupied by X atoms with probability y. Intermediate formation of the tetragonal (space group $P4/mmm$) M_2X superstructure in the third phase transformation sequence can be excluded due to the thermodynamic instability of such a phase in MX_y compounds with the basic structure $B1$. The notation 'vac' in unit cells of M_2X superstructures indicates vacant sites.

compound MX_y to the low-symmetry trigonal phase M_2X (in the hexagonal arrangement). The overall symmetry reduction is equal to the product of rotational and translational reductions. For this reason, in the disordered cubic (space group $Fm\bar{3}m$) MX_y phase → ordered trigonal (space group $R\bar{3}m$) M_2X phase transition, the overall symmetry reduction is given by $N = n(G)/n(G_{\mathrm{D}}) = 6$, where $n(G)$ and $n(G_{\mathrm{D}})$ are the orders of space groups G and G_{D} relevant to high- and low-symmetry phases.

The cubic (space group $Fd\bar{3}m$) M_2X superstructure has the same point symmetry group $m\bar{3}m$ as the disordered MX_y phase; therefore, the rotational symmetry reduction equals 1. Translational symmetry reduction during transition from the disordered MX_y phase to the cubic (space group $Fd\bar{3}m$) M_2X phase equals 8. Due to this, the overall symmetry reduction in the disordered cubic (space group $Fm\bar{3}m$) MX_y phase → ordered cubic (space group $Fd\bar{3}m$) M_2X phase transition is equal to 8.

Although the point symmetry group of the trigonal (space group $R\bar{3}m$) M_2X superstructure is a subgroup of the point group of the cubic (space group $Fd\bar{3}m$) M_2X superstructure, transition from the cubic (space group $Fd\bar{3}m$) M_2X superstructure to the trigonal one is impossible because, in this case, symmetry would raise rather than reduce. It follows from a comparison of symmetry reduction during formation of trigonal and cubic M_2X superstructures that their formation is equally probable. Indeed, Ref. [37] reports that these superstructures arise in different concentration regions. It may be supposed that in nonstoichiometric MX_y compounds differing in the amount of nonmetal y, parallel disorder–order transitions are possible from the cubic (space group $Fm\bar{3}m$) disordered MX_y phase to the cubic (space group $Fd\bar{3}m$) ordered M_2X phase and from the cubic (space group $Fm\bar{3}m$) disordered MX_y phase to the trigonal (space group $R\bar{3}m$) ordered M_2X phase.

Tetragonal (space group $P4/mmm$ and $I4_1/amd$) M_2X superstructures have the same point symmetry group $4/mmm$ (D_{4h}) that includes 16 symmetry elements h_1-h_4, $h_{13}-h_{16}$, $h_{25}-h_{28}$, and $h_{37}-h_{40}$ [1, 2, 34]. Thus, the rotational symmetry reduction during formation of tetragonal M_2X superstructures proceeds in a similar fashion and equals 3. The change in translational symmetry in disorder–order transitions resulting in tetragonal M_2X superstructures with space groups $P4/mmm$ and $I4_1/amd$ equals 1/2 and 2, while the overall symmetry reduction in these transitions is equal to 3/2 and 6, respectively.

It is clear from the ratio of symmetry elements h_I that the point group $4/mmm$ of tetragonal M_2X superstructures is not a subgroup of group $\bar{3}m$ of a trigonal superstructure. This means that order–order transitions from a trigonal superstructure to any of the two tetragonal M_2X superstructures with decreasing temperature are impossible. Order–order transitions from a cubic M_2X superstructure to any of the two tetragonal M_2X superstructures with decreasing temperature are equally impossible, because symmetry would raise rather than reduce.

Bearing in mind changes in general and translational symmetries, the tetragonal (space group $P4/mmm$) M_2X superstructure can be formally regarded as highly symmetric with respect to the M_2X superstructure with the space group $I4_1/amd$. In this case, the overall reduction in symmetry during the order–order transition from M_2X (space group $P4/mmm$) to M_2X (space group $I4_1/amd$) equals 4.

On the whole, the above analysis demonstrates the possibility of three sequences of transformations involving ordered M_2X phases with a decrease in temperature (Fig. 5). The first and second sequences are the cubic (space group $Fm\bar{3}m$) disordered MX_y phase → cubic (space group $Fd\bar{3}m$) ordered M_2X phase and cubic (space group $Fm\bar{3}m$) disordered MX_y phase → trigonal (space group $R\bar{3}m$)

ordered M_2X phase transitions; they may occur in nonstoichiometric MX_y type compounds with different y compositions and include only disorder–order transformations. The alternative sequence is the cubic (space group $Fm\bar{3}m$) disordered MX_y phase → tetragonal (space group $P4/mmm$) ordered M_2X phase transformation; it includes disorder–order and order–order transformations. In the absence of an ordered phase in experiment, the transformation sequences remain physically valid anyway, even without this phase.

The above transformation sequences were found from symmetry considerations. It was shown in Refs [1, 2, 5, 53] by the order parameter functional method that the formation of cubic, trigonal, and tetragonal (space group $I4_1/amd$) M_2X superstructures is equally probable from the thermodynamic point of view and must occur at closely spaced temperatures. As regards the tetragonal (space group $P4/mmm$) M_2X superstructure, it has a higher (absolute) free energy than other M_2X type superstructures and therefore cannot arise in nonstoichiometric MX_y compounds with structure $B1$, meaning that the tetragonal (space group $P4/mmm$) M_2X superstructure can be excluded from the third sequence. Then, the third sequence takes the form of the cubic (space group $Fm\bar{3}m$) disordered MX_y phase → tetragonal (space group $I4_1/amd$) ordered M_2X phase transformation and also includes only disorder–order transitions.

It was shown in experiment that the first and second sequences of disorder–order transformations with the production of cubic and trigonal M_2X phases are realized in nonstoichiometric carbides of different compositions, especially in titanium carbide. According to Ref. [37], ordering in nonstoichiometric carbide TiC_y leads to the formation of the cubic (space group $Fd\bar{3}m$) M_2X superstructure in the region from $\mathrm{TiC}_{0.49-0.51}$ to $\mathrm{TiC}_{0.54–0.55}$, while the trigonal (space group $R\bar{3}m$) M_2X superstructure has the homogeneity interval $\mathrm{TiC}_{0.55}-\mathrm{TiC}_{0.59}$. The disorder–order transition temperature for both superstructures falls in the range of 990–1020 K. The third transformation sequence, i.e., disorder–order transition with the formation of a tetragonal (space group $I4_1/amd$) M_2X superstructure, occurs in nonstoichiometric nitrides. It can be supposed that the realization of one sequence or another is related to the macroscopic state of a nonstoichiometric compound, namely to grain size and morphology in the disordered phase and the origin of formation of the primary ordered phase on a certain crystallographic surface, as well as to the distinctions in $M-\mathrm{C}$ and $M-\mathrm{N}$ interatomic interactions.

4. M_3X_2 superstructures

4.1 Monoclinic M_3X_2 superstructure

The unit cell of a monoclinic [space group $C2$ ($B112$)] M_3X_2 superstructure is depicted in Fig. 6. Its translation vectors and coordinates of atoms and vacancies in an ideal monoclinic M_3X_2 superstructure are presented in Table 4. In Ref. [26], the space group of this superstructure was determined incorrectly; therefore, certain atoms and vacancies in the unit cell were disregarded. This error was repeated in later publications [1, 2, 6].

The monoclinic [space group $C2$ ($B112$)] M_3X_2 superstructure forms via the phase transition channel involving six rays of the $\{\mathbf{k}_4\}$ star with parameter $\mu_4 = 1/3$ (Table 5).

Table 4. Monoclinic [space group No. 5 — $C2$ ($B112$) (C_2^3)] M_3X_2 superstructure: $Z = 6$, $V = 9a_{B1}^3/2$, $\mathbf{a}_\mathrm{m} = (1/2)\langle 112\rangle_{B1}$, $\mathbf{b}_\mathrm{m} = \langle 11\bar{1}\rangle_{B1}$, and $\mathbf{c}_\mathrm{m} = (3/2)\langle 1\bar{1}0\rangle_{B1}$.

Atom	Position and multiplicity	Atomic coordinates in perfectly ordered structure			Values of distribution function $n(x_\mathrm{I}, y_\mathrm{I}, z_\mathrm{I})$
		x/a_m	y/b_m	z/c_m	
$X1$ (vacancy)	2(b)	1/2	1/2	2/3	$n_1 = y - 2\eta_4/3$
$X2$ (vacancy)	4(c)	1/6	1/6	0	$n_1 = y - 2\eta_4/3$
$X3$	2(b)	1/2	1/2	0	$n_2 = y + \eta_4/3$
$X4$	2(b)	1/2	1/2	1/3	$n_2 = y + \eta_4/3$
$X5$	4(c)	1/6	1/6	1/3	$n_2 = y + \eta_4/3$
$X6$	4(c)	1/6	1/6	2/3	$n_2 = y + \eta_4/3$
$M1$	2(a)	0	0	1/6	
$M2$	2(a)	0	0	1/2	
$M3$	2(a)	0	0	5/6	
$M4$	4(c)	1/6	2/3	0	
$M5$	4(c)	1/6	2/3	1/3	
$M6$	4(c)	1/6	2/3	2/3	

The monoclinic M_3X_2 superstructure is described by the distribution function

$$n(x_\mathrm{I}, y_\mathrm{I}, z_\mathrm{I}) = y - \frac{\eta_4}{3}\left\{\cos\left[\frac{4\pi(x_\mathrm{I}+z_\mathrm{I})}{3}\right] - \frac{\sqrt{3}}{3}\sin\left[\frac{4\pi(x_\mathrm{I}+z_\mathrm{I})}{3}\right] - \frac{2\sqrt{3}}{3}\sin\left[\frac{4\pi(y_\mathrm{I}+z_\mathrm{I})}{3}\right] + \cos\left[\frac{4\pi(x_\mathrm{I}-y_\mathrm{I})}{3}\right] + \frac{\sqrt{3}}{3}\sin\left[\frac{4\pi(x_\mathrm{I}-y_\mathrm{I})}{3}\right]\right\}. \qquad (14)$$

Parameters γ_4 and $\varphi_4^{(j)}$ of function (14) are presented in Table 5. For the completely ordered M_3X_2 phase, the quantity $y_\mathrm{st} = 2/3$. Figure 6 shows that coordinates $(x_\mathrm{I}, y_\mathrm{I}, z_\mathrm{I})$ are related to the coordinates of the monoclinic M_3X_2 superstructure, presented in Table 4, by the following

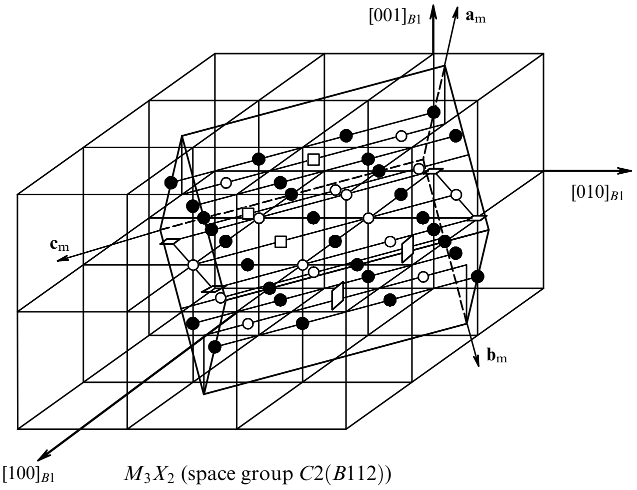

Figure 6. Position of the monoclinic [space group $C2$ ($B112$)] unit cell of the M_3X_2 superstructure in the lattice with the basic structure $B1$: (○) interstitial atom, (●) metal atom, and (□) vacancy. Although angles α, β, and γ of an ideal unit cell are equal to 90°, this structure is monoclinic rather than orthorhombic in terms of symmetry. The origin of coordinates of the monoclinic M_3X_2 superstructure has coordinates $(-1/4\ -1/4\ 0)_{B1}$ of the basic lattice with structure $B1$.

Table 5. Channels of disorder–order $MX_y - M_3X_2$ phase transitions and the parameters of distribution functions $n(x_{\rm I}, y_{\rm I}, z_{\rm I})$ describing M_3X_2 superstructures.

Symmetry	Space group	Disorder–order transition channel		Parameters of the distribution function	
		$\{\mathbf{k}_s\}$ star	$\mathbf{k}_s^{(j)}$ rays of the $\{\mathbf{k}_s\}$ star	γ_s	$\varphi_s^{(j)}$
Monoclinic	No. 5 $C2$ ($B112$) (C_2^3)	$\{\mathbf{k}_4\}$	$\mathbf{k}_4^{(3)} = (\mathbf{b}_2 - \mathbf{b}_1)/3$,	$\gamma_4 = \sqrt{3}/9$	$\varphi_4^{(3)} = \pi/3$
		$\{\mathbf{k}_4\}$	$\mathbf{k}_4^{(4)} = -\mathbf{k}_4^{(3)}$,	$\gamma_4 = \sqrt{3}/9$	$\varphi_4^{(4)} = -\pi/3$
		$\{\mathbf{k}_4\}$	$\mathbf{k}_4^{(5)} = (\mathbf{b}_1 + 2\mathbf{b}_2 + \mathbf{b}_3)/3$,	$\gamma_4 = \sqrt{3}/9$	$\varphi_4^{(5)} = \pi$
		$\{\mathbf{k}_4\}$	$\mathbf{k}_4^{(6)} = -\mathbf{k}_4^{(5)}$,	$\gamma_4 = \sqrt{3}/9$	$\varphi_4^{(6)} = -\pi$
		$\{\mathbf{k}_4\}$	$\mathbf{k}_4^{(9)} = (2\mathbf{b}_1 + \mathbf{b}_2 + \mathbf{b}_3)/3$,	$\gamma_4 = \sqrt{3}/9$	$\varphi_4^{(9)} = 7\pi/6$
		$\{\mathbf{k}_4\}$	$\mathbf{k}_4^{(10)} = -\mathbf{k}_4^{(9)}$	$\gamma_4 = \sqrt{3}/9$	$\varphi_4^{(10)} = -7\pi/6$
Orthorhombic	No. 71 $Immm$ (D_{2h}^{25})	$\{\mathbf{k}_4\}$	$\mathbf{k}_4^{(1)} = (\mathbf{b}_1 + \mathbf{b}_2 + 2\mathbf{b}_3)/3$,	$\gamma_4 = 1/3$	$\varphi_4^{(1)} = \pi$
		$\{\mathbf{k}_4\}$	$\mathbf{k}_4^{(2)} = -\mathbf{k}_4^{(1)}$	$\gamma_4 = 1/3$	$\varphi_4^{(2)} = -\pi$
Orthorhombic	No. 20 $C222_1$ (D_2^5)	$\{\mathbf{k}_4\}$	$\mathbf{k}_4^{(1)} = (\mathbf{b}_1 + \mathbf{b}_2 + 2\mathbf{b}_3)/3$,	$\gamma_4 = 1/6$	$\varphi_4^{(1)} = 4\pi/3$
		$\{\mathbf{k}_4\}$	$\mathbf{k}_4^{(2)} = -\mathbf{k}_4^{(1)}$,	$\gamma_4 = 1/6$	$\varphi_4^{(2)} = -4\pi/3$
		$\{\mathbf{k}_3\}$	$\mathbf{k}_3^{(3)} = -(7\mathbf{b}_1 + \mathbf{b}_2 + 2\mathbf{b}_3)/12$,	$\gamma_3 = \sqrt{6}/12$	$\varphi_3^{(3)} = 11\pi/12$
		$\{\mathbf{k}_3\}$	$\mathbf{k}_3^{(4)} = -\mathbf{k}_3^{(3)}$,	$\gamma_3 = \sqrt{6}/12$	$\varphi_3^{(4)} = -11\pi/12$
		$\{\mathbf{k}_3\}$	$\mathbf{k}_3^{(5)} = (\mathbf{b}_1 - 5\mathbf{b}_2 + 2\mathbf{b}_3)/12$,	$\gamma_3 = \sqrt{6}/12$	$\varphi_3^{(5)} = 7\pi/12$
		$\{\mathbf{k}_3\}$	$\mathbf{k}_3^{(6)} = -\mathbf{k}_3^{(5)}$	$\gamma_3 = \sqrt{6}/12$	$\varphi_3^{(6)} = -7\pi/12$
Trigonal	No. 164 $P\bar{3}m1$ (D_{3d}^3)	$\{\mathbf{k}_5\}$	$\mathbf{k}_5^{(5)} = -\mathbf{b}_2/3$,	$\gamma_5 = 1/3$	$\varphi_5^{(5)} = \pi$
		$\{\mathbf{k}_5\}$	$\mathbf{k}_5^{(6)} = -\mathbf{k}_5^{(5)}$	$\gamma_5 = 1/3$	$\varphi_5^{(6)} = -\pi$

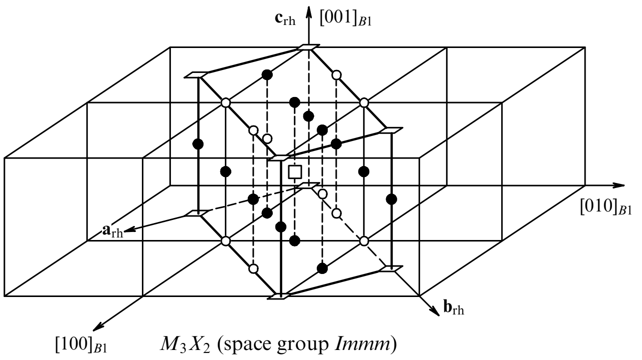

Figure 7. Position of the orthorhombic (space group $Immm$) unit cell of the M_3X_2 superstructure in the lattice with structure $B1$: (○) interstitial atom, (●) metal atom, and (□) vacancy.

equations: $x_{\rm I} = x_{\rm m}/2 + y_{\rm m} + 3z_{\rm m}/2 - 1/4$, $y_{\rm I} = x_{\rm m}/2 + y_{\rm m} - 3z_{\rm m}/2 - 1/4$, and $z_{\rm I} = x_{\rm m} - y_{\rm m}$. The distribution function (14) assumes two values, n_1 and n_2, at sites of the nonmetal fcc sublattice (see Table 4).

In the completely ordered monoclinic [space group $C2$ ($B112$)] M_3X_2 ($y = 2/3$, $\eta_4 = 1$) superstructure, one third of the sites of each nonmetal atomic plane $(1\bar{1}1)_{B1}$ are vacant, while the remaining ones are occupied by interstitial atoms.

4.2 Orthorhombic M_3X_2 superstructures

The literature describes two orthorhombic M_3X_2 superstructures with space groups $Immm$ (Fig. 7) and $C222_1$ (Fig. 8). Translation vectors of the unit cells of these superstructures, as well as the coordinates of atoms and vacancies in them, are listed in Table 6.

The disorder–order $MX_y - M_3X_2$ (space group $Immm$) phase transition channel includes two rays $\mathbf{k}_4^{(1)}$ and $\mathbf{k}_4^{(2)}$ of the $\{\mathbf{k}_4\}$ star with parameter $\mu_4 = 1/3$ (see Table 5). The orthorhombic (space group $Immm$) M_3X_2 superstructure is described by the distribution function

$$n(x_{\rm I}, y_{\rm I}, z_{\rm I}) = y - \frac{2\eta_4}{3} \cos\left[\frac{4\pi(x_{\rm I} + y_{\rm I})}{3}\right]. \tag{15}$$

For the fully ordered M_3X_2 phase, the quantity $y_{\rm st} = 2/3$. In accordance with Fig. 7, coordinates $(x_{\rm I}, y_{\rm I}, z_{\rm I})$ are related to the coordinates of the orthorhombic (space group $Immm$) M_3X_2 superstructure, presented in Table 6, by the equations $x_{\rm I} = x_{\rm rh}/2 + 3y_{\rm rh}/2$, $y_{\rm I} = -x_{\rm rh}/2 + 3y_{\rm rh}/2$, and $z_{\rm I} = z_{\rm rh}$.

In the ordering under consideration, the nonmetal sublattice of the disordered MX_y compound splits into two nonequivalent sublattices differing in probabilities n_1 and n_2 of site occupation by interstitial X atoms (see Table 6).

The orthorhombic unit cell of the M_3X_2 superstructure with the space group $C222_1$ is depicted in Fig. 8. The presence of the ordered (space group $C222_1$) M_3X_2 phase in titanium carbide $\rm TiC_{0.64}$ was shown by a Monte Carlo computation in Ref. [23]. Traces of the orthorhombic (space group $C222_1$) ordered $\rm Ti_3C_2$ (M_3X_2) phase were observed in experiment [37]. The M_3X_2 superstructure forms via the transition channel involving two rays of the $\{\mathbf{k}_4\}$ star and four rays of the $\{\mathbf{k}_3\}$ star (see Table 5). The actual parameters of the $\{\mathbf{k}_4\}$ and $\{\mathbf{k}_3\}$ stars are $\mu_4 = 1/3$ and $\mu_3 = 1/12$, respectively.

The distribution function of interstitial atoms in the orthorhombic (space group $C222_1$) M_3X_2 superstructure has the form

$$\begin{aligned} n(x_{\rm I}, y_{\rm I}, z_{\rm I}) = y &- \frac{\eta_4}{3}\left\{\frac{1}{2}\cos\left[\frac{4\pi(x_{\rm I} + y_{\rm I})}{3}\right]\right. \\ &\left. - \frac{\sqrt{3}}{2}\sin\left[\frac{4\pi(x_{\rm I} + y_{\rm I})}{3}\right]\right\} \\ &- \frac{\eta_3}{2}\left\{\left(\frac{1}{2} + \frac{\sqrt{3}}{6}\right)\cos\left[\frac{\pi(2x_{\rm I} - 4y_{\rm I} - 3z_{\rm I})}{3}\right]\right. \end{aligned}$$

Table 6. Orthorhombic M_3X_2 superstructures.

Space group	Translation vectors of unit cell	V *	Atom	Position and multiplicity	Atomic coordinates in ideal ordered structure			Values of distribution function $n(x_{\rm I}, y_{\rm I}, z_{\rm I})$
					$x/a_{\rm rh}$	$y/b_{\rm rh}$	$z/c_{\rm rh}$	
No. 71 *Immm* (D_{2h}^{25})	$\mathbf{a}_{\rm rh} = \frac{1}{2}\langle 1\bar{1}0\rangle_{B1}$, $\mathbf{b}_{\rm rh} = \frac{3}{2}\langle 110\rangle_{B1}$, $\mathbf{c}_{\rm rh} = \langle 001\rangle_{B1}$	$3a_{B1}^3/2$	$X1$ (vacancy)	$2(a)$	0	0	0	$n_1 = y - 2\eta_4/3$
			$X2$	$4(g)$	0	1/3	0	$n_2 = y + \eta_4/3$
			$M1$	$2(c)$	1/2	1/2	0	
			$M2$	$4(h)$	0	2/3	1/2	
					$x/a_{\rm rh}$	$y/b_{\rm rh}$	$z/c_{\rm rh}$	
No. 20 $C222_1$ (D_2^5)	$\mathbf{a}_{\rm rh} = \langle 1\bar{1}0\rangle_{B1}$, $\mathbf{b}_{\rm rh} = \langle 330\rangle_{B1}$, $\mathbf{c}_{\rm rh} = \langle 002\rangle_{B1}$	$12a_{B1}^3$	$X1$ (vacancy)	$4(b)$	0	1/6	1/4	$n_1 = y - \eta_4/6 - \eta_3/2$
			$X2$ (vacancy)	$4(b)$	0	1/3	1/4	$n_1 = y - \eta_4/6 - \eta_3/2$
			$X3$ (vacancy)	$8(c)$	1/4	5/12	0	$n_1 = y - \eta_4/6 - \eta_3/2$
			$X4$	$4(b)$	0	0	1/4	$n_2 = y + \eta_4/3$
			$X5$	$4(b)$	0	1/2	1/4	$n_2 = y + \eta_4/3$
			$X6$	$4(b)$	0	2/3	1/4	$n_3 = y - \eta_4/6 + \eta_3/2$
			$X7$	$4(b)$	0	5/6	1/4	$n_3 = y - \eta_4/6 + \eta_3/2$
			$X8$	$8(c)$	1/4	1/12	0	$n_3 = y - \eta_4/6 + \eta_3/2$
			$X9$	$8(c)$	1/4	1/4	0	$n_2 = y + \eta_4/3$
			$M1$	$4(a)$	0	0	0	
			$M2$	$4(a)$	1/2	0	0	
			$M3$	$8(c)$	1/4	1/12	1/4	
			$M4$	$8(c)$	1/4	1/4	1/4	
			$M5$	$8(c)$	1/4	5/12	1/4	
			$M6$	$8(c)$	0	1/6	1/4	
			$M7$	$8(c)$	0	1/3	1/2	

* The volume of the unit cell of a superstructure expressed through parameter a_{B1} of the unit cell of the disordered basic $B1$ type structure.

$$+\left(\frac{1}{2}-\frac{\sqrt{3}}{6}\right)\sin\left[\frac{\pi(2x_{\rm I}-4y_{\rm I}-3z_{\rm I})}{3}\right]$$
$$+\left(\frac{1}{2}-\frac{\sqrt{3}}{6}\right)\cos\left[\frac{\pi(-2x_{\rm I}+4y_{\rm I}-3z_{\rm I})}{3}\right]$$
$$+\left(\frac{1}{2}+\frac{\sqrt{3}}{6}\right)\sin\left[\frac{\pi(-2x_{\rm I}+4y_{\rm I}-3z_{\rm I})}{3}\right]\Bigg\}. \qquad (16)$$

As in the preceding case, the quantity $y_{\rm st} = 2/3$. Function (16) takes three values at all sites located in different positions on the nonmetal sublattice of the M_3X_2 structure (see Table 6). As follows from Fig. 8, coordinates $(x_{\rm I}, y_{\rm I}, z_{\rm I})$ are related to the coordinates of the M_3X_2 structure, listed in Table 6, by the following equations: $x_{\rm I} = x_{\rm rh} + 3y_{\rm rh} - 1/2$, $y_{\rm I} = -x_{\rm rh}+3y_{\rm rh} - 1/2$, and $z_{\rm I} = 2z_{\rm rh} - 1/2$.

Parameters γ_s and $\varphi_s^{(j)}$ of distribution functions (15) and (16) are presented in Table 5.

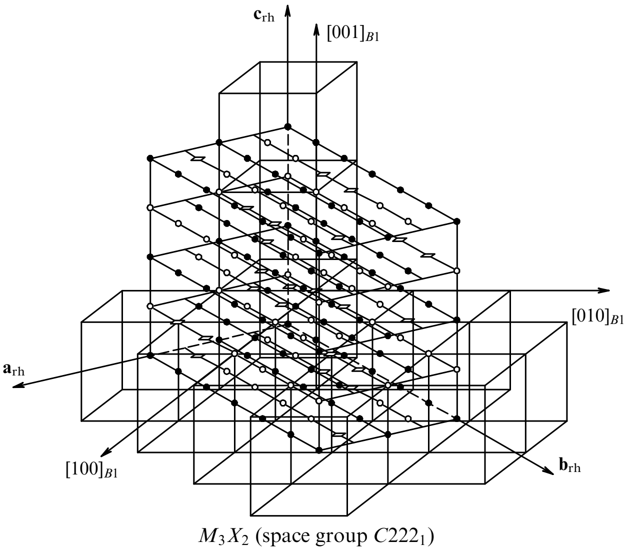

M_3X_2 (space group $C222_1$)

Figure 8. Position of the orthorhombic (space group $C222_1$) unit cell of the M_3X_2 superstructure in the lattice with structure $B1$: (○) interstitial atom, (●) metal atom, and (□) vacancy.

4.3 Trigonal M_3X_2 superstructure

The unit cell of a model trigonal (space group $P\bar{3}m1$) M_3X_2 superstructure is depicted in Fig. 9. Translation vectors of this unit cell and coordinates of atoms and vacancies are given in Table 7. The trigonal (space group $P\bar{3}m1$) M_3X_2 superstructure forms via the transition channel involving two rays, $\mathbf{k}_5^{(5)}$ and $\mathbf{k}_5^{(6)}$, of the $\{\mathbf{k}_5\}$ star (see Table 5). In this superstructure. the actual parameter μ_5 of $\{\mathbf{k}_5\}$ star rays equals 1/3.

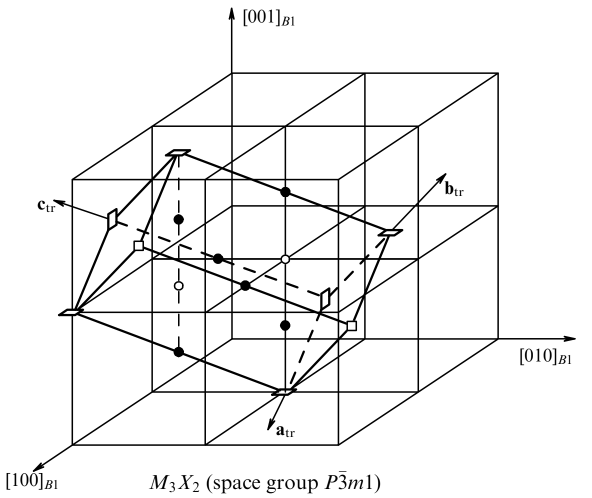

Figure 9. Position of the trigonal (space group $P\bar{3}m1$) unit cell of the M_3X_2 superstructure in the lattice with structure $B1$: (○) interstitial atom, (●) metal atom, and (□) vacancy. The origin of coordinates of the trigonal M_3X_2 superstructure has coordinates $(1/2\ 1\ 1/2)_{B1}$ of the basic lattice with structure $B1$.

Table 7. Trigonal [space group No. 164 — $P\bar{3}m1$ (D^3_{3d})] M_3X_2 superstructure: $Z=1$, $V=3a^3_{B1}/4$, $\mathbf{a}_{\rm tr}=(1/2)\langle 10\bar{1}\rangle_{B1}$, $\mathbf{b}_{\rm tr}=(1/2)\langle 01\bar{1}\rangle_{B1}$ and, $\mathbf{c}_{\rm tr}=\langle 1\bar{1}1\rangle_{B1}$.

Atom	Position and multiplicity	Atomic coordinates in perfectly ordered structure			Values of distribution function $n(x_{\rm I}, y_{\rm I}, z_{\rm I})$
		$x/a_{\rm tr}$	$y/b_{\rm tr}$	$z/c_{\rm tr}$	
$X1$ (vacancy)	$1(a)$	0	0	0	$n_1 = y - 2\eta_5/3$
$X2$	$2(d)$	1/3	2/3	1/3	$n_2 = y + \eta_5/3$
$M1$	$1(b)$	0	0	1/2	
$M2$	$2(d)$	1/3	2/3	5/6	

The distribution function for the trigonal M_3X_2 superstructure has the form

$$n(x_{\rm I}, y_{\rm I}, z_{\rm I}) = y - \frac{2\eta_5}{3}\cos\left[\frac{2\pi(x_{\rm I} - y_{\rm I} + z_{\rm I})}{3}\right]. \qquad (17)$$

As follows from Fig. 9, coordinates $(x_{\rm I}, y_{\rm I}, z_{\rm I})$ are related to the coordinates of the M_3X_2 superstructure presented in Table 7 by the following equations: $x_{\rm I} = x_{\rm tr}/2 + z_{\rm tr} + 1/2$, $y_{\rm I} = y_{\rm tr}/2 - z_{\rm tr} + 1$, and $z_{\rm I} = -x_{\rm tr}/2 + y_{\rm tr}/2 + z_{\rm tr} + 1/2$. Distribution function (17) assumes two values at all sites of the nonmetal fcc sublattice (see Table 7). For the completely ordered trigonal M_3X_2 phase, the quantity $y_{\rm st} = 2/3$. Parameters γ_5 and $\varphi_5^{(j)}$ of (17) are presented in Table 5.

Given that only the nonmetal sublattice of the trigonal (space group $P\bar{3}m1$) M_3X_2 superstructure is considered, two complete atomic planes, all sites of which are occupied by interstitial atoms, and one defective plane having all sites vacant alternate successively in the $[1\bar{1}1]_{B1}$ direction. The formation of such a superstructure in nonstoichiometric MX_y compounds with structure $B1$ is unlikely. This inference is consistent with thermodynamic calculations by the order parameter functional method [1, 2, 5, 53], showing that the formation of the trigonal (space group $P\bar{3}m1$) M_3X_2 superstructure in nonstoichiometric MX_y compounds is impossible.

4.4 Sequence of M_3X_2 superstructure formation

Thermodynamic calculations [1–6] of phase equilibria in Ti–C, Zr–C, Hf–C, and Ti–N systems, including nonstoichiometric MX_y compounds with the basic cubic $B1$ structure, confirm the possibility of forming ordered M_3X_2 type phases with the exception of the trigonal (space group $P\bar{3}m1$) phase. We shall perform a symmetry analysis of three other M_3X_2 type superstructures and discuss the sequence of their formation with decreasing temperature.

Point symmetry groups of monoclinic and orthorhombic M_3X_2 superstructures take the part of the subgroups of the $m\bar{3}m$ (O_h) point symmetry group of the disordered cubic (space group $Fm\bar{3}m$) MX_y phase. Therefore, the transition from phase MX_y to any of these superstructures is a disorder–order phase transformation.

The determination of $MX_y - M_3X_2$ phase transition channels showed that the formation of monoclinic and orthorhombic M_3X_2 superstructures is associated with the symmetry distortion affecting one ($\{\mathbf{k}_4\}$) or two ($\{\mathbf{k}_4\}$ or $\{\mathbf{k}_3\}$) non-Lifshitz stars. Moreover, for orthorhombic (space groups $Immm$ and $C222_1$) superstructures, $3\mathbf{k}_4^{(1)} = \langle 220\rangle$, and for the monoclinic (space group $C2$) superstructure, $3\mathbf{k}_4^{(5)} = \langle 202\rangle$. This means that condition (13) is not fulfilled and the formation of these M_3X_2 type superstructures is a first-order phase transformation.

Among the three M_3X_2 superstructures being discussed, the orthorhombic (space group $Immm$) M_3X_2 phase exhibits the highest symmetry. It has a point symmetry group mmm (D_{2h}) that includes 8 symmetry elements, $h_1 - h_4$ and $h_{25} - h_{28}$, whereas the point group $m\bar{3}m$ (O_h) of the basic cubic disordered phase includes 48 elements; for this reason, the rotational reduction in symmetry equals 6. The volume of the unit cell of this superstructure is $V = 3a^3_{B1}/2$ (see Table 6); therefore, the translational symmetry reduction is 3/2. The overall symmetry reduction equals $6 \times 3/2 = 9$.

Another orthorhombic (space group $C222_1$) M_3X_2 phase has the point symmetry group 222 (D_2) including 2 symmetry elements, h_1 and h_2. The volume of the unit cell of this superstructure is $V = 12a^3_{B1}$. Accordingly, rotational and translational symmetry reductions equal 24 and 12, while the overall symmetry reduction during the formation of the orthorhombic (space group $C222_1$) M_3X_2 superstructure equals $24 \times 12 = 288$.

The monoclinic [space group $C2$ ($B112$)] M_3X_2 superstructure possesses the point symmetry group 2 ($C2$) that includes two symmetry elements, h_1 and h_4. Therefore, the rotational symmetry reduction during its formation in a nonstoichiometric compound with structure $B1$ equals 24. The reduction in translational symmetry during formation of this superstructure is 9/2, and the overall symmetry reduction reaches $24 \times 9/2 = 108$.

Point symmetry groups of orthorhombic (space group $C222_1$) and monoclinic (space group $C2$ ($B112$)] M_3X_2 superstructures are subgroups of the point symmetry group of the orthorhombic (space group $Immm$) M_3X_2 phase. Thus, the highest-symmetry orthorhombic (space group $Immm$) M_3X_2 superstructure may be a high-temperature phase as compared with orthorhombic (space group $C222_1$) and monoclinic (space group $C2$) M_3X_2 phases. More likely is the order–order orthorhombic (space group $Immm$) M_3X_2 phase → orthorhombic (space group $C222_1$) M_3X_2 phase transition, since it is associated with the maximum overall symmetry reduction equal to 32. In the order–order orthorhombic (space group $Immm$) M_3X_2 phase → monoclinic (space group $C2$) M_3X_2 phase transition, the overall reduction in symmetry is 12, and this transition cannot be excluded. The point symmetry group of the monoclinic (space group

$C2$) M_3X_2 phase is not a subgroup of the point symmetry group of the orthorhombic (space group $C222_1$) M_3X_2 phase; therefore, the orthorhombic (space group $C222_1$) M_3X_2 phase → monoclinic (space group $C2$) M_3X_2 phase transformation is impossible. Moreover, such a transition would be accompanied by a symmetry raising instead of reduction.

The above analysis indicates that a drop in temperature in MX_y type nonstoichiometric compounds with structure $B1$ may cause two alternative phase transformation sequences involving ordered M_3X_2 type phases, namely the cubic (space group $Fm\bar{3}m$) disordered MX_y phase → orthorhombic (space group $C222_1$) ordered M_3X_2 phase transition and the cubic (space group $Fm\bar{3}m$) disordered MX_y phase → orthorhombic (space group $Immm$) ordered M_3X_2 phase → monoclinic (space group $C2$) ordered M_3X_2 phase transition. Both sequences include disorder–order and order–order transformations. The former sequence ending in the formation of an orthorhombic (space group $C222_1$) M_3X_2 superstructure appears more likely, taking into consideration the overall symmetry reduction.

5. M_4X_3 superstructures

5.1 Cubic and tetragonal superstructures of type M_4X_3

Unit cells of cubic (space group $Pm\bar{3}m$) and tetragonal (space group $I4/mmm$) M_4X_3 superstructures are shown in Fig. 10. Translation vectors of the unit cell of the former superstructure coincide with those of the basic crystal lattice with structure $B1$; coordinates of the atoms and vacancies in an ideal cubic M_4X_3 superstructure are presented in Table 8. The cubic (space group $Pm\bar{3}m$) ordered M_4X_3 phase forms via the phase transition channel involving all three rays of the $\{\mathbf{k}_{10}\}$ star (Table 9).

The distribution function describing the cubic M_4X_3 superstructure has the form

$$n(x_{\rm I}, y_{\rm I}, z_{\rm I}) = y - \frac{\eta_{10}}{4}\left(\cos(2\pi x_{\rm I}) + \cos(2\pi y_{\rm I}) + \cos(2\pi z_{\rm I})\right). \tag{18}$$

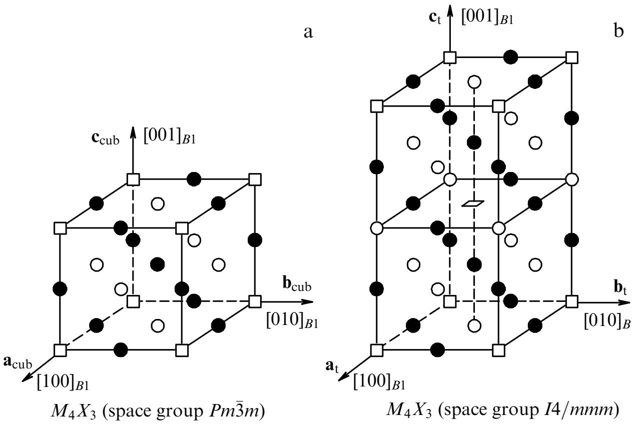

Figure 10. Positions of (a) cubic (space group $Pm\bar{3}m$) and (b) tetragonal (space group $I4/mmm$) unit cells of M_4X_3 type superstructures in a lattice with structure $B1$: (○) interstitial atom, (●) metal atom, and (□) vacancy.

Coordinates $(x_{\rm I}, y_{\rm I}, z_{\rm I})$ of the basic nonmetal fcc sublattice coincide with the coordinates of the cubic M_4X_3 superstructure. Distribution function (18) at sites located in different positions of the nonmetal sublattice takes the following values: $n_1 = y - 3\eta_{10}/4$, and $n_2 = y + \eta_{10}/4$ (see Table 8). Parameters γ_{10} and $\varphi_{10}^{(j)}$ of function (18) are given in Table 9. For the completely ordered M_4X_3 phase, the relative stoichiometric concentration of interstitial atoms $y_{\rm st}$ is equal to 3/4. The same function describes the cubic (space group $Pm\bar{3}m$) substitution A_3B superstructure (of the $\rm Cu_3Au$ type).

The unit cell of a tetragonal (space group $I4/mmm$) M_4X_3 superstructure is depicted in Fig. 10b. Translation vectors of these cell and coordinates of the atoms and vacancies are presented in Table 8. The disorder–order $MX_y - M_4X_3$ (space group $I4/mmm$) transition channel includes one ray of the $\{\mathbf{k}_{10}\}$ star and two rays of the $\{\mathbf{k}_8\}$ star (see Table 9).

The tetragonal interstitial M_4X_3 structure is described by the distribution function that depends on two long-range order parameters, η_{10} and η_8:

$$n(x_{\rm I}, y_{\rm I}, z_{\rm I}) = y - \frac{\eta_{10}}{4}\cos(2\pi z_{\rm I}) - \frac{\eta_8}{2}\cos\left[\pi(2x_{\rm I} + z_{\rm I})\right]. \tag{19}$$

Table 8. Superstructures of type M_4X_3.

Symmetry	Space group	Translation vectors of unit cell	V*	Atom	Position and multiplicity	Atomic coordinates in ideal ordered structure			Values of distribution function $n(x_{\rm I}, y_{\rm I}, z_{\rm I})$
						$x/a_{\rm cub}$	$y/b_{\rm cub}$	$z/c_{\rm cub}$	
Cubic	No. 221 $Pm\bar{3}m$ (O_h^1)	$\mathbf{a}_{\rm cub} = \langle 100\rangle_{B1}$, $\mathbf{b}_{\rm cub} = \langle 010\rangle_{B1}$, $\mathbf{c}_{\rm cub} = \langle 001\rangle_{B1}$	a_{B1}^3	$X1$ (vacancy)	1(a)	0	0	0	$n_1 = y - 3\eta_{10}/4$
				$X2$	3(c)	1/2	0	1/2	$n_2 = y + \eta_{10}/4$
				$M1$	1(b)	1/2	1/2	1/2	
				$M2$	3(d)	0	1/2	0	
						$x/a_{\rm t}$	$y/b_{\rm t}$	$z/c_{\rm t}$	
Tetragonal	No. 139 $I4/mmm$ (D_{4h}^{17})	$\mathbf{a}_{\rm t} = \langle 100\rangle_{B1}$, $\mathbf{b}_{\rm t} = \langle 010\rangle_{B1}$, $\mathbf{c}_{\rm t} = \langle 002\rangle_{B1}$	$2a_{B1}^3$	$X1$ (vacancy)	2(a)	0	0	0	$n_1 = y - \eta_{10}/4 - \eta_8/2$
				$X2$	2(b)	0	0	1/2	$n_2 = y - \eta_{10}/4 + \eta_8/2$
				$X3$	4(d)	0	1/2	1/4	$n_3 = y + \eta_{10}/4$
				$M1$	4(c)	0	1/2	0	
				$M2$	4(c)	0	0	1/4	

* The volume of the unit cell of a superstructure expressed through parameter a_{B1} of the unit cell of the basic disordered $B1$ type structure.

Table 9. The channels of disorder–order $MX_y - M_4X_3$ phase transitions and the parameters of distribution functions $n(x_{\mathrm{I}}, y_{\mathrm{I}}, z_{\mathrm{I}})$ describing M_4X_3 superstructures.

Symmetry	Space group	Disorder–order transition channel		Parameters of the distribution function	
		$\{\mathbf{k}_s\}$ star	$\mathbf{k}_s^{(j)}$ rays of the $\{\mathbf{k}_s\}$ star	γ_s	$\varphi_s^{(j)}$
Cubic	No. 221	$\{\mathbf{k}_{10}\}$	$\mathbf{k}_{10}^{(1)} = (\mathbf{b}_1 + \mathbf{b}_2)/2$,	$\gamma_{10} = 1/4$	$\varphi_{10}^{(1)} = \pi$
	$Pm\bar{3}m$	$\{\mathbf{k}_{10}\}$	$\mathbf{k}_{10}^{(2)} = (\mathbf{b}_1 + \mathbf{b}_3)/2$,	$\gamma_{10} = 1/4$	$\varphi_{10}^{(2)} = \pi$
	(O_h^1)	$\{\mathbf{k}_{10}\}$	$\mathbf{k}_{10}^{(3)} = (\mathbf{b}_2 + \mathbf{b}_3)/2$,	$\gamma_{10} = 1/4$	$\varphi_{10}^{(3)} = \pi$
Tetragonal	No. 139	$\{\mathbf{k}_{10}\}$	$\mathbf{k}_{10}^{(1)} = (\mathbf{b}_1 + \mathbf{b}_2)/2$,	$\gamma_{10} = 1/4$	$\varphi_{10}^{(1)} = \pi$
	$I4/mmm$	$\{\mathbf{k}_8\}$	$\mathbf{k}_8^{(1)} = (\mathbf{b}_1 + 3\mathbf{b}_2 + 2\mathbf{b}_3)/4$,	$\gamma_8 = 1/4$	$\varphi_8^{(1)} = \pi$
	(D_{4h}^{17})	$\{\mathbf{k}_8\}$	$\mathbf{k}_8^{(2)} = -\mathbf{k}_8^{(1)}$,	$\gamma_8 = 1/4$	$\varphi_8^{(2)} = -\pi$

In accordance with Fig. 10b, coordinates $(x_{\mathrm{I}}, y_{\mathrm{I}}, z_{\mathrm{I}})$ are related by expressions $x_{\mathrm{I}} = x_{\mathrm{t}}$, $y_{\mathrm{I}} = y_{\mathrm{t}}$, and $z_{\mathrm{I}} = z_{\mathrm{t}}/2$ to the coordinates of this superstructure, listed in Table 8. Distribution function (19) takes three values at the sites pertaining to different positions of the nonmetal fcc sublattice (see Table 8). For the totally ordered M_4X_3 phase, the relative stoichiometric concentration of interstitial atoms is $y_{\mathrm{st}} = 3/4$.

Distribution function (19) also describes the tetragonal (space group $I4/mmm$) substitution A_3B superstructure characteristic of, e.g., $\mathrm{Al_3Ti}$ and $\mathrm{Ni_3V}$.

Superstructures of type M_4X_3 in nonstoichiometric MX_y compounds with the $B1$ structure have never been observed in experiment. Thermodynamic calculations by the order parameter functional method [1–6, 53] have given evidence that type M_4X_3 superstructures do not form in nonstoichiometric MX_y compounds with the $B1$ structure.

The cubic (space group $Pm\bar{3}m$) M_4X_3 superstructure possesses a higher symmetry than the tetragonal (space group $I4/mmm$) M_4X_3 superstructure. It follows, thus, from the symmetry analysis that the cubic (space group $Fm\bar{3}m$) disordered MX_y phase → cubic (space group $Pm\bar{3}m$) ordered M_4X_3 phase → tetragonal (space group $I4/mmm$) ordered M_4X_3 phase transition is formally possible as temperature decreases. The phase transformation sequence remains physically valid, despite the lack of an ordered phase in experiment.

5.2 Ordering in the trigonal ζ-$\mathrm{Ta_4C_{3-x}}$ phase

The high nonstoichiometry of the nonmetal sublattice is characteristic not only of cubic and tetragonal carbides but also of trigonal ζ-$M_4\mathrm{C}_{3-x}$ ($M_4\mathrm{C}_{3-x}\square_{1+x}$, $0.20 < x < 0.56$) vanadium, niobium, and tantalum carbides. The large concentration of structural vacancies $\square$ in the carbon sublattice of nonstoichiometric trigonal ζ-$M_4\mathrm{C}_{3-x}$ phases amounting to tens of at.% is a prerequisite for their atomic-vacancy ordering.

The first investigations into the ordering in nonstoichiometric ζ-$M_4\mathrm{C}_{3-x}$ phases were carried out using the ζ-phase of tantalum carbide [54–56].

In Refs [57–59], formation of ζ-$\mathrm{Ta_4C_{3-x}}$ was erroneously interpreted as ordering involving cubic carbide TaC_y. However, this transformation is not a disorder–order transition between the disordered cubic TaC_y carbide and trigonal ζ-$\mathrm{Ta_4C_{3-x}}$ carbide, because cubic symmetry of the basic metal fcc sublattice of disordered TaC_y carbide is not preserved in ζ-$\mathrm{Ta_4C_{3-x}}$.

Disordered ζ-$M_4\mathrm{C}_{3-x}$ (M = V, Nb, Ta) carbide phases have a trigonal (space group $R\bar{3}m$) structure in which 12 metal atoms twice occupy $6(c)$ positions, while sites of the nonmetal sublattice are located in $3(a)$, $3(b)$, and $6(c)$ positions having coordinates (000), (00 1/2), and (00 ∼ 5/12), respectively (from here on, atomic coordinates and parameters of unit cells of the ζ-phases are expressed in hexagonal axes).

In ζ-$M_4\mathrm{C}_{3-x}\square_{1+x}$ phases, even at $x = 0$, a quarter of all positions of the nonmetal sublattice are vacant. Carbon atoms fill all $6(c)$ positions, while the remaining C atoms and structural vacancies occupy $3(a)$ and $3(b)$ positions. The location of C atoms and $\square$ vacancies in $3(a)$ and $3(b)$ positions may become statistic or ordered. For statistical distribution, C atoms equiprobably, $(1-x)/2$, occupy $3(a)$ and $3(b)$ positions in the nonmetal sublattice. An ordered distribution is possible in two variants. In one of them, the atoms occupy $3(a)$ positions with a probability of $(1-x)$, while $3(b)$ positions are vacant. During such ordering, new crystallographic positions do not appear, and the lattice retains its trigonal symmetry. An X-ray and neutronographic experiments [54–56] confirmed the validity of this variant. According to these studies, the other variant with C atoms and vacancies occupying $3(b)$ and $3(a)$ positions, respectively, with probability $(1-x)$, does not agree with available experiments.

The unit cell of a disordered trigonal ζ-$\mathrm{Ta_4C_{3-x}}$ phase shown in Fig. 11a in hexagonal axes contains three $\mathrm{Ta_4C_{3-x}}$ formula units. In disordered ζ-$\mathrm{Ta_4C_{3-x}}$ carbide, C atoms and $\square$ vacancies statistically, with the same probability $(1-x)/2$, occupy $3(a)$ and $3(b)$ positions in the nonmetal sublattice. The unit cell of an ordered trigonal ζ-phase of tantalum carbide also contains three $\mathrm{Ta_4C_{3-x}}$ formula units. Coordinates of the atoms and vacancies in this cell are presented in Table 10. The composition of an ideal ζ-phase corresponds to $\sim \mathrm{TaC_{0.67}}$ ($\mathrm{TaC_{2/3}}$) or $\mathrm{Ta_4C_{3-x}}$ with $x = 1/3$. Tantalum atoms occupying $6(c)$ positions with coordinates (00 ∼ 1/8) in the planes normal to the c-axis of the unit cell are displaced toward carbon sublattice planes formed by the sites at $3(b)$ positions and away from carbon sublattice planes formed by $3(a)$ sites (Fig. 11b). The presence of such displacements indirectly suggests different populations of $3(a)$ and $3(b)$ positions by C atoms, i.e., their possible ordering.

The ζ-$\mathrm{Ta_4C_{3-x}}$ phase has a close-packed metal sublattice transitional between hexagonal close-packed (HCP) and fcc metal sublattices of hexagonal and cubic $\mathrm{Ta_2C}$ and TaC_y carbides.

Taking account of the ordered distribution of C atoms and $\square$ vacancies over $3(a)$ and $3(b)$ positions, the structural formula of the ζ-phase can be represented as $\mathrm{Ta_4C_2C_{1-x}}\square_{1+x}$. If the distribution of carbon atoms and vacancies between $3(a)$ and $3(b)$ positions is described by the long-range order

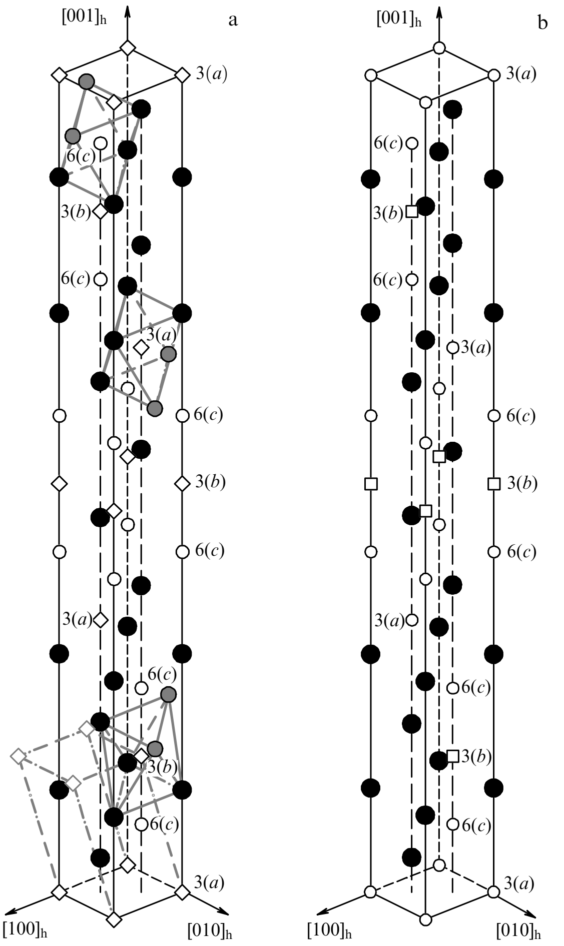

Figure 11. Arrangement of atoms in the unit cell of disordered (a) and ordered (b) trigonal (space group $R\bar{3}m$) ζ-Ta_4C_{3-x} phases (the cell is shown in hexagonal axes): (●) Ta atoms, (◉) Ta atoms outside the cell, (○) C atoms, (□) structural vacancies, (◇) $3(a)$ and $3(b)$ positions of the nonmetal sublattice of the disordered phase statistically, with probability $(1-x)/2$, occupied by C atoms and vacancies. (a) Dashed-dotted lines show the primitive cell of the disordered ζ-Ta_4C_{3-x} phase formed by $3(a)$ and $3(b)$ sites, and also $3(a)$, $3(b)$, and $6(c)$ positions of the nonmetal sublattice octahedrally surrounded by tantalum atoms. (b) Ordered distribution of C atoms over $3(a)$ positions and structural vacancies □ over $3(b)$ positions.

parameter η, ideal ordering with the long-range order parameter $\eta_{max} = 1$ is achieved at $x = 0$, when all $3(a)$ positions are occupied by C atoms and $3(b)$ positions are vacant. If x increases, i.e., with a rise in vacancy concentration, parameter η_{max} decreases, since vacancies appear in $3(a)$ positions. The dependence of the maximum value of the long-range order parameter on the ζ-phase composition has the form $\eta_{max}(x) = 1 - x$. In the disordered ζ-phase, $3(1-x)$ carbon atoms equiprobably occupy $3(a)$ and $3(b)$ positions; therefore, the relative concentration of carbon atoms involved in the ordering process amounts to $(1-x)/2$. Then, the function describing the distribution of C atoms over $3(a)$ and $3(b)$ sites in a nonmetal sublattice of the trigonal ζ-phase can be represented as

$$n(\mathbf{r}) = \frac{1-x}{2} + \frac{\eta}{2}\cos(6\pi z_h)\,, \qquad (20)$$

where $\mathbf{r} = (x_h, y_h, z_h)$ is the site of the nonmetal sublattice occupying either the $3(a)$ or $3(b)$ position. Distribution function (20) defines the probability of detecting carbon atoms at $\mathbf{r}$ sites relevant to the $3(a)$ and $3(b)$ positions in the nonmetal sublattice of the ζ-Ta_4C_{3-x} phase. With a maximum long-range order parameter, $\eta_{max}(x) = 1 - x$, function (20) at all $3(a)$ sites assumes the value of $(1-x)$ but vanishes into $3(b)$ sites. In other words, the probability of detecting C atoms at $3(a)$ and $3(b)$ sites at the maximum long-range order parameter is $(1-x)$ and 0, respectively. For lack of ordering, when $\eta = 0$, the distribution function $n(\mathbf{r}) = (1-x)/2$ at all $3(a)$ and $3(b)$ sites of the nonmetal sublattice. The values of function (20) at the sites of the nonmetal sublattice of the ζ-Ta_4C_{3-x} phase are given in Table 10.

Table 10. Trigonal [space group No. 166 — $R\bar{3}m$ (D^5_{3d})] ζ-$Ta_4C_{3-x} \equiv Ta_4C_2C_{1-x}\square_{1+x}$ carbide: $Z = 3$, $a_h = b_h = 0.3123$, and $c_h = 3.0053$ nm.

Atom	Position and multiplicity	Atomic coordinates in hexagonal axes			Values of distribution function $n(x_h, y_h, z_h)$
		x/a_h	y/b_h	z/c_h	
C1*	$3(a)^*$	0	0	0	$n_2 = (1-x)/2 + \eta/2$
C2 (vacancy)	$3(b)$	0	0	0.5	$n_1 = (1-x)/2 - \eta/2$
C3	$6(c)$	0	0	0.4170	
Ta1	$6(c)$	0	0	0.1274	
Ta2	$6(c)$	0	0	0.2910	

* Carbon C atoms occupy all 3(a) positions in ζ-Ta_4C_{3-x} carbide at $x = 0$ and the maximum long-range order parameter; for $x > 0$ and the maximum long-range order parameter, C atoms occupy only part of the $3(a)$ positions, while their remaining part is vacant; $3(b)$ positions are always vacant regardless of composition and order parameter; $6(c)$ positions of nonmetal lattice are always filled with carbon atoms.

6. M_6X_5 superstructures

The literature contains a wealth of data on carbide superstructures M_6C_5 ($M_6C_5\square$) for which $t = 3$. Experiments have demonstrated the formation of M_6C_5 superstructures differing in symmetry and distribution of C atoms and □ vacancies over the lattice sites in strongly nonstoichiometric cubic (space group $Fm\bar{3}m$) MC_y carbides of group V transition metals (M = V, Nb, Ta) with a relative carbon content of $0.79 \leqslant y \leqslant 0.88$ at temperatures below 1300 K. Trigonal (space group $P3_1$ or $P3_112$) and monoclinic (space group $C2/m$, $C2$ or $C2/c$) M_6C_5 superstructures have been proposed in the literature for ordered nonstoichiometric vanadium and niobium carbides. The formation of an incommensurate M_6C_5-like ordered phase was observed in nonstoichiometric tantalum carbide TaC_y [60–62].

The sequence of phase transformations accompanying the formation of M_6C_5 superstructures in nonstoichiometric MC_y carbides was discussed in Ref. [63]. However, reports published after 2008 propose updated structures with new space groups for ordered M_6X_5 (M_6C_5) phases. These data were summarized by the authors of Ref. [64], who revised the transformation sequence during the formation of M_6X_5 type superstructures in nonstoichiometric MX_y compounds with the $B1$ structure. The discussion below takes account of the new information on superstructures of type M_6X_5.

6.1 Trigonal M_6X_5 superstructure

The formation of an axial trigonal ordered V_6C_5 phase has been established by the electron diffraction method, electron microscopy, and NMR method [65–67]. In terms of symme-

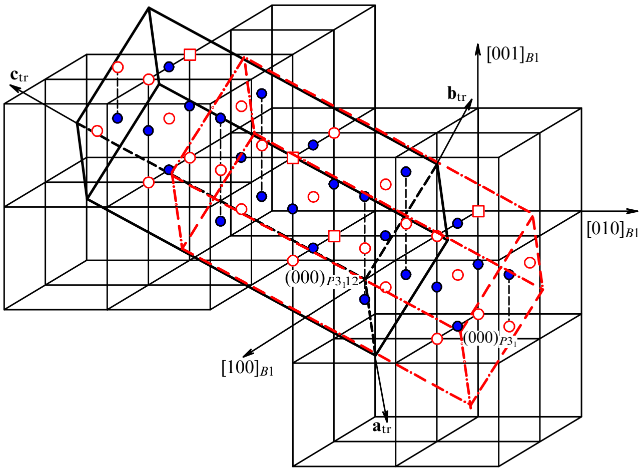

M_6X_5 (M_6X_5□) (space group $P3_112$ and $P3_1$)

Figure 12. Position of trigonal (space group $P3_112$ and $P3_1$) unit cells of M_6X_5 ($M_6\mathrm{C}_5$) superstructure in a lattice with the basic structure $B1$. The contours of the unit cells are shown by solid and dashed-dotted lines, respectively. The origin of coordinates $(000)_{P3_112}$ of the trigonal (space group $P3_112$) unit cell has cubic coordinates $(2/3\ \bar{5}/6\ \bar{1}/2)_{B1}$, and the origin of coordinates $(000)_{B1}$ of the trigonal (space group $P3_1$) unit cell has cubic coordinates $(0\ \bar{1}/6\ \bar{7}/6)_{B1}$. (●) metal atom, (○) interstitial atom X (C), and (□) vacancy.

try, this superstructure belongs to the space group $P3_1$ or enantiomorphic space group $P3_2$. The authors of Refs [68, 69] used structural neutronography to elucidate the structure of the trigonal $\mathrm{V_6C_5}$ phase and showed that it has the space group $P3_112$. Later on, the authors of Ref. [70] reconsidered the experimental data [65] on the crystalline structure of ordered nonstoichiometric vanadium carbide and demonstrated that the trigonal $\mathrm{V_6C_5}$ superstructure possesses the space group $P3_112$ rather than $P3_1$.

Trigonal (space groups $P3_112$ and $P3_1$) unit cells of M_6X_5 ($M_6\mathrm{C}_5$) superstructure are demonstrated in Fig. 12. Coordinates of the atoms and vacancies in ideal trigonal (space groups $P3_112$ and $P3_1$) M_6X_5 superstructures are presented in Table 11. Both unit cells have identical translation vectors (see Table 11). The unit cell of the M_6X_5 superstructure with the space group $P3_112$ is displaced one third of the $\mathbf{c}_{\rm tr}$-axis length from the trigonal (space group $P3_1$) cell, i.e., by vector $\mathbf{c}_{\rm tr}/3 = (2/3)\langle 1\bar{1}1\rangle_{B1}$.

Trigonal (space groups $P3_112$ and $P3_1$) M_6X_5 ($M_6\mathrm{C}_5$) superstructures are formed via the phase transition channel involving 13 $\mathbf{k}_s^{(j)}$ rays of the three $\{\mathbf{k}_9\}$, $\{\mathbf{k}_4\}$, and $\{\mathbf{k}_3\}$ stars (Table 12).

The identical disorder–order transition channel corresponding to trigonal (space groups $P3_112$ and $P3_1$) M_6X_5 superstructures suggests that they are described by one and the same distribution function depending on three long-range order parameters: η_9, η_4, and η_3, corresponding to $\{\mathbf{k}_9\}$, $\{\mathbf{k}_4\}$, and $\{\mathbf{k}_3\}$ stars:

$$
\begin{aligned}
n(x_{\rm I}, y_{\rm I}, z_{\rm I}) &= y - \frac{\eta_9}{6}\cos\left[\pi(x_{\rm I} - y_{\rm I} + z_{\rm I})\right] \\
&- \frac{\eta_4}{6}\left\{\cos\left[\frac{4\pi(x_{\rm I} + y_{\rm I})}{3}\right] - \frac{\sqrt{3}}{3}\sin\left[\frac{4\pi(x_{\rm I} + y_{\rm I})}{3}\right]\right. \\
&- \frac{2\sqrt{3}}{3}\sin\left[\frac{4\pi(x_{\rm I} - z_{\rm I})}{3}\right] + \cos\left[\frac{4\pi(y_{\rm I} + z_{\rm I})}{3}\right] \\
&\left. + \frac{\sqrt{3}}{3}\sin\left[\frac{4\pi(y_{\rm I} + z_{\rm I})}{3}\right]\right\} - \frac{\eta_3}{6}\left\{\cos\left[\frac{\pi(x_{\rm I} - 5y_{\rm I} - 3z_{\rm I})}{3}\right]\right. \\
&- \frac{\sqrt{3}}{3}\sin\left[\frac{\pi(x_{\rm I} - 5y_{\rm I} - 3z_{\rm I})}{3}\right] \\
&+ \frac{2\sqrt{3}}{3}\sin\left[\frac{\pi(5x_{\rm I} + 3y_{\rm I} + z_{\rm I})}{3}\right] + \cos\left[\frac{\pi(3x_{\rm I} + y_{\rm I} - 5z_{\rm I})}{3}\right] \\
&\left. + \frac{\sqrt{3}}{3}\sin\left[\frac{\pi(3x_{\rm I} + y_{\rm I} - 5z_{\rm I})}{3}\right]\right\}. \qquad (21)
\end{aligned}
$$

Referring to Fig. 12, coordinates $(x_{\rm I}, y_{\rm I}, z_{\rm I}$ are related to the coordinates of the trigonal (space group $P3_112$) M_6X_5

Table 11. Trigonal [space group No. 151 — $P3_112$ (D_3^3) and No. 144 — $P3_1$ (C_3^2)] M_6X_5 ($M_6\mathrm{C}_5$) type superstructures: $Z = 3$, $V = 9a_{B1}^3/2$, and $\mathbf{a}_{\rm tr} = (1/2)\langle 21\bar{1}\rangle_{B1}$, $\mathbf{b}_{\rm tr} = (1/2)\langle \bar{1}12\rangle_{B1}$, $\mathbf{c}_{\rm tr} = 2\langle 1\bar{1}1\rangle_{B1}$.

Atom	Space group $P3_112$				Space group $P3_1$				Values of distribution function $n(x_{\rm I}, y_{\rm I}, z_{\rm I})$
	Position and multiplicity	Atomic coordinates in ideal ordered structure			Position and multiplicity	Atomic coordinates in ideal ordered structure			
		$x/a_{\rm tr}$	$y/b_{\rm tr}$	$z/c_{\rm tr}$		$x/a_{\rm tr}$	$y/b_{\rm tr}$	$z/c_{\rm tr}$	
$X1$ (vacancy)	$3(b)$	1/9	2/9	1/6	$3(a)$	1/9	2/9	1/2	$n_1 = y - \eta_9/6 - \eta_4/3 - \eta_3/3$
$X2$	$3(b)$	4/9	8/9	1/6	$3(a)$	4/9	8/9	1/2	$n_3 = y - \eta_9/6 + \eta_4/6 + \eta_3/6$
$X3$	$3(b)$	7/9	5/9	1/6	$3(a)$	7/9	5/9	1/2	$n_3 = y - \eta_9/6 + \eta_4/6 + \eta_3/6$
$X4$	$3(a)$	1/9	8/9	1/3	$3(a)$	1/9	8/9	2/3	$n_2 = y + \eta_9/6 - \eta_4/3 + \eta_3/3$
$X5$	$3(a)$	4/9	5/9	1/3	$3(a)$	4/9	5/9	2/3	$n_4 = y + \eta_9/6 + \eta_4/6 - \eta_3/6$
$X6$	$3(a)$	7/9	2/9	1/3	$3(a)$	7/9	2/9	2/3	$n_4 = y + \eta_9/6 + \eta_4/6 - \eta_3/6$
$M1$	$6(c)$	4/9	5/9	1/12	$3(a)$	4/9	5/9	5/12	
		4/9	5/9	7/12	$3(a)$	4/9	5/9	11/12	
$M2$	$6(c)$	1/9	8/9	1/12	$3(a)$	1/9	8/9	5/12	
		1/9	8/9	7/12	$3(a)$	1/9	8/9	11/12	
$M3$	$6(c)$	7/9	2/9	1/12	$3(a)$	7/9	2/9	5/12	
		7/9	2/9	7/12	$3(a)$	7/9	2/9	11/12	

Table 12. Disorder–order $MX_y - M_6X_5$ phase transition channels and parameters of the distribution functions $n(x_{\rm I}, y_{\rm I}, z_{\rm I})$ describing M_6X_5 (M_6C$_5$) superstructures.

Symmetry	Space group	Disorder–order transition channel		Parameters of distribution functions	
		$\{\mathbf{k}_s\}$ star	$\mathbf{k}_s^{(j)}$ rays of the $\{\mathbf{k}_s\}$ star	γ_s	$\varphi_s^{(j)}$
Trigonal	No 151	$\{\mathbf{k}_9\}$	$\mathbf{k}_9^{(3)} = \mathbf{b}_2/2$,	$\gamma_9 = 1/6$	$\varphi_9^{(3)} = \pi$
	$P3_112$	$\{\mathbf{k}_4\}$	$\mathbf{k}_4^{(1)} = (\mathbf{b}_1 + \mathbf{b}_2 + 2\mathbf{b}_3)/3$,	$\gamma_4 = \sqrt{3}/18$	$\varphi_4^{(1)} = 7\pi/6$
	(D_3^3)	$\{\mathbf{k}_4\}$	$\mathbf{k}_4^{(2)} = -\mathbf{k}_4^{(1)}$,	$\gamma_4 = \sqrt{3}/18$	$\varphi_4^{(2)} = -7\pi/6$
	or	$\{\mathbf{k}_4\}$	$\mathbf{k}_4^{(7)} = (\mathbf{b}_3 - \mathbf{b}_1)/3$,	$\gamma_4 = \sqrt{3}/18$	$\varphi_4^{(7)} = 3\pi/2$
	No. 144	$\{\mathbf{k}_4\}$	$\mathbf{k}_4^{(8)} = -\mathbf{k}_4^{(7)}$,	$\gamma_4 = \sqrt{3}/18$	$\varphi_4^{(8)} = -3\pi/2$
	$P3_1$	$\{\mathbf{k}_4\}$	$\mathbf{k}_4^{(9)} = (2\mathbf{b}_1 + \mathbf{b}_2 + \mathbf{b}_3)/3$,	$\gamma_4 = \sqrt{3}/18$	$\varphi_4^{(9)} = 5\pi/6$
	(C_3^2)	$\{\mathbf{k}_4\}$	$\mathbf{k}_4^{(10)} = -\mathbf{k}_4^{(9)}$,	$\gamma_4 = \sqrt{3}/18$	$\varphi_4^{(10)} = -5\pi/6$
		$\{\mathbf{k}_3\}$	$\mathbf{k}_3^{(3)} = -(4\mathbf{b}_1 + \mathbf{b}_2 + 2\mathbf{b}_3)/3$,	$\gamma_3 = \sqrt{3}/18$	$\varphi_3^{(3)} = 7\pi/6$
		$\{\mathbf{k}_3\}$	$\mathbf{k}_3^{(4)} = -\mathbf{k}_3^{(3)}$,	$\gamma_3 = \sqrt{3}/18$	$\varphi_3^{(4)} = -7\pi/6$
		$\{\mathbf{k}_3\}$	$\mathbf{k}_3^{(9)} = (2\mathbf{b}_1 + 3\mathbf{b}_2 + 4\mathbf{b}_3)/6$,	$\gamma_3 = \sqrt{3}/18$	$\varphi_3^{(9)} = \pi/2$
		$\{\mathbf{k}_3\}$	$\mathbf{k}_3^{(10)} = -\mathbf{k}_3^{(9)}$,	$\gamma_3 = \sqrt{3}/18$	$\varphi_3^{(10)} = -\pi/2$
		$\{\mathbf{k}_3\}$	$\mathbf{k}_3^{(23)} = (2\mathbf{b}_1 + \mathbf{b}_2 - 2\mathbf{b}_3)/6$,	$\gamma_3 = \sqrt{3}/18$	$\varphi_3^{(23)} = -5\pi/6$
		$\{\mathbf{k}_3\}$	$\mathbf{k}_3^{(24)} = -\mathbf{k}_3^{(23)}$	$\gamma_3 = \sqrt{3}/18$	$\varphi_3^{(24)} = 5\pi/6$
Monoclinic	No. 15	$\{\mathbf{k}_9\}$	$\mathbf{k}_9^{(3)} = \mathbf{b}_2/2$,	$\gamma_9 = 1/6$	$\varphi_9^{(3)} = \pi$
	$C2/c$	$\{\mathbf{k}_4\}$	$\mathbf{k}_4^{(1)} = (\mathbf{b}_1 + \mathbf{b}_2 + 2\mathbf{b}_3)/3$,	$\gamma_4 = 1/12$	$\varphi_4^{(1)} = 4\pi/3$
	$(C12/c1)$	$\{\mathbf{k}_4\}$	$\mathbf{k}_4^{(2)} = -\mathbf{k}_4^{(1)}$,	$\gamma_4 = 1/12$	$\varphi_4^{(2)} = -4\pi/3$
	(C_{2h}^6)	$\{\mathbf{k}_3\}$	$\mathbf{k}_3^{(3)} = -(4\mathbf{b}_1 + \mathbf{b}_2 + 2\mathbf{b}_3)/3$,	$\gamma_3 = 1/12$	$\varphi_3^{(3)} = 4\pi/3$
	or	$\{\mathbf{k}_3\}$	$\mathbf{k}_3^{(4)} = -\mathbf{k}_3^{(3)}$,	$\gamma_3 = 1/12$	$\varphi_3^{(4)} = -4\pi/3$
	No. 5	$\{\mathbf{k}_0\}$	$\mathbf{k}_0^{(4)} = (4\mathbf{b}_1 + \mathbf{b}_2 - 4\mathbf{b}_3)/12$,	$\gamma_0 = \sqrt{3}/12$	$\varphi_0^{(4)} = -7\pi/6$
	$C2$ $(C121)$	$\{\mathbf{k}_0\}$	$\mathbf{k}_0^{(28)} = -\mathbf{k}_0^{(4)}$,	$\gamma_0 = \sqrt{3}/12$	$\varphi_0^{(28)} = 7\pi/6$
	(C_2^3)	$\{\mathbf{k}_0\}$	$\mathbf{k}_0^{(13)} = -(8\mathbf{b}_1 + 5\mathbf{b}_2 + 4\mathbf{b}_3)/12$,	$\gamma_0 = \sqrt{3}/12$	$\varphi_0^{(13)} = -7\pi/6$
		$\{\mathbf{k}_0\}$	$\mathbf{k}_0^{(37)} = -\mathbf{k}_0^{(13)}$	$\gamma_0 = \sqrt{3}/12$	$\varphi_3^{(37)} = 7\pi/6$
Monoclinic	No. 12	$\{\mathbf{k}_9\}$	$\mathbf{k}_9^{(3)} = \mathbf{b}_2/2$,	$\gamma_9 = 1/6$	$\varphi_9^{(3)} = \pi$
	$C2/m$	$\{\mathbf{k}_4\}$	$\mathbf{k}_4^{(1)} = (\mathbf{b}_1 + \mathbf{b}_2 + 2\mathbf{b}_3)/3$,	$\gamma_4 = 1/6$	$\varphi_4^{(1)} = \pi$
	$(C12/m1)$	$\{\mathbf{k}_4\}$	$\mathbf{k}_4^{(2)} = -\mathbf{k}_4^{(1)}$,	$\gamma_4 = 1/6$	$\varphi_4^{(2)} = -\pi$
	(C_{2h}^3)	$\{\mathbf{k}_3\}$	$\mathbf{k}_3^{(3)} = -(4\mathbf{b}_1 + \mathbf{b}_2 + 2\mathbf{b}_3)/3$,	$\gamma_3 = 1/6$	$\varphi_3^{(3)} = \pi$
		$\{\mathbf{k}_3\}$	$\mathbf{k}_3^{(4)} = -\mathbf{k}_3^{(3)}$	$\gamma_3 = 1/6$	$\varphi_3^{(4)} = -\pi$

superstructure, listed in Table 11, by the following expressions: $x_{\rm I} = x_{\rm tr} - y_{\rm tr}/2 + 2z_{\rm tr} + 2/3$, $y_{\rm I} = x_{\rm tr}/2 + y_{\rm tr}/2 - 2z_{\rm tr} - 5/6$, and $z_{\rm I} = -x_{\rm tr}/2 + y_{\rm tr} + 2z_{\rm tr} - 1/2$. Parameters γ_s and $\varphi_s^{(j)}$ of function (21) are presented in Table 12. Distribution function (21) describing trigonal M_6X_5 (M_6C$_5$) superstructures takes four values: n_1, n_2, n_3, and n_4 at the sites of the basic nonmetal fcc sublattice (see Table 11), meaning that the nonmetal sublattice of the disordered nonstoichiometric MX_y (MC$_y$) compound splits into four nonequivalent sublattices in the ordering being considered. For ideal M_6X_5 (M_6C$_5$) superstructures, quantity y in distribution function (21), i.e., the relative concentration of interstitial X atoms, equals $5/6$.

The identity of the phase transition channel and the distribution function means that for the trigonal M_6X_5 phase only one of the two trigonal structural models is valid. Given that the usual requirements for a unit cell are fulfilled (correspondence to crystal symmetry, maximum number of right angles and minimum volume), its choice in one and the same lattice is controversial and possible in a variety of ways [71]. This explains why one and the same crystal is described differently in experimental studies. As a matter of fact, the requirements for the choice of a unit cell are reduced to a single condition: it must possess the highest possible symmetry. Given an equal volume of cells, this means that the point symmetry group of the selected unit cell must include the maximum number of symmetry elements (operations).

The point symmetry group 322 (D_3) of a trigonal (space group $P3_112$) M_6X_5 superstructure comprises 6 symmetry elements: h_1, h_5, h_9, h_{13}, h_{17}, and h_{21}, and the point symmetry group 3 (C_3) of a trigonal (space group $P3_1$) M_6C$_5$ superstructure has three elements: h_1, h_5, and h_9 [1, 2, 31]. This means that the trigonal (space group $P3_112$) structural model of the M_6X_5 phase possesses a higher symmetry than the trigonal model of the M_6X_5 phase with space group $P3_1$. In other words, the former model more adequately describes the crystalline structure of the ordered M_6X_5 ($M_6X_5\square$) phase than the latter one. Thus, the trigonal (space group $P3_112$) M_6X_5 (M_6C$_5$) superstructures observed in experiments [65–67, 72, 73] and described later in reviews [1–6, 26] actually belong to the space group $P3_112$.

6.2 Monoclinic M_6X_5 superstructure: $C2/c$ or $C2$ space group?

A solid boron solution in fcc palladium, PdB$_y$, was recently investigated in Refs [74, 75] by structural neutronography, X-ray, and electron diffraction techniques. The disordered solid PdB$_y$ solution has a basic cubic structure $B1$. The authors of Refs [74, 75] took advantage of the analogy with

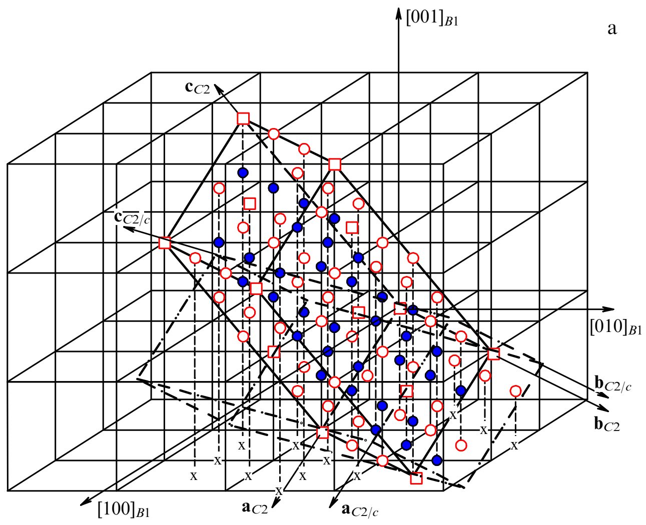

M_6X_5 (M_6X_5□) (space group $C2$)

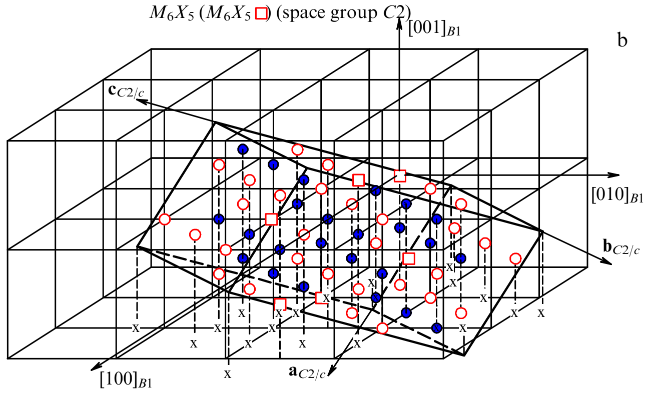

M_6X_5 (M_6X_5□) (space group $C2/c$)

Figure 13. Position of monoclinic unit cells of the M_6X_5 (M_6C_5) superstructure in a lattice with the basic structure $B1$: (a) the cell with space group $C2$, and (b) the cell with space group $C2/c$. Dashed-dotted lines in figure (a) additionally show the contour of the monoclinic cell with space group $C2/c$. The origin of coordinates $(000)_{C2/c}$ of the monoclinic (space group $C2/c$) unit cell has cubic coordinates $(\bar{1}/2\ 1/4\ \bar{1}/4)_{B1}$, i.e., it is displaced by vector $(1/4)\langle\bar{2}1\bar{1}\rangle_{B1}$ with respect to the origin of coordinates $(000)_{B1} \equiv (000)_{C2}$ of the monoclinic (space group $C2$) unit cell. Vertical dashed lines show projections (×) of atoms, vacancies, and vertices of unit cells onto the plane $(x\,y\,0)_{B1}$. (●) metal atom, (○) interstitial atom X (C), and (□) vacancy.

ordered nonstoichiometric M_6C_5 carbides [1, 2, 26, 34] and arrived at a conclusion about the formation of a monoclinic [space group $C2/c$ ($C12/c1$)] Pd_6B (M_6X) superstructure. The monoclinic (space group $C2/c$) Pd_6B superstructure corresponds to the inverse M_6X_5 superstructure with the same space group. In the present case, by inversion is meant the inversion of populations of octahedral interstices (a vacant interstice is replaced by the one occupied by a nonmetal interstitial atom and vice versa).

The disorder–order transition channel for the inverse monoclinic (space group $C2/c$) M_6X_5 (M_6C_5) superstructure was studied in Refs [76, 77]. It turned out to be identical with the disorder–order transition channel via which the monoclinic M_6C_5 superstructure with a space group $C2$ forms. Let us clarify if there is a physical difference between monoclinic M_6X_5 (M_6C_5) superstructures with space groups $C2/c$ and $C2$.

Figure 13a shows the position of the unit cell of the monoclinic (space group $C2$) M_6X_5 superstructure and the contour of the unit cell of the monoclinic (space group $C2/c$) M_6X_5 phase. Figure 13b illustrates the arrangement of atoms and vacancies in the unit cell of the monoclinic (space group $C2/c$) M_6X_5 (M_6X_5□) phase. Referring to Fig. 13, the origin of coordinates $(000)_{C2/c}$ of this superstructure has cubic coordinates $(\bar{1}/2\ 1/4\ \bar{1}/4)_{B1}$, i.e., it is displaced by vector $(1/4)\langle\bar{2}1\bar{1}\rangle_{B1}$ with respect to the origin of coordinates $(000)_{B1} \equiv (000)_{C2}$ of the monoclinic (space group $C2$) unit cell of the M_6X_5 (M_6C_5) superstructure. Coordinates of atoms and vacancies in ideal monoclinic (space groups $C2/c$ and $C2$) M_6X_5 (M_6X_5□) superstructures and translation vectors of unit cells are presented in Table 13. The unit cells of monoclinic superstructures comprise four M_6X_5 formula units and have equal volumes $V = 6a^3_{B1}$.

Figure 13 demonstrates that translation vectors of the unit cell of the monoclinic (space group $C2/c$) M_6X_5 phase have the same length and direction as those of the monoclinic (space group $C2$) M_6X_5 phase or are their linear combinations: $\mathbf{a}_{C2/c} = \mathbf{a}_{C2}$, $\mathbf{b}_{C2/c} = \mathbf{b}_{C2}$, and $\mathbf{c}_{C2/c} = \mathbf{a}_{C2} + \mathbf{c}_{C2}$, the volumes of both unit cells being equal. Due to the invariance of determinants in formula (1) with respect to addition and subtraction of the rows, the superstructure vectors of the reciprocal lattice of the monoclinic (space group $C2/c$) M_6X_5 phase also coincide or are combinations of the vectors of the reciprocal lattice of the monoclinic (space group $C2$) M_6X_5 phase: $\mathbf{a}^*_{C2/c} = \mathbf{a}^*_{C2} - \mathbf{c}^*_{C2} = (1/4)\langle 1\bar{1}\bar{3}\rangle$, $\mathbf{b}^*_{C2/c} = \mathbf{b}^*_{C2} = (1/3)\langle\bar{1}\bar{1}0\rangle$, and $\mathbf{c}^*_{C2/c} = \mathbf{c}^*_{C2} = (1/4)\langle 1\bar{1}1\rangle$. Monoclinic (space groups $C2/c$ and $C2$) M_6C_5 phases are formed via the same disorder–order transition channel involving 9 vectors belonging to the Lifshitz star $\{\mathbf{k}_9\}$, non-Lifshitz stars $\{\mathbf{k}_4\}$, $\{\mathbf{k}_3\}$, and non-Lifshitz star $\{\mathbf{k}_0\}$ with 48 rays (see Table 12).

Taking account of this channel, the distribution function of interstitial atoms X (C) in monoclinic (space groups $C2/c$ and $C2$) M_6X_5 (M_6C_5) superstructures depends on four long-range order parameters, η_9, η_4, η_3, and η_0, corresponding to stars $\{\mathbf{k}_9\}$, $\{\mathbf{k}_4\}$, $\{\mathbf{k}_3\}$, and $\{\mathbf{k}_0\}$, and has the form

$$\begin{aligned} n(x_{\mathrm{I}}, y_{\mathrm{I}}, z_{\mathrm{I}}) &= y - \frac{\eta_9}{6}\cos\left[\pi(x_{\mathrm{I}} - y_{\mathrm{I}} + z_{\mathrm{I}})\right] \\ &- \frac{\eta_4}{12}\left\{\cos\left[\frac{4\pi(x_{\mathrm{I}} + y_{\mathrm{I}})}{3}\right] - \sqrt{3}\sin\left[\frac{4\pi(x_{\mathrm{I}} + y_{\mathrm{I}})}{3}\right]\right\} \\ &- \frac{\eta_3}{12}\left\{\cos\left[\frac{\pi(x_{\mathrm{I}} - 5y_{\mathrm{I}} - 3z_{\mathrm{I}})}{3}\right] - \sqrt{3}\sin\left[\frac{\pi(x_{\mathrm{I}} - 5y_{\mathrm{I}} - 3z_{\mathrm{I}})}{3}\right]\right\} \\ &- \frac{\eta_0}{12}\left\{3\cos\left[\frac{\pi(x_{\mathrm{I}} + 7y_{\mathrm{I}} + 9z_{\mathrm{I}})}{6}\right] - \sqrt{3}\sin\left[\frac{\pi(x_{\mathrm{I}} + 7y_{\mathrm{I}} + 9z_{\mathrm{I}})}{6}\right]\right. \\ &\left. + 3\cos\left[\frac{\pi(7x_{\mathrm{I}} + y_{\mathrm{I}} - 9z_{\mathrm{I}})}{6}\right] - \sqrt{3}\sin\left[\frac{\pi(7x_{\mathrm{I}} + y_{\mathrm{I}} - 9z_{\mathrm{I}})}{6}\right]\right\}. \end{aligned} \tag{22}$$

Referring to Fig. 13, coordinates $(x_{\mathrm{I}}, y_{\mathrm{I}}, z_{\mathrm{I}})$ of the disordered cubic $B1$ structure are related to the coordinates of the monoclinic (space group $C2/c$) M_6X_5 superstructure (see Table 13) by the expressions $x_{\mathrm{I}} = x_{\mathrm{m}}/2 + 3y_{\mathrm{m}}/2 + 3z_{\mathrm{m}}/2 - 1/2$, $y_{\mathrm{I}} = -x_{\mathrm{m}}/2 + 3y_{\mathrm{m}}/2 - 3z_{\mathrm{m}}/2 + 1/4$, and $z_{\mathrm{I}} = -x_{\mathrm{m}} + z_{\mathrm{m}} - 1/4$. Distribution function (22) describing monoclinic (space groups $C2/c$ and $C2$) M_6X_5 (M_6C_5) superstructures at all sites of the basic nonmetal fcc sublattice takes 5 different values, n_1, n_2, n_3, n_4, and n_5 (see Table 13). The similarity of distribution functions means that only one of the two monoclinic (space groups $C2/c$ and $C2$) structural models holds for the M_6X_5 phase. Since the volumes of the unit cells are equal, the higher symmetry cell should be chosen here.

Table 13. Monoclinic superstructures of type M_6X_5 (M_6C$_5$) [space group No. 15 — $C2/c$ ($C12/c1$) (C_{2h}^6) and No. 5 — $C2$ ($C121$) (C_2^3)]: $Z = 4$, $V = 6a_{B1}^3$; $\mathbf{a}_{C2/c} = (1/2)\langle 1\bar{1}\bar{2}\rangle_{B1}$, $\mathbf{b}_{C2/c} = (1/2)\langle 330\rangle_{B1}$, $\mathbf{c}_{C2/c} = (1/2)\langle 3\bar{3}2\rangle_{B1}$; $\mathbf{a}_{C2} = (1/2)\langle 1\bar{1}\bar{2}\rangle_{B1}$, $\mathbf{b}_{C2} = (1/2)\langle 330\rangle_{B1}$, $\mathbf{c}_{C2} = \langle 1\bar{1}2\rangle_{B1}$.

Atom	Space group $C2/c$				Space group $C2$				Values of distribution function $n(x_\mathrm{I}, y_\mathrm{I}, z_\mathrm{I})$
	Position and multiplicity	Atomic coordinates in ideal ordered structure			Position and multiplicity	Atomic coordinates in ideal ordered structure			
		x/a_tr	y/b_tr	z/c_tr		x/a_tr	y/b_tr	z/c_tr	
$X1$ (vacancy)	4(e)	0	1/12	1/4	2(a)	0	0	0	$n_1 = y - \eta_9/6 - \eta_4/12 - \eta_3/12 - \eta_0/2$
		1/2	5/12	3/4	2(b)	2(b)	1/3	1/2	$n_1 = y - \eta_9/6 - \eta_4/12 - \eta_3/12 - \eta_0/2$
$X2$	4(e)	0	5/12	1/4	2(a)	0	1/3	0	$n_5 = y - \eta_9/6 - \eta_4/12 - \eta_3/12 + \eta_0/2$
		0	7/12	3/4	2(b)	1/2	1/2	1/2	$n_5 = y - \eta_9/6 - \eta_4/12 - \eta_3/12 + \eta_0/2$
$X3$	4(e)	0	3/4	1/4	2(a)	0	2/3	0	$n_3 = y - \eta_9/6 + \eta_4/6 + \eta_3/6$
		0	1/4	3/4	2(b)	1/2	1/6	1/2	$n_3 = y - \eta_9/6 + \eta_4/6 + \eta_3/6$
$X4$	4(c)	1/4	3/4	1/2	4(c)	1/2	2/3	1/4	$n_4 = y + \eta_9/6 + \eta_4/6 - \eta_3/6$
$X5$	8(f)	1/4	5/12	1/2	4(c)	1/2	1/3	1/4	$n_2 = y + \eta_9/6 - \eta_4/12 + \eta_3/12$
		1/4	1/12	1/2	4(c)	1/2	0	1/4	$n_2 = y + \eta_9/6 - \eta_4/12 + \eta_3/12$
$M1$	8(f)	1/8	1/4	3/8	4(c)	1/4	1/6	1/8	
		1/8	3/4	7/8	4(c)	3/4	2/3	5/8	
$M2$	8(f)	5/8	5/12	3/8	4(c)	3/4	1/3	1/8	
		3/8	7/12	5/8	4(c)	3/4	1/2	3/8	
$M3$	8(f)	1/8	7/12	3/8	4(c)	1/4	1/2	1/8	
		5/8	1/12	3/8	4(c)	3/4	0	1/8	

Table 14. Monoclinic [space group No. 12 — $C2/m$ ($C12/m1$) (C_{2h}^3)] M_6X_5 superstructures: $Z = 2$, $V = 3a_{B1}^3$, $\mathbf{a}_{C2/m} = (1/2)\langle 1\bar{1}\bar{2}\rangle_{B1}$, $\mathbf{b}_{C2/m} = (1/2)\langle 330\rangle_{B1}$, and $\mathbf{c}_{C2/m} = (1/2)\langle 1\bar{1}2\rangle_{B1}$.

Atom	Position and multiplicity	Atomic coordinates in ideal ordered structure			Values of distribution function $n(x_\mathrm{I}, y_\mathrm{I}, z_\mathrm{I})$
		$x/a_\mathrm{C2/m}$	$y/b_\mathrm{C2/m}$	$z/c_\mathrm{C2/m}$	
$X1$ (vacancy)	2(a)	0	0	0	$n_1 = y - \eta_9/6 - \eta_4/3 - \eta_3/3$
$X2$	2(d)	0	1/2	1/2	$n_2 = y + \eta_9/6 - \eta_4/3 + \eta_3/3$
$X3$	4(g)	0	1/3	0	$n_3 = y - \eta_9/6 + \eta_4/6 + \eta_3/6$
$X4$	4(h)	0	1/6	1/2	$n_4 = y + \eta_9/6 + \eta_4/6 - \eta_3/6$
$M1$	4(i)	1/4	0	3/4	
$M2$	8(j)	1/4	2/3	3/4	

The point symmetry group $2/m$ (C_{2h}) of the monoclinic (space group $C2/c$) M_6X_5 (M_6C$_5$) phase includes 4 symmetry elements (rotations h_1, h_4, h_{25}, and h_{28}), whereas group 2 ($C2$) of the monoclinic (space group $C2$) M_6X_5 (M_6C$_5$) phase comprises only two symmetry elements, h_1 and h_4. Therefore, it is inferior to the monoclinic (space group $C2/c$) structural model of the M_6X_5 phase in terms of symmetry. Thus, the monoclinic (space group $C2/c$) model more adequately describes the crystalline structure of the ordered M_6X_5 ($M_6X_5\square$) phase than the model with a space group $C2$. To sum up, the monoclinic (space group $C2$) M_6X_5 (M_6C$_5$) superstructures observed in experiments [78–81] and also described in reviews [1–6, 26] actually belong to the space group $C2/c$.

6.3 Monoclinic (space group $C2/m$) M_6X_5 superstructure

The unit cell of the monoclinic (space group $C2/m$) M_6X_5 (M_6C$_5$) superstructure includes two M_6X_5 formula units (Fig. 14). Translation vectors of the unit cell and coordinates of atoms and vacancies are given in Table 14. The disorder–

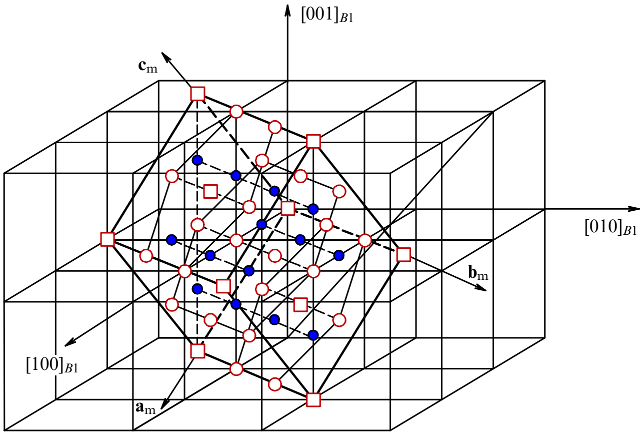

M_6X_5 ($M_6X_5\square$) (space group $C2/m$)

Figure 14. Position of the monoclinic (space group $C2/m$) unit cell of M_6X_5 (M_6C$_5$) superstructure in a lattice with the basic structure $B1$. (●) metal atom, (○) interstitial atom X (C), and (□) vacancy.

order transition channel associated with the formation of the monoclinic (space group $C2/m$) M_6X_5 (M_6C_5) superstructure involves five nonequivalent superstructure vectors of three stars, $\{\mathbf{k}_9\}$, $\{\mathbf{k}_4\}$, and $\{\mathbf{k}_3\}$ (see Table 12). Taking this into account, the distribution function of carbon atoms in monoclinic (space group $C2/m$) M_6X_5 (M_6C_5) superstructures depends on three long-range order parameters, η_9, η_4, and η_3:

$$n(x_{\rm I}, y_{\rm I}, z_{\rm I}) = y - \frac{\eta_9}{6}\cos\left[\pi(x_{\rm I} - y_{\rm I} + z_{\rm I})\right] - \frac{\eta_4}{3}\cos\left[\frac{4\pi(x_{\rm I} + y_{\rm I})}{3}\right] - \frac{\eta_3}{3}\cos\left[\frac{\pi(x_{\rm I} - 5y_{\rm I} - 3z_{\rm I})}{3}\right]. \quad (23)$$

In accordance with Fig. 14, coordinates $(x_{\rm I}, y_{\rm I}, z_{\rm I})$ of the basic disordered $B1$ structure are related to the coordinates of the monoclinic (space group $C2/m$) M_6X_5 superstructure by the expressions $x_{\rm I} = x_{\rm m}/2 + 3y_{\rm m}/2 + z_{\rm m}/2$, $y_{\rm I} = -x_{\rm m}/2 + 3y_{\rm m}/2 - z_{\rm m}/2$, and $z_{\rm I} = -x_{\rm m} + z_{\rm m}$. The distribution function (23) at all sites of the basic nonmetal fcc sublattice takes the same 4 values (see Table 14) as distribution function (21) describing the trigonal M_6X_5 superstructure (see Table 11). However, the relative positions of the sites of four sublattices in the monoclinic (space group $C2/m$) ordered superstructure differ from those in the trigonal (space group $P3_112$) M_6X_5 superstructure. The long-range order in the distribution of carbon atoms and vacancies in the monoclinic (space group $C2/m$) M_6X_5 superstructure under consideration is also different from that in the monoclinic (space group $C2/c$) M_6X_5 superstructure.

The monoclinic (space group $C2/m$) superstructure of type M_6X_5 (M_6C_5) was observed in experiments with nonstoichiometric niobium carbide NbC_y [32, 33, 82–86]. According to paper [73], solidification of vanadium-rich Fe alloys is accompanied by dispersed precipitation of the ordered $\mathrm{V_6C_5}$ phase that also has the monoclinic (space group $C2/m$) structure.

6.4 Sequence of M_6X_5 superstructure formation

The above symmetry analysis of M_6X_5 (M_6C_5) superstructures gives evidence that the ordering of nonstoichiometric MX_y ($M\mathrm{C}_y$) compounds with $y \approx 5/6$ results in formation of one trigonal (space group No. 151 — $P3_112$) and two monoclinic (space groups No. 12 — $C2/m$ and No. 15 — $C2/c$) M_6X_5 (M_6C_5) phases. The ordering of X atoms and $\square$ structural vacancies occurs in the basic nonmetal fcc sublattice of the disordered cubic (space group $Fm\bar{3}m$) MX_y phase and is associated with the splitting of high-symmetry $4(b)$ positions into two or more positions of the low-symmetry ordered phase. The disordered cubic (space group $Fm\bar{3}m$) MX_y phase has a point symmetry group $m\bar{3}m$ (O_h) that includes 48 symmetry elements, $h_1 - h_{48}$ [1, 2, 30, 31].

Point symmetry groups of trigonal (space group $P3_112$), monoclinic (space group $C2/c$), and monoclinic (space group $C2/m$) M_6X_5 (M_6C_5) superstructures include six (h_1, h_5, h_9, h_{13}, h_{17}, h_{21}), four (h_1, h_4, h_{25}, h_{28}), and again four (h_1, h_4, h_{25}, h_{28}) symmetry elements, respectively. They are subgroups of the point symmetry group of the basic disordered cubic (space group $Fm\bar{3}m$) MX_y ($M\mathrm{C}_y$) phase; therefore, the transition from the disordered MX_y ($M\mathrm{C}_y$) compound to any of these superstructures represents a disorder–order phase transformation. The formation of these M_6X_5 superstructures proceeds with a symmetry distortion over three or four irreducible representations, meaning that $MX_y \to M_6X_5$ phase transitions do not satisfy the Landau group-theoretical criterion for second-order phase transitions: they are realized through a first-order transition mechanism.

The point symmetry group 322 (D_3) of the trigonal (space group $P3_112$) M_6X_5 superstructure includes 6 symmetry elements: h_1, h_5, h_9, h_{13}, h_{17}, and h_{21}, while the point symmetry group $m\bar{3}m$ (O_h) of the basic cubic disordered $M\mathrm{C}_y$ phase contains 48 elements, $h_1 - h_{48}$; therefore, the rotational symmetry reduction equals 8. The reduction in translational symmetry upon the transition from the high-symmetry disordered MX_y ($M\mathrm{C}_y$) phase to a low-symmetry trigonal M_6X_5 (M_6C_5) superstructure equals 4.5. The overall symmetry reduction is the product of rotational and translational reductions. Therefore, the overall symmetry reduction in the disordered nonstoichiometric cubic (space group $Fm\bar{3}m$) MX_y phase → ordered trigonal (space group $P3_112$) M_6X_5 phase transition amounts to $N = 36$. The point symmetry group $2/m$ (C_{2h}) of monoclinic (space group $C2/m$ and $C2/c$) ordered M_6X_5 phases involves 4 symmetry elements, h_1, h_4, h_{25}, and h_{28}; hence, the rotational symmetry reduction in the disorder–order transition reaches 12. The reduction in translational symmetry during the transition from the disordered MX_y phase to the monoclinic (space group $C2/m$) M_6X_5 superstructure would run to 3 and equals 6 in the transition to the monoclinic M_6X_5 phase with a space group $C2/c$. The overall symmetry reduction in disorder–order MX_y (space group $Fm\bar{3}m$) → M_6X_5 (space group $C2/m$) and MX_y (space group $Fm\bar{3}m$) → M_6X_5 (space group $C2/c$) transitions amounts to 36 and 72, respectively.

As far as transitions between individual M_6X_5 (M_6C_5) superstructures are concerned, it is clear from the relationship between symmetry elements h_i that a trigonal superstructure is unrelated to monoclinic M_6X_5 superstructures in terms of symmetry, because its point group is neither a group nor a subgroup of the point groups of monoclinic superstructures. Therefore, the transition between the trigonal and any of the two monoclinic M_6X_5 phases cannot be an order–order transition but is possible as a polymorphic transformation.

The order–order phase transformation is only possible for monoclinic (space groups $C2/m$ and $C2/c$) M_6X_5 superstructures. Since the point symmetry groups of these superstructures are identical, a transition between them does not affect rotational symmetry. A reduction in translational symmetry in an order–order transition equals the ratio between unit cell volumes of low- and high-symmetry ordered phases or the ratio between site numbers in the unit cells of these phases. For the monoclinic (space groups $C2/m$ and $C2/c$) M_6X_5 (M_6C_5) superstructures under consideration, the reduction in translational symmetry equaling 2 will occur during the order–order M_6X_5 (space group $C2/m$) → M_6X_5 (space group $C2/c$) transition. Therefore, the order–order monoclinic (space group $C2/m$) M_6X_5 phase → monoclinic (space group $C2/c$) M_6X_5 phase transformation occurs with a two-fold overall symmetry reduction.

Thus, a decrease in temperature is accompanied by two transition sequences involving M_6X_5 (M_6C_5) phases (Fig. 15). The first one covers a cubic (space group $Fm\bar{3}m$) disordered MX_y phase → monoclinic (space group $C2/m$) ordered M_6X_5 phase → monoclinic (space group $C2/c$) ordered M_6X_5 phase transformations, including only disorder–order and order–order transitions with symmetry reduction by a factor of 36 and 2, respectively. The alternative sequence embraces a cubic (space group $Fm\bar{3}m$) disordered MX_y phase → trigonal (space group $P3_112$) ordered M_6X_5 phase → monoclinic (space

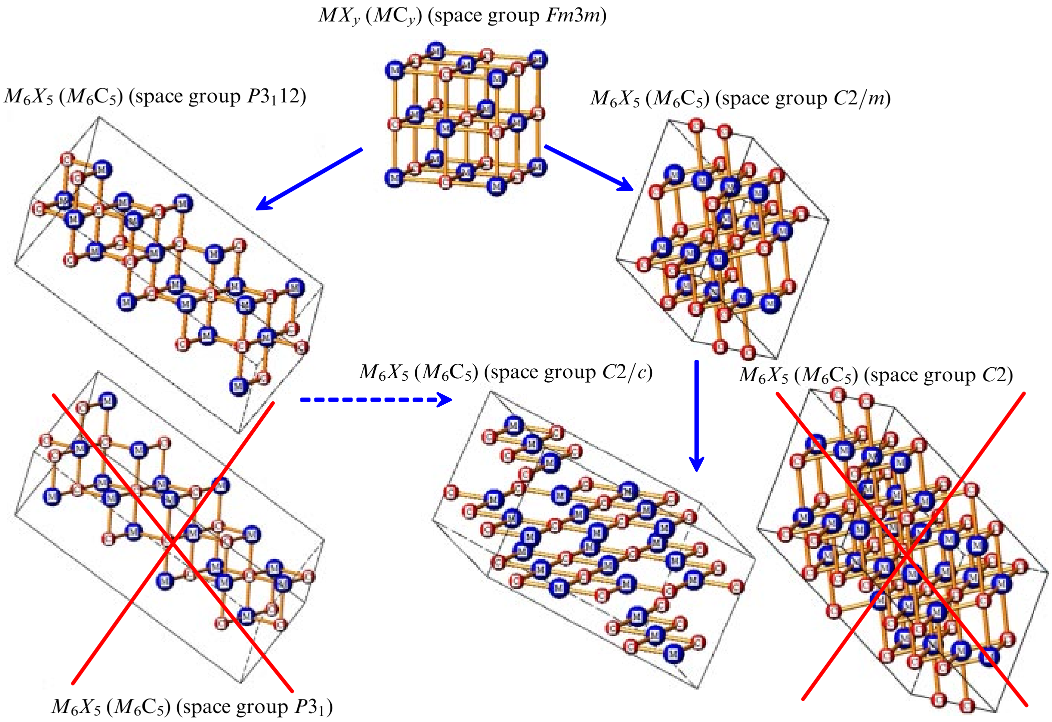

Figure 15. (Color online.) Physically admissible sequences of disorder–order and order–order phase transformations proceeding with a decrease in temperature and producing superstructures of type M_6X_5 (M_6C_5) in strongly nonstoichiometric MX_y (MC_y) compounds with the basic $B1$ structure. The topmost unit cell of the nonstoichiometric MX_y (MC_y) compound has a basic cubic (space group $Fm\bar{3}m$) structure; the sites of the nonmetal sublattice in this cell are statistically occupied by X (C) atoms with probability y. According to verified data, M_6X_5 (M_6C_5) superstructures belong to the space groups $P3_112$ and $C2/c$ (space groups $P3_1$ and $C2$ were identified incorrectly). Of the two possible sequences, the cubic (space group $Fm\bar{3}m$) disordered MX_y (MC_y) phase → monoclinic (space group $C2/m$) ordered M_6X_5 phase → monoclinic (space group $C2/c$) ordered M_6X_5 phase transformation is most likely to occur. The vacant sites of the nonmetal sublattice of M_6X_5 (M_6C_5) superstructures are not shown.

group $C2/c$) M_6X_5 phase transformations, including disorder–order transitions with symmetry reduction by a factor of 36 and polymorphic transformation of the trigonal phase into the monoclinic one. Experimental data suggest a higher probability of the former sequence.

7. M_8X_7 cubic superstructures

Unit cells of cubic (space groups $Fm\bar{3}m$ and $P4_332$) superstructures of type M_8X_7 have similar translation vectors but differ in the relative positions of occupied and vacant sites in M_8X_7 phases (Fig. 16). Translation vectors of unit cells and the coordinates of atoms and vacancies in these phases are presented in Table 15.

The phase transition channel associated with the formation of a cubic (space group $Fm\bar{3}m$) M_8X_7 superstructure includes all rays of $\{\mathbf{k}_{10}\}$ and $\{\mathbf{k}_9\}$ stars (Table 16). The distribution function of interstitial atoms in the cubic (space group $Fm\bar{3}m$) M_8X_7 phase has the form

$$n(x_\mathrm{I}, y_\mathrm{I}, z_\mathrm{I}) = y - \frac{\eta_{10}}{8}\left[\cos(2\pi x_\mathrm{I}) + \cos(2\pi y_\mathrm{I}) + \cos(2\pi z_\mathrm{I})\right]$$
$$- \frac{\eta_9}{8}\Big\{\cos\left[\pi(x_\mathrm{I} + y_\mathrm{I} + z_\mathrm{I})\right] + \cos\left[\pi(x_\mathrm{I} - y_\mathrm{I} + z_\mathrm{I})\right]$$
$$+ \cos\left[\pi(x_\mathrm{I} + y_\mathrm{I} - z_\mathrm{I})\right] + \cos\left[\pi(-x_\mathrm{I} + y_\mathrm{I} + z_\mathrm{I})\right]\Big\} \qquad (24)$$

and depends on two long-range order parameters, η_{10} and η_9. Referring to Fig. 16a, coordinates $(x_\mathrm{I}, y_\mathrm{I}, z_\mathrm{I})$ of the basic disordered $B1$ structure are related to the coordinates of the cubic (space group $Fm\bar{3}m$) M_8X_7 superstructure given in Table 15 by the expressions $x_\mathrm{I} = 2x_\mathrm{cub}$, $y_\mathrm{I} = 2y_\mathrm{cub}$, and $z_\mathrm{I} = 2z_\mathrm{cub}$. The values of function (24) at sites located in different positions of the nonmetal sublattice are presented in Table 15, and the values of parameters γ_s and $\varphi_s^{(j)}$ of this function in Table 16. The same distribution function (24) describes the cubic (space group $Fm\bar{3}m$) substitution superstructure A_7B (of the Pt$_7$Cu type).

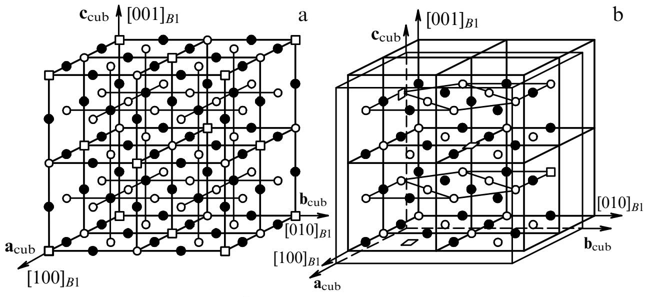

M_8X_7 (space group $Fm\bar{3}m$) M_8X_7 (space group $P4_332$)

Figure 16. Position of cubic (space group $Fm\bar{3}m$) unit cells of M_8X_7 superstructures in a lattice with the basic structure $B1$: (a) space group $Fm\bar{3}m$, and (b) space group $P4_332$ (the origin of coordinates $(000)_{M_8X_7}$ of this superstructure M_8X_7 has coordinates $(-1/4\ -1/4\ -1/4)_{B1}$ of the basic structure of type $B1$). (○) interstitial atom, (●) metal atom, and (□) vacancy.

The cubic (space group $P4_332$) M_8X_7 superstructure forms via the transition channel involving all rays of $\{\mathbf{k}_9\}$, $\{\mathbf{k}_8\}$, and $\{\mathbf{k}_4\}$ stars with $\mu_4 = 1/4$ (see Table 16). The distribution function describing this superstructure depends

Table 15. Cubic superstructures of type M_8X_7.

Symmetry	Space group	Translation vectors of unit cell	V *	Atom	Position and multiplicity	Atomic coordinates in ideal ordered structure			Values of distribution function $n(x_{\rm I}, y_{\rm I}, z_{\rm I})$
						$x/a_{\rm cub}$	$y/b_{\rm cub}$	$z/c_{\rm cub}$	
Cubic	No. 225 $Fm\bar{3}m$ (O_h^5)	$\mathbf{a}_{\rm cub} = \langle 200\rangle_{B1}$, $\mathbf{b}_{\rm cub} = \langle 020\rangle_{B1}$, $\mathbf{c}_{\rm cub} = \langle 002\rangle_{B1}$	$8a_{B1}^3$	$X1$ (vacancy)	$4(a)$	0	0	0	$n_1 = y - 3\eta_{10}/8 - \eta_9/2$
				$X2$	$4(b)$	1/2	1/2	1/2	$n_2 = y - 3\eta_{10}/8 + \eta_9/2$
				$X3$	$24(d)$	0	1/4	1/4	$n_3 = y + \eta_{10}/8$
				$M1$	$8(c)$	1/2	1/4	1/4	
				$M2$	$24(e)$	1/4	0	0	
						$x/a_{\rm cub}$	$y/b_{\rm cub}$	$z/c_{\rm cub}$	
Cubic	No. 212 $P4_332$ (O^6)	$\mathbf{a}_{\rm cub} = \langle 200\rangle_{B1}$, $\mathbf{b}_{\rm cub} = \langle 020\rangle_{B1}$, $\mathbf{c}_{\rm cub} = \langle 002\rangle_{B1}$	$8a_{B1}^3$	$X1$ (vacancy)	$4(b)$	5/8	5/8	5/8	$n_1 = y - \eta_9/8 - 3\eta_8/8 - 3\eta_4/8$
				$X2$	$4(a)$	1/8	1/8	1/8	$n_2 = y + \eta_9/8 + 3\eta_8/8 - 3\eta_4/8$
				$X3$	$12(d)$	1/8	5/8	5/8	$n_3 = y + \eta_9/8 - \eta_8/8 + \eta_4/8$
				$X4$	$12(d)$	1/8	3/8	7/8	$n_4 = y - \eta_9/8 + \eta_8/8 + \eta_4/8$
				$M1$	$8(c)$	3/8	3/8	3/8	
				$M2$	$24(e)$	1/8	3/8	1/8	

* The volume of the unit cell of a superstructure expressed through parameter a_{B1} of the unit cell of the basic disordered $B1$ structure.

Table 16. Disorder–order $MX_y - M_8X_7$ phase transition channels and parameters of the distribution functions describing superstructures of type M_8X_7.

Symmetry	Space group	Disorder–order transition channel		Parameters of distribution functions	
		$\{\mathbf{k}_s\}$ star	$\mathbf{k}_s^{(j)}$ rays of the $\{\mathbf{k}_s\}$ star	γ_s	$\varphi_s^{(j)}$
Cubic	No. 225 $Fm\bar{3}m$ (O_h^5)	$\{\mathbf{k}_{10}\}$	$\mathbf{k}_{10}^{(1)}, \mathbf{k}_{10}^{(2)}, \mathbf{k}_{10}^{(3)}$	$\gamma_{10} = 1/8$	$\varphi_{10}^{(1)} = \varphi_{10}^{(2)} = \varphi_{10}^{(3)} = \pi$
		$\{\mathbf{k}_9\}$	$\mathbf{k}_9^{(1)}, \mathbf{k}_9^{(2)}, \mathbf{k}_9^{(3)}, \mathbf{k}_9^{(4)}$	$\gamma_9 = 1/8$	$\varphi_9^{(1)} = \varphi_9^{(2)} = \varphi_9^{(3)} = \varphi_9^{(4)} = \pi$
Cubic	No. 212 $P4_332$ (O^6)	$\{\mathbf{k}_9\}$	$\mathbf{k}_9^{(1)}, \mathbf{k}_9^{(2)}, \mathbf{k}_9^{(3)}, \mathbf{k}_9^{(4)}$	$\gamma_9 = 1/16$	$\varphi_9^{(1)} = \pi$, $\varphi_9^{(2)} = \varphi_9^{(3)} = \varphi_9^{(4)} = 0$
		$\{\mathbf{k}_8\}$	$\mathbf{k}_8^{(1)}, \mathbf{k}_8^{(3)}, \mathbf{k}_8^{(5)}$	$\gamma_8 = \sqrt{2}/16$	$\varphi_8^{(1)} = \varphi_8^{(3)} = \varphi_8^{(5)} = 5\pi/4$
		$\{\mathbf{k}_8\}$	$\mathbf{k}_8^{(2)}, \mathbf{k}_8^{(4)}, \mathbf{k}_8^{(6)}$	$\gamma_8 = \sqrt{2}/16$	$\varphi_8^{(2)} = \varphi_8^{(4)} = \varphi_8^{(6)} = -5\pi/4$
		$\{\mathbf{k}_4\}$	$\mathbf{k}_4^{(1)}, \mathbf{k}_4^{(5)}, \mathbf{k}_4^{(9)}$	$\gamma_4 = 1/16$	$\varphi_4^{(1)} = \varphi_4^{(5)} = \varphi_4^{(9)} = \pi$
		$\{\mathbf{k}_4\}$	$\mathbf{k}_4^{(2)}, \mathbf{k}_4^{(6)}, \mathbf{k}_4^{(10)}$	$\gamma_4 = 1/16$	$\varphi_4^{(2)} = \varphi_4^{(6)} = \varphi_4^{(10)} = -\pi$
		$\{\mathbf{k}_4\}$	$\mathbf{k}_4^{(3)}, \mathbf{k}_4^{(11)}$	$\gamma_4 = 1/16$	$\varphi_4^{(3)} = \varphi_4^{(11)} = \pi/2$
		$\{\mathbf{k}_4\}$	$\mathbf{k}_4^{(4)}, \mathbf{k}_4^{(12)}$	$\gamma_4 = 1/16$	$\varphi_4^{(4)} = \varphi_4^{(12)} = -\pi/2$
		$\{\mathbf{k}_4\}$	$\mathbf{k}_4^{(7)}, \mathbf{k}_4^{(8)}$	$\gamma_4 = 1/16$	$\varphi_4^{(7)} = 3\pi/2$, $\varphi_4^{(8)} = -3\pi/2$

on three long-range order parameters, η_9, η_8, and η_4:

$$
\begin{aligned}
n(x_{\rm I}, y_{\rm I}, z_{\rm I}) = y - \frac{\eta_9}{16}\Big\{&\cos\big[\pi(x_{\rm I} + y_{\rm I} + z_{\rm I})\big] \\
&- \cos\big[\pi(x_{\rm I} - y_{\rm I} + z_{\rm I})\big] - \cos\big[\pi(x_{\rm I} + y_{\rm I} - z_{\rm I})\big] \\
&- \cos\big[\pi(-x_{\rm I} + y_{\rm I} + z_{\rm I})\big]\Big\} - \frac{\eta_8}{8}\Big\{-\cos\big[\pi(2x_{\rm I} + z_{\rm I})\big] \\
&+ \sin\big[\pi(2x_{\rm I} + z_{\rm I})\big] - \cos\big[\pi(y_{\rm I} + 2z_{\rm I})\big] + \sin\big[\pi(y_{\rm I} + 2z_{\rm I})\big] \\
&- \cos\big[\pi(x_{\rm I} + 2y_{\rm I})\big] + \sin\big[\pi(x_{\rm I} + 2y_{\rm I})\big]\Big\} \\
&- \frac{\eta_4}{8}\Big\{\cos\big[\pi(x_{\rm I} + y_{\rm I})\big] + \cos\big[\pi(x_{\rm I} + z_{\rm I})\big] \\
&+ \cos\big[\pi(y_{\rm I} + z_{\rm I})\big] + \sin\big[\pi(x_{\rm I} - y_{\rm I})\big] \\
&- \sin\big[\pi(x_{\rm I} - z_{\rm I})\big] + \sin\big[\pi(y_{\rm I} - z_{\rm I})\big]\Big\}\,. \qquad (25)
\end{aligned}
$$

The values of parameters γ_s and $\varphi_s^{(j)}$ of function (25) are presented in Table 16. As Fig. 16b shows, coordinates $(x_{\rm I}, y_{\rm I}, z_{\rm I})$ of the basic disordered $B1$ structure are related to the coordinates of the cubic (space group $P4_332$) M_8X_7 superstructure (see Table 15) by expressions $x_{\rm I} = 2x_{\rm cub} - 1/4$, $y_{\rm I} = 2y_{\rm cub} - 1/4$, and $z_{\rm I} = 2z_{\rm cub} - 1/4$. The probabilities of filling sites in these sublattices by interstitial X atoms, i.e., the values of the distribution function (25), are given in Table 15. In such ordering, the nonmetal sublattice of the disordered MX_y compound breaks up into four nonequivalent sublattices.

The cubic (space group $P4_332$) superstructure of type M_8X_7 has been observed experimentally in vanadium carbide VC$_y$ [87–92], and in dispersed vanadium carbide precipitates from Fe–Va alloys [73].

In completely ordered cubic superstructures of type M_8X_7, the relative content of interstitial atoms in the nonmetal sublattice is $y_{\rm st} = 7/8$.

Cubic M_8X_7 superstructures have unit cells of equal volume, $V = 8a_{B1}^3$, but the point symmetry group 432 (O) in M_8X_7 with the space group $P4_332$ contains 24 symmetry elements, $h_1 - h_{24}$, whereas the point symmetry group $m\bar{3}m$ (O_h) of the cubic (space group $Fm\bar{3}m$) M_8X_7 superstructure includes 48 elements, $h_1 - h_{48}$. Evidently, one of these two cubic M_8X_7 superstructures, namely that with the space group $P4_332$, is a low-symmetry and, accordingly, low-temperature structure. The cubic (space group $Fm\bar{3}m$) M_8X_7 superstructure is intermediate between the high-temperature disordered MX_y phase and the M_8X_7 superstructure with space group $P4_332$. The sequence of possible phase transformations that occur as temperature decreases and give rise to M_8X_7 superstructures in MX_y compound with structure $B1$ has the following form: disordered nonstoichiometric cubic (space group $Fm\bar{3}m$) MX_y phase → ordered cubic (space group $Fm\bar{3}m$) M_8X_7 phase → ordered cubic (space group $P4_332$) M_8X_7 phase. In these disorder–order and order–order transitions, the overall symmetry reduction equals 8 and 2, respectively.

8. Superstructures of lower hexagonal M_2C_y carbides

Ordering in lower nonstoichiometric carbides and nitrides $M_2X_{y'} \equiv MX_{y'/2}$ $(0.40 \leqslant y'/2 \leqslant 0.50)$ with the basic hexagonal structure of type $L'3$ is known much less than that in nonstoichiometric MX_y compounds with the basic cubic structure $B1$. Ordering of lower hexagonal nonstoichiometric $M_2X_{y'}$ compounds most frequently gives rise to superstructures of type M_2X with a different symmetry. A detailed description of such superstructures exemplified by lower tungsten carbide W_2C can be found in monograph [93]. In what follows, they are considered as typical M_2X superstructures with a basic hexagonal lattice.

The lower tungsten carbide W_2C_y belong in the group of strongly nonstoichiometric interstitial compounds and has a homogeneity interval extending from $WC_{0.34}$ to $WC_{0.52}$ at ~ 3000 K [94] and narrowing as temperature drops. The literature reports a disordered hexagonal [space group $P6_3/mmc$ (D_{6h}^4)] β-W_2C phase and three ordered phases of lower tungsten carbide W_2C_y, viz. orthorhombic β′-W_2C [space group No. 60 — $Pbcn$ (D_{2h}^{14})] with the ζ-Fe_2N (Mo_2C) structure, rhombohedral β″-W_2C [space group No. 164 — $P\bar{3}m1$ (D_{3d}^3)] with the $C6$ (anti-CdI_2) structure, and trigonal ε-W_2C [space group No. 162 — $P\bar{3}1m$ (D_{3d}^1)] with the ε-Fe_2N structure. In all modifications of W_2C_y carbide, the tungsten atoms make up a close-packed hexagonal metal sublattice in which from 34 to 50% of the interstices can be occupied by carbon atoms. Lower W_2C_y carbide can be either disordered at a high temperature or ordered at a lower temperature, depending on the arrangement of carbon (C) atoms and □ vacancies.

The basic β-W_2C phase has a hexagonal (space group $P6_3/mmc$) $L'3$ structure with a disordered arrangement of C atoms and □ structural vacancies in $2(a)$ positions of the nonmetal sublattice. The unit cell of the β-W_2C phase is depicted in Fig. 17a. The volume $V_{L'3}$ of the unit cell in β-W_2C carbide is $(\sqrt{3}/2)a^2c$. In disordered β-W_2C carbide with the $L'3$ structure, the Ising lattice in which atomic-vacancy ordering may occur is formed by the hexagonal nonmetal sublattice. For the β-W_2C carbide, lattice periods $a_x = a_y = a$, and period a_z of the primitive (as regards the nonmetal sublattice) translation cell in direction [001] is half the period c of the unit cell, i.e., $a_z = c/2$ (Fig. 17a). Structural vectors of the reciprocal lattice for the basic hexagonal lattice are $\mathbf{b}_1 = \langle 100 \rangle$ and $\mathbf{b}_2 = \langle 010 \rangle$ in $4\pi/(a\sqrt{3})$ units, and $\mathbf{b}_3 = \langle 001 \rangle$ in $4\pi/c$ units.

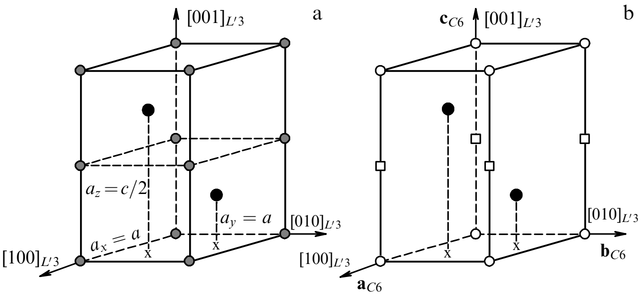

β-W_2C ($L'3$, space group $P6_3/mmc$) β″-W_2C ($C6$, space group $P\bar{3}m1$)

Figure 17. Unit cell of the basic disordered hexagonal (space group $P6_3/mmc$) β-W_2C phase with $L'3$ type structure (a) and position of the unit cell of the rhombohedral (space group $P\bar{3}m1$) ordered β″-W_2C phase of type $C6$ (b) in the basic lattice with $L'3$ structure. Periods of the unit cell of the disordered β-W_2C phase equal a in directions $[100]_{L'3}$ and $[010]_{L'3}$; the period in the $[001]_{L'3}$ direction is c. The primitive (as regards nonmetal sublattice) unit cell of the β-W_2C phase is shown by dashed lines; its periods a_x and a_y coincide with the respective periods of the unit cell of the β-W_2C phase, and period a_z of the primitive cell in direction $[001]_{L'3}$ is half the period c of the unit cell of the disordered β-W_2C phase, i.e., $a_z = c/2$. (●) tungsten (W) atoms, (◉) sites of the nonmetal sublattice of the disordered β-W_2C phase statistically (with probability 1/2) occupied by carbon (C) atoms, (○) carbon (C) atoms, and (□) vacant sites of nonmetal sublattice.

8.1 Rhombohedral β″-W_2C superstructure

The unit cell of a rhombohedral (space group $P\bar{3}m1$) ordered β″-W_2C phase with the $C6$ type structure is shown in Fig. 17b. Translation vectors of this unit cell coincide with translation vectors of the unit cell of the disordered hexagonal phase and equal $\mathbf{a}_{C6} = [100]_{L'3}$, $\mathbf{b}_{C6} = [010]_{L'3}$, and $\mathbf{c}_{C6} = [001]_{L'3}$. Due to this, the volume of the unit cell of the rhombohedral phase, $V_{C6} = (\sqrt{3}/2)a^2c$, coincides with that of the unit cell of the disordered β-W_2C carbide. Coordinates of the atoms and vacancies in an ideal rhombohedral (space group $P\bar{3}m1$) β″-W_2C phase are presented in Table 17. It is clear from a comparison of the disordered β-W_2C carbide and the rhombohedral β″-W_2C phase (see Fig. 17) that rhombohedral ordering results in splitting $2(a)$ positions statistically half-filled with C atoms into positions $1(a)$ and $(1b)$, one of which is occupied by carbon atom, while the other is vacant.

The β″-W_2C superstructure forms via the disorder–order transition channel involving $\mathbf{k}_{17}^{(1)} = \mathbf{b}_3/2$ ray of the $\{\mathbf{k}_{17}\}$ star of the hexagonal lattice (the numbering and description of $\{\mathbf{k}_s\}$ stars of the wave vectors of the hexagonal lattice and their $\mathbf{k}_s^{(j)}$ rays are in accordance with monographs [30, 31]). Notice that vector $\mathbf{k}_{17}^{(1)} = \mathbf{b}_3/2 = (0\,0\,1/2)$ in $4\pi/c$ units or (001) in $2\pi/c$ units. Accordingly, the distribution function of carbon atoms at $\mathbf{r}$ sites of the nonmetal sublattice in the ordered rhombohedral β″-W_2C (WC_y) phase depends on a single long-range order parameter η_{17} and has the form

$$n(x_{\mathrm{I}}, y_{\mathrm{I}}, z_{\mathrm{I}}) = y + \frac{\eta_{17}}{2} \cos(2\pi z_{\mathrm{I}}) , \tag{26}$$

where $y \leqslant 0.5$ is the relative carbon concentration in β″-W_2C (WC_y) carbide, and $x_{\mathrm{I}}, y_{\mathrm{I}}, z_{\mathrm{I}}$ are the coordinates of $\mathbf{r}$ sites in the nonmetal sublattice of the basic disordered hexagonal phase. Referring to Fig. 17b, coordinates $(x_{\mathrm{I}}, y_{\mathrm{I}}, z_{\mathrm{I}})$ of the disordered hexagonal $L'3$ structure are related by simple

Table 17. M_2X type superstructures of lower hexagonal tungsten carbide W_2C.

Symmetry	Space group	Translation vectors of unit cell	V *	Atom	Position and multiplicity	Atomic coordinates in ideal ordered structure			Values of distribution function $n(x_I, y_I, z_I)$
						x/a_{C6}	y/b_{C6}	z/c_{C6}	
Rhombohedral	No. 164 $P\bar{3}m1$ (D^3_{3d})	$\mathbf{a}_{C6} = \langle 100 \rangle_{L'3}$, $\mathbf{b}_{C6} = \langle 010 \rangle_{L'3}$, $\mathbf{c}_{C6} = \langle 001 \rangle_{L'3}$	$V_{L'3}$	C1 (vacancy)	$1(b)$	0	0	1/2	$n_1 = y - \eta_{17}/2$
				C2	$1(a)$	0	0	0	$n_2 = y + \eta_{17}/2$
				$M1$ (W1)	$2(d)$	1/3	2/3	1/4	
						x/a_ε	y/b_ε	z/c_ε	
Trigonal	No. 162 $P\bar{3}1m$ (D^1_{3d})	$\mathbf{a}_\varepsilon = \langle 1\bar{1}0 \rangle_{L'3}$, $\mathbf{b}_\varepsilon = \langle 120 \rangle_{L'3}$, $\mathbf{c}_\varepsilon = \langle 001 \rangle_{L'3}$	$3V_{L'3}$	C1 (vacancy)	$1(b)$	0	0	1/2	$n_1 = y + \eta_{17}/6 - 2\eta_{15}/3$
				C2 (vacancy)	$2(c)$	1/3	2/3	0	$n_2 = y - \eta_{17}/6 - \eta_{15}/3$
				C3	$1(a)$	0	0	0	$n_3 = y - \eta_{17}/6 + 2\eta_{15}/3$
				C4	$2(d)$	1/3	2/3	1/2	$n_4 = y + \eta_{17}/6 + \eta_{15}/3$
				$M1$ (W1)	$6(k)$	1/3	0	1/4	
						x/a_{orth}	y/b_{orth}	z/c_{orth}	
Orthorhombic	No. 60 $Pbcn$ (D^{14}_{2h})	$\mathbf{a}_{\text{orth}} = \langle 001 \rangle_{L'3}$, $\mathbf{b}_{\text{orth}} = 2\langle 100 \rangle_{L'3}$, $\mathbf{c}_{\text{orth}} = \langle 120 \rangle_{L'3}$	$4V_{L'3}$	C1 (vacancy)	$4(c)$	0	7/8	1/4	$n_1 = y - \eta_{14}/2$
				C2	$4(c)$	0	3/8	1/4	$n_2 = y + \eta_{14}/2$
				$M1$ (W1)	$8(d)$	1/4	1/8	1/12	

* The volume of the unit cell of a superstructure expressed through volume $V_{L'3} = (\sqrt{3}/2)a^2c$ of the unit cell of the basic disordered structure of type $L'3$.

expressions $x_I = x_{C6}$, $y_I = y_{C6}$, and $z_I = z_{C6}$ to the coordinates of the rhombohedral (space group $P\bar{3}m1$) β''-W_2C superstructure (see Table 17) . The values of distribution function (26) at the sites of the nonmetal sublattice of the rhombohedral superstructure are listed in Table 17.

The authors of Ref. [95] postulated the existence of the ordered rhombohedral β''-W_2C phase without furnishing strong structural evidence by a mere reference to Ref. [96], where W_2C carbide obtained by carbidization of a thin metallic tungsten film was studied using the electron diffraction technique. In Ref. [96], based on limited data and taking no account of other models, the researchers hypothesized that lower β''-W_2C carbide has a rhombohedral (space group $P\bar{3}m1$) structure of type $C6$. The authors of Ref. [95] argued that the β''-W_2C phase exists at temperatures from 2300 to 1500 K. Reference [97] reports without any structural proof finding the β''-W_2C phase in lower tungsten carbide obtained at 2420–2520 K. The existence of the rhombohedral β''-W_2C phase has never been confirmed in later studies.

8.2 Trigonal ε-W_2C superstructure

The trigonal (space group $P\bar{3}1m$) ε-W_2C phase possesses a unit cell of volume $V_\varepsilon = (3\sqrt{3}/2)a^2c$ (Fig. 18). Its translation vectors and coordinates of atoms and vacancies are presented in Table 17. For the trigonal ε-W_2C superstructure in the first Brillouin zone of the disordered hexagonal nonmetal sublattice, there are three nonequivalent superstructure vectors corresponding to ray $\mathbf{k}_{17}^{(1)} = \mathbf{b}_3/2$ of the single-ray Lifshitz star $\{\mathbf{k}_{17}\}$ and two rays $\mathbf{k}_{15}^{(1)} = (\mathbf{b}_1 + \mathbf{b}_2)/3 + \mathbf{b}_3/2$ and $\mathbf{k}_{15}^{(2)} = -\mathbf{k}_{15}^{(1)}$ of the two-ray Lifshitz star $\{\mathbf{k}_{15}\}$. Thus, the disorder–order phase transition channel involved in the formation of the ordered trigonal ε-W_2C phase comprises three superstructure vectors, $\mathbf{k}_{15}^{(1)}$, $\mathbf{k}_{15}^{(2)}$, and $\mathbf{k}_{17}^{(1)}$. It should be noted that vector $\mathbf{b}_3/2 = (0\ 0\ 1/2)$ in $4\pi/c$ units or (001) in $2\pi/c$ units. If $2\pi/c$ units are utilized, vectors $\mathbf{k}_{17}^{(1)} = \mathbf{b}_3/2 = (001)$ and $\mathbf{k}_{15}^{(1)} = (\mathbf{b}_1 + \mathbf{b}_2)/3 + \mathbf{b}_3/2 = (1/3\ 1/3\ 1)$. Therefore, the distribution function of carbon atoms in the ordered trigonal ε-$W_2C_{y'}$ (WC_y, $y \leqslant 0.5$) phase has the form

$$n(x_I, y_I, z_I) = y - \frac{\eta_{17}}{6}\cos(2\pi z_I) + \frac{2\eta_{15}}{3}\cos\left[\frac{2\pi}{3}(x_I + y_I + 3z_I)\right]. \tag{27}$$

Referring to Fig. 18, coordinates (x_I, y_I, z_I) of the disordered hexagonal $L'3$ structure are related to the coordinates of the trigonal (space group $P\bar{3}1m$) ε-W_2C superstructure (see Table 17) by the following expressions: $x_I = x_\varepsilon + y_\varepsilon$, $y_I = -x_\varepsilon + 2y_\varepsilon$, and $z_I = z_\varepsilon$. Distribution function (27) depends on two long-range order parameters, η_{17} and η_{15}, corresponding to $\{\mathbf{k}_{17}\}$ and $\{\mathbf{k}_{15}\}$ stars, and takes four different values at the sites of the nonmetal sublattice of the trigonal ε-W_2C phase (see Table 17).

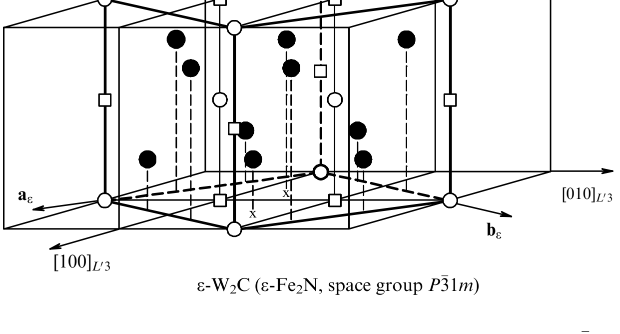

ε-W_2C (ε-Fe_2N, space group $P\bar{3}1m$)

Figure 18. Position of the unit cells of the trigonal (space group $P\bar{3}1m$) ordered ε-W_2C phase of type ε-Fe_2N in the basic lattice with the $L'3$ structure: (●) tungsten (W) atoms, (○) carbon (C) atoms, and (□) vacant sites of the nonmetal sublattice.

The trigonal (space group $P\bar{3}1m$) ε-W_2C phase was found in W_2C samples produced by solid-phase sintering of $W-C$ mixtures at 2370–2670 K [98], 1920 K [99], and 2070 K [100], and by arc melting such mixtures [101]. In Refs [101–104], the W_2C samples were ground and the resulting powders were annealed at 1470 K for 100 h. Neutronographic [103] and electron diffraction [101] studies revealed that the main phase in the annealed powders is ordered trigonal (space group $P\bar{3}1m$) ε-W_2C carbide with the ε-Fe_2N type structure. According to Ref. [103], the temperature of the disorder–order β-W_2C $\leftrightarrow$ ε-W_2C transition depends on the carbon concentration in carbides and varies from 1920 to 2100 K. The authors of Refs [105, 106] found that disordered β-W_2C carbide is transformed into a trigonal ordered ε-W_2C phase at $\sim$ 2120 K. The authors of Ref. [106] maintain that the ε-W_2C phase is thermodynamically stable in a temperature range of 2120–1520 K.

Detailed neutronographic and X-ray investigations into the structure of lower tungsten carbide obtained under various conditions in a temperature range of $\sim$ 3600–1370 K are reported in Refs [100, 107–109]. These experiments demonstrated that lower tungsten carbide W_2C is thermodynamically stable in a range from the melting point of $\sim$ 3050 to 1370 K, where it resists decomposition. It was shown in Refs [100, 107–109] that the sole ordered phase of lower tungsten carbide W_2C in a range from $\sim$ 2700 to 1370 K is the trigonal (space group $P\bar{3}1m$) ε-W_2C phase.

8.3 Orthorhombic β′-W_2C superstructure

The unit cell of the orthorhombic (space group *Pbcn*) ordered β′-W_2C phase with the structure of type ζ-Fe_2N is depicted in Fig. 19. Its volume $V_{\text{orth}} = (2\sqrt{3})a^2c$, i.e., four times that of the unit cell of disordered β-W_2C carbide. Coordinates of atoms and vacancies in an ideal orthorhombic (space group *Pbcn*) β′-W_2C phase are presented in Table 17.

The disorder–order β-W_2C (space group $P6_3/mmc$) $\rightarrow$ β′-W_2C (space group *Pbcn*) transition channel involves one superstructure $\mathbf{k}_{14}^{(3)}$ vector of the $\{\mathbf{k}_{14}\}$ star. Because vector $\mathbf{b}_3/2 = (0\ 0\ 1/2)$ in $4\pi/c$ units or (001) in $2\pi/c$ units, vector $\mathbf{k}_{14}^{(3)} = -(\mathbf{b}_1 + \mathbf{b}_2 - \mathbf{b}_3)/2 = -(1/2\ 1/2\ -1)$ in $2\pi/c$ units. The distribution function of carbon atoms in the orthorhombic (space group *Pbcn*) β′-W_2C phase takes the form

$$n(x_{\text{I}}, y_{\text{I}}, z_{\text{I}}) = y + \frac{\eta_{14}}{2}\cos\left[\pi(x_{\text{I}} + y_{\text{I}} - 2z_{\text{I}})\right]. \tag{28}$$

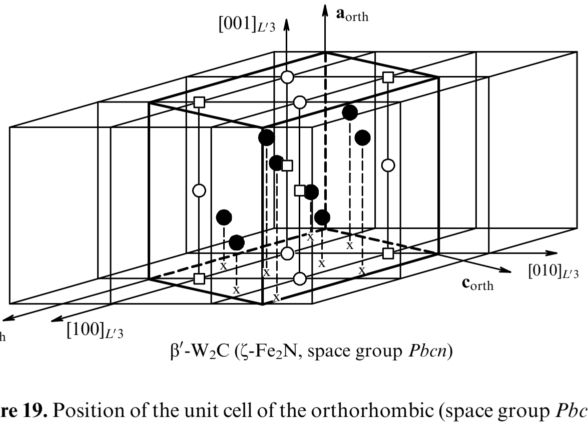

Figure 19. Position of the unit cell of the orthorhombic (space group *Pbcn*) ordered β′-W_2C (ζ-W_2C) phase of type ζ-Fe_2N in the basic lattice with the $L'3$ structure: (●) tungsten (W) atoms, (○) carbon (C) atoms, and (□) vacant sites of the nonmetal sublattice.

In accordance with Fig. 19, coordinates $(x_{\text{I}}, y_{\text{I}}, z_{\text{I}})$ of the disordered hexagonal $L'3$ structure are related to the coordinates of the orthorhombic (space group *Pbcn*) β′-W_2C superstructure in Table 17 by the following expressions: $x_{\text{I}} = 2y_{\text{orth}} + z_{\text{orth}} - 1$, $y_{\text{I}} = 2z_{\text{orth}} - 1/2$, and $z_{\text{I}} = x_{\text{orth}}$. Distribution function (28) takes two values at sites relevant to different positions of the nonmetal sublattice of the orthorhombic β′-W_2C superstructure (see Table 17).

The authors of Ref. [95] hypothesized the existence of an orthorhombic β′-W_2C phase. Röntgenograms of W_2C ($WC_{0.50}$) samples annealed for $T \leqslant 1270$ K in Refs [110, 111] gave evidence of diffraction reflections of the orthorhombic β′-W_2C phase with a structure of type ζ-Fe_2N. Samples of W_2C annealed at 870, 1070, and 1270 K for 3000, 1500, and 750 h, respectively, retained the ordered orthorhombic (space group *Pbcn*) β′-W_2C phase [111]. A neutronographic study [112] of W_2C ($WC_{0.50}$) samples annealed at 1070–1270 K for 600 h confirmed the existence of the ordered orthorhombic (space group *Pbcn*) phase of lower tungsten carbide.

The orthorhombic β′-W_2C phase was also observed in Refs [97, 102, 103, 113]. Neutronographic data [102, 103] indicated that this superstructure was present in W_2C samples only after annealing for $T < 1300$ K. It may be argued based on the results of Refs [97, 102, 103, 110–113] that the orthorhombic (space group *Pbcn*) modification of β′-W_2C phase occurs at temperatures below 1300 K.

8.4 Sequence of disorder–order and order–order transformations in W_2C_y

Let us consider changes in symmetry during the formation of various superstructures for the determination of a physically admissible disorder–order and order–order phase transformation sequence in W_2C_y with decreasing temperature.

The point symmetry group $\bar{3}m$ (D_{3d}) of rhombohedral β″-W_2C carbide includes 12 symmetry elements: H_1, H_3, H_5, H_8, H_{10}, H_{12}, H_{13}, H_{15}, H_{17}, H_{20}, H_{22}, and H_{24}, of the 24 $H_1 - H_{24}$ elements, making up the $6/mmm$ hexagonal group [1, 2, 30, 31]; therefore, rotational symmetry reduction reaches 2. The drop in translational symmetry equals the ratio between unit cell volumes of ordered and disordered phases or the ratio between site numbers in these cells. The overall symmetry reduction N is the product of rotational symmetry reduction and the translational symmetry fall. Because the unit cell volume remains unaltered in a disorder–order transition, translational symmetry reduction equals 1, and the overall symmetry reduction in the putative β-W_2C (space group $P6_3/mmc$) $\rightarrow$ β″-W_2C (space group $P\bar{3}m1$) phase transformation is 2.

The point symmetry group $\bar{3}m$ of trigonal ε-W_2C carbide includes 12 symmetry elements; therefore, rotational symmetry reduction equals 2. The unit cell volume increases by a factor of 3 in the transition from disordered β-W_2C carbide to trigonal ε-W_2C carbide. The overall symmetry reduction in the β-W_2C (space group $P6_3/mmc$) $\rightarrow$ ε-W_2C (space group $P\bar{3}1m$) transition reaches 6.

The point symmetry group mmm (D_{2h}) of orthorhombic β′-W_2C carbide includes 8 symmetry elements H_i; therefore, rotational symmetry reduction is 3. The drop in translational symmetry equals 4, and the overall symmetry reduction in the β-W_2C (space group $P6_3/mmc$) $\rightarrow$ β′-W_2C (space group *Pbcn*) transition amounts to 12.

Symmetry changes during the formation of putative orthorhombic and rhombohedral phases are such that the hexagonal disordered β-W_2C phase → orthorhombic ordered β′-W_2C phase → rhombohedral ordered β″-W_2C phase transition sequence proposed in Ref. [95] is physically inadmissible, because the β′-W_2C → β″-W_2C transition would be accompanied by a rise in symmetry rather than a fall.

When all three superstructures are formed at different stages of W_2C carbide ordering, the results of symmetry analysis allow us to propose the sole possible sequence of phase transformations that occur with decreasing temperature and agree with the symmetry variations, viz. the hexagonal (space group $P6_3/mmc$) disordered β-W_2C phase → rhombohedral (space group $P\bar{3}m1$) ordered β″-W_2C phase → trigonal (space group $P\bar{3}1m$) ordered ε-W_2C phase → orthorhombic (space group $Pbcn$) ordered β′-W_2C phase transitions. In this case, symmetry reduces twofold during the transition from hexagonal to rhombohedral carbide, then threefold in the transition from rhombohedral to trigonal carbide, and, finally, twofold in the transition from trigonal to orthorhombic carbide. The transition sequences remain physically valid even in the absence of observing the ordered phase in experiment.

The sole ordered phase of lower tungsten carbide W_2C in a temperature range of $\sim 2700-1370$ K is the trigonal (space group $P\bar{3}1m$) ε-W_2C phase [107–109]. The existence of the rhombohedral (space group $P\bar{3}m1$) ordered β″-W_2C phase in this temperature range remains to be confirmed. Nor have any traces of the orthorhombic (space group $Pbcn$) ordered β′-W_2C phase been observed after prolonged annealing at 1370 K [100, 107–109]. It may be supposed that the transition from the trigonal ordered ε-W_2C phase to the orthorhombic (space group $Pbcn$) ordered β′-W_2C phase occurs at temperatures below 1370 K, since it is consistent with the physically admissible phase transition sequence. Indeed, the orthorhombic (space group $Pbcn$) β′-W_2C phase with the ζ-Fe_2N structure has been observed in lower tungsten carbide samples annealed at temperatures below 1300 K [103, 111, 112].

Thus, a symmetry analysis and the available experimental data [100, 103, 107–112] suggests that ordering of lower tungsten carbide with decreasing temperature leads to the following sequence of phase transformations: hexagonal (space group $P6_3/mmc$) disordered β-W_2C phase → trigonal (space group $P\bar{3}1m$) ordered ε-W_2C phase → orthorhombic (space group $Pbcn$) ordered β′-W_2C phase.

Calculations of electronic structure and energy stability of disordered and three possible ordered phases of lower tungsten carbide W_2C [114] by the nonempirical band FLAPW-GGA method[1] agree with this experimentally adopted transition sequence. According to Ref. [114], trigonal ε-W_2C and orthorhombic β′-W_2C phases are the most stable ones having similar formation energies (−0.04 and −0.02 eV per formula unit). The rhombohedral (space group $P\bar{3}m1$) ordered β″-W_2C phase is characterized by a very high formation energy, +0.19 eV per formula unit, and cannot exist. The formation energy of disordered β-W_2C carbide is close to zero, which accounts for its metastability at low temperatures. Indeed, disordered β-W_2C carbide is found in thermodynamic equilibrium between ~ 2300 K and the melting point; it undergoes a disorder–order phase transformation at temperatures below approximately 2000–2300 K.

9. Superstructures of nonstoichiometric Ti_xO_z and V_xO_z oxides with double defectiveness

Besides nonstoichiometric compounds with a single defective sublattice, there are nonstoichiometric compounds containing about 10–15 at.% of structural vacancies simultaneously in two sublattices: cubic titanium and vanadium monoxides, Ti_xO_z and V_xO_z, with the basic crystalline $B1$ structure [1, 2].

The ordering in cubic titanium monoxide TiO_y ($Ti_x\blacksquare_{1-x}O_z\square_{1-z}$, where $y = z/x$, $\blacksquare$ and $\square$ are vacancies in metal and oxygen sublattices, respectively) has been studied in great detail [115–125]. In titanium monoxide TiO_y, the ordered phases with cubic, tetragonal, rhombic, or monoclinic sublattices are formed, depending on the composition and thermal treatment conditions. The variety of superstructures in cubic titanium monoxide, TiO_y, is due to the presence of structural vacancies in both titanium and oxygen sublattices at a time. Of greatest interest is ordering of equiatomic titanium monoxide $Ti_{0.83}O_{0.83}$ in which monoclinic [116, 118, 120, 121, 124, 125] and cubic [117, 126–128] superstructures of type Ti_5O_5 arise. During the formation of the Ti_5O_5 superstructure, Ti atoms and metal vacancies $\blacksquare$ are ordered within the metal fcc sublattice, whereas oxygen atoms and nonmetal $\square$ vacancies undergo ordering at the sites of the nonmetal fcc sublattice. In other words, equiatomic titanium monoxide is characterized by the ordering of two atomic species in two different but equitype Ising lattices.

Vanadium oxides containing less than 50–55 at.% oxygen also possess wide homogeneity intervals. However, cubic vanadium monoxide VO_y ($V_x\blacksquare_{1-x}O_z\square_{1-z} \equiv V_xO_z$) contains only one ordered $V_{52}O_{64}$ phase, despite its apparent similarity to titanium monoxide TiO_y [129–135]. This phase exhibits tetragonal symmetry and forms in the $VO_{1.2}-VO_{1.3}$ region, i.e., in monoxide containing vacancies only in the vanadium sublattice. Its structure is significantly different from that of the known ordered phases in titanium monoxide TiO_y and from the structures of other nonstoichiometric compounds.

Nonstoichiometric vanadium oxides adjoin a solid oxygen solution in vanadium, V(O), called the β-phase. In this phase, oxygen (O) atoms and $\square$ structural vacancies make up a substitution solution. The high vacancy concentration in the β-phase creates prerequisites for atomic-vacancy ordering. Ordering of the β-phase gives rise to a γ-phase, i.e., the monoclinic vanadium suboxide $V_{14}O_6$ ($V_{14}O_6\square_8$) superstructure [136–141].

9.1 Monoclinic Ti_5O_5 superstructure

The unit cell of the monoclinic (space group $C2/m$) $Ti_5O_5 \equiv Ti_5\blacksquare O_5\square$ ($Ti_{10}\blacksquare_2O_{10}\square_2$) superstructure formed in titanium monoxide $TiO_y \equiv Ti_xO_z$ with vacancies located simultaneously in titanium and oxygen sublattices is depicted in Fig. 20. It contains two formula units $Ti_5\blacksquare O_5\square$, and translation vectors, the coordinates of atoms and vacancies for this cell are presented in Table 18. The Ti_5O_5 superstructure forms via a transition channel involving 5 vectors, viz. $\mathbf{k}_{10}^{(1)}$ ray of the $\{\mathbf{k}_{10}\}$ star, two rays $\mathbf{k}_4^{(5)}$ and $\mathbf{k}_4^{(6)}$ of the $\{\mathbf{k}_4\}$ star with parameter $\mu_4 = 1/3$, and two $\mathbf{k}_1^{(7)}$ and $\mathbf{k}_1^{(8)}$ rays of the $\{\mathbf{k}_1\}$ star with parameters $\mu_1^{(1)} = 1/3$ and $\mu_1^{(2)} = 1/6$.

Calculations done in Refs [120, 121] showed that the distribution function of titanium atoms in the monoclinic (space group $C2/m$) superstructure of titanium monoxide

---

[1] The fullong-range order parameter potential linear augmented plane wave (FLAPW) method with generalized gradient approximation (GGA) of the exchange-correlation potential.

Table 18. Monoclinic [space group No. 12 — $C2/m$ ($A12/m1$) (C_{2h}^3)] Ti_5O_5 ($Ti_5■_1O_5□_1$) superstructure of Ti_xO_z monoxide: $Z=2$, $V=3a_{B1}^3$, $\mathbf{a}_m = \langle 10\bar{1}\rangle_{B1}$, $\mathbf{b}_m = \langle 010\rangle_{B1}$, and $\mathbf{c}_m = \langle 102\rangle_{B1}$.

Atom	Position and multiplicity	Atomic coordinates in ideal ordered structure			Values of distribution functions $n_{Ti}(x_I, y_I, z_I)$ and $n_O(x_I, y_I, z_I)$
		x/a_m	y/b_m	z/c_m	
Ti1 (vacancy ■)	2(a)	0	0	0	$n_{1(Ti)} = x - \eta_{10}/6 - \eta_4/3 - \eta_1/3$
Ti2	2(d)	1/2	1/2	1/2	$n_{2(Ti)} = x + \eta_{10}/6 - \eta_4/3 + \eta_1/3$
Ti3	4(i)	1/6	0	1/3	$n_{4(Ti)} = x + \eta_{10}/6 + \eta_4/6 - \eta_1/6$
Ti4	4(i)	1/3	0	2/3	$n_{3(Ti)} = x - \eta_{10}/6 + \eta_4/6 + \eta_1/6$
O1 (vacancy □)	2(c)	1/2	0	1/2	$n_{1(O)} = z - \eta_{10}/6 - \eta_4/3 - \eta_1/3$
O2	2(b)	0	1/2	0	$n_{2(O)} = z + \eta_{10}/6 - \eta_4/3 + \eta_1/3$
O3	4(i)	1/3	0	1/6	$n_{4(O)} = z + \eta_{10}/6 + \eta_4/6 - \eta_1/6$
O4	4(i)	1/6	0	5/6	$n_{3(O)} = z - \eta_{10}/6 + \eta_4/6 + \eta_1/6$

Ti_xO_z has the form

$$n_{Ti}(x_I, y_I, z_I) = x - \frac{\eta_{10}}{6}\cos(2\pi z_I) - \frac{\eta_4}{3}\cos\left[\frac{4\pi(x_I + z_I)}{3}\right] - \frac{\eta_1}{3}\cos\left[\frac{2\pi(2x_I - z_I)}{3}\right], \qquad (29)$$

with $\gamma_{10} = 1/6$, $\varphi_{10}^{(1)} = \pi$, $\gamma_4 = 1/6$, $\varphi_4^{(1)} = \pi$, $\varphi_4^{(2)} = -\pi$, $\gamma_1 = 1/6$, $\varphi_1^{(1)} = \pi$, and $\varphi_1^{(2)} = -\pi$. The distribution of oxygen atoms in the monoclinic (space group $C2/m$) superstructure of titanium monoxide Ti_xO_z is described by the function

$$n_O(x_I, y_I, z_I) = z + \frac{\eta_{10}}{6}\cos(2\pi z_I) - \frac{\eta_4}{3}\cos\left[\frac{4\pi(x_I + z_I)}{3}\right] + \frac{\eta_1}{3}\cos\left[\frac{2\pi(2x_I - z_I)}{3}\right] \qquad (30)$$

with parameters $\gamma_{10} = 1/6$, $\varphi_{10}^{(1)} = 0$, $\gamma_4 = 1/6$, $\varphi_4^{(1)} = \pi$, $\varphi_4^{(2)} = -\pi$, $\gamma_1 = 1/6$, $\varphi_1^{(1)} = 0$, and $\varphi_1^{(2)} = 2\pi$.

Referring to Fig. 20, coordinates (x_I, y_I, z_I) of the disordered cubic $B1$ structure are related to the coordinates of the monoclinic (space group $C2/m$) Ti_5O_5 superstructure presented in Table 18, by the following expressions: $x_I = x_m + z_m$, $y_I = y_m$, and $z_I = -x_m + 2z_m$. The completely ordered state of titanium monoxide is reached when all long-range order parameters equal 1, i.e., $\eta_{10} = \eta_4 = \eta_1 = 1$. It follows from distribution functions (29) and (30) that in this case the relative concentration of Ti atoms in the metal sublattice is $x = 5/6$, while the analogous quantity for oxygen atoms in the nonmetal sublattice is $z = 5/6$. In other words, the stoichiometric composition of an ideal monoclinic superstructure can be represented as $Ti_{5/6}O_{5/6}$ ($Ti_{0.83}O_{0.83}$) or Ti_5O_5 ($Ti_5■O_5□$).

Distribution function (29) of Ti atoms at the sites of the metal sublattice of ordered titanium monoxide takes four different values: $n_{1(Ti)}$, $n_{2(Ti)}$, $n_{3(Ti)}$, and $n_{4(Ti)}$; distribution function (30) of O atoms at the sites of the nonmetal sublattice assumes 4 similar values (see Table 18). Thus, ordering in the cubic titanium monoxide under discussion results in the splitting of each sublattice into four nonequivalent sublattices. In the case of equal long-range order parameters, the distribution functions take only two values each, and each sublattice undergoing ordering breaks up only into two sublattices. It can be seen from Fig. 20 that the relative positions of oxygen vacancies are exactly the same as those of titanium vacancies. In fact, the oxygen vacancy sublattice is displaced by vector $(1/2)\langle 101\rangle_{C2/m} \equiv (1/2)\langle 201\rangle_{B1}$ with respect to the titanium vacancy sublattice.

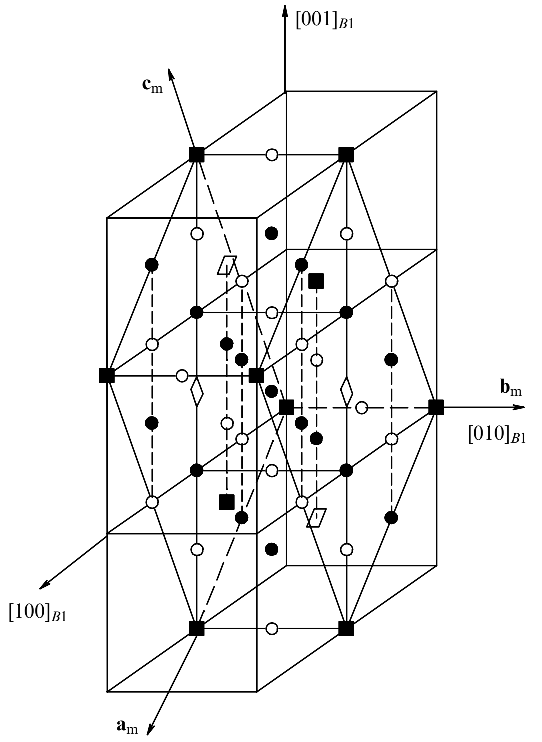

$Ti_5■O_5□$ (space group $C2/m$)

Figure 20. Position of the monoclinic (space group $C2/m$) unit cell of the $Ti_5■O_5□$ superstructure in a lattice with the basic structure $B1$: (○) oxygen atom, (●) titanium atom, (□) vacancy in the nonmetal sublattice (oxygen vacancy), and (■) vacancy in the metal sublattice (titanium vacancy).

9.2 Cubic Ti_5O_5 superstructure

The ordered cubic Ti_5O_5 phase was mentioned without any experimental evidence in one of the first publications on titanium monoxide, dated 1968 [117]. According to this report, the cubic Ti_5O_5 phase exists in a temperature range from 1250 to 1520 K and, unlike disordered titanium monoxide, has a triple-period lattice; in terms of symmetry, it belongs to one of the space groups $Fm\bar{3}$, $F432$, $F\bar{4}3m$, or $Fm\bar{3}m$. Experiments in subsequent decades failed to demonstrate the cubic Ti_5O_5 ($Ti_5■O_5□$) superstructure, nor has its

Table 19. Ideal ordered cubic [space group No. 221 — $Pm\bar{3}m$ ($P4/m\bar{3}2/m$) (O_h^1)] $Ti_5■O_5□$ phase of titanium monoxide Ti_xO_z: $Z = 18$, $V = 27a_{B1}^3$, $\mathbf{a}_{cub} = \langle 300\rangle_{B1}$, $\mathbf{b}_{cub} = \langle 030\rangle_{B1}$, and $\mathbf{c}_{cub} = \langle 003\rangle_{B1}$.

Atom	Position and multiplicity	Atomic coordinates in ideal ordered structure			Values of distribution functions $n_{Ti}(x_I, y_I, z_I)$ and $n_O(x_I, y_I, z_I)$
		x/a_{cub}	y/b_{cub}	z/c_{cub}	
Ti1	1(b)	1/2	1/2	1/2	$n_{1(Ti)} = x - \eta_{10}/2 - \eta_7/3 - \eta_{6(1)}/6 - \eta_{6(2)}/6 + \eta_{4(1)}/3 + \eta_{4(2)}/3 + 2\eta_1/3$
Ti2	3(d)	1/2	0	0	$n_{2(Ti)} = x + \eta_{10}/6 + \eta_7/9 + \eta_{6(1)}/18 - \eta_{6(2)}/6 - \eta_{4(1)}/9 + \eta_{4(2)}/3 - 2\eta_1/9$
Ti3	6(e)	1/6	0	0	$n_{3(Ti)} = x + \eta_{10}/6 - \eta_7/18 + 5\eta_{6(1)}/36 - \eta_{6(2)}/12 + 2\eta_{4(1)}/9 - 2\eta_1/9$
Ti4 (vacancy ■)	6(f)	1/6	1/2	1/2	$n_{4(Ti)} = x - \eta_{10}/2 - \eta_7/6 - \eta_{6(1)}/12 - \eta_{6(2)}/12$
Ti5	8(g)	1/6	1/6	1/6	$n_{5(Ti)} = x - \eta_{10}/2 + \eta_7/6 + \eta_{6(1)}/12 + \eta_{6(2)}/12 + \eta_{4(1)}/12 + \eta_{4(2)}/12 + \eta_1/6$
Ti6	12(h)	1/3	1/2	0	$n_{6(Ti)} = x + \eta_{10}/6 + \eta_7/9 - \eta_{6(1)}/36 - \eta_{6(2)}/12 - \eta_{4(1)}/9 + \eta_1/9$
Ti7 (vacancy ■)	12(j_1)	1/2	1/6	1/6	$n_{7(Ti)} = x - \eta_{10}/2 - \eta_{4(1)}/12 - \eta_{4(2)}/12 - \eta_1/6$
Ti8	12(j_2)	1/2	1/3	1/3	$n_{8(Ti)} = x + \eta_{10}/6 + \eta_7/9 - \eta_{6(1)}/9 + 5\eta_{4(1)}/36 - \eta_{4(2)}/12 - \eta_1/18$
Ti9	24(k)	0	1/6	1/3	$n_{9(Ti)} = x + \eta_{10}/6 - \eta_7/18 + \eta_{6(1)}/18 - \eta_{4(1)}/36 - \eta_{4(2)}/12 + \eta_1/9$
Ti10	24(m)	1/3	1/3	1/6	$n_{10(Ti)} = x + \eta_{10}/6 - \eta_7/18 - \eta_{6(1)}/36 + \eta_{6(2)}/12 - \eta_{4(1)}/36 + \eta_{4(2)}/12 - \eta_1/18$
O1	1(a)	0	0	0	$n_{1(O)} = z - \eta_{10}/2 - \eta_7/3 - \eta_{6(1)}/6 - \eta_{6(2)}/6 + \eta_{4(1)}/3 + \eta_{4(2)}/3 + 2\eta_1/3$
O2	3(c)	0	1/2	1/2	$n_{2(O)} = z + \eta_{10}/6 + \eta_7/9 + \eta_{6(1)}/18 - \eta_{6(2)}/6 - \eta_{4(1)}/9 + \eta_{4(2)}/3 - 2\eta_1/9$
O3 (vacancy □)	6(e)	1/3	0	0	$n_{3(O)} = z - \eta_{10}/2 - \eta_7/6 - \eta_{6(1)}/12 - \eta_{6(2)}/12$
O4	6(f)	1/3	1/2	1/2	$n_{4(O)} = z + \eta_{10}/6 - \eta_7/18 + 5\eta_{6(1)}/36 - \eta_{6(2)}/12 + \eta_{4(1)}/9 - \eta_1/9$
O5	8(g)	1/3	1/3	1/3	$n_{5(O)} = z - \eta_{10}/2 + \eta_7/6 + \eta_{6(1)}/12 + \eta_{6(2)}/12 + \eta_{4(1)}/12 + \eta_{4(2)}/12 + \eta_1/6$
O6	12(h)	1/6	1/2	0	$n_{6(O)} = z + \eta_{10}/6 + \eta_7/9 - \eta_{6(1)}/36 - \eta_{6(2)}/12 - \eta_{4(1)}/9 + \eta_1/9$
O7 (vacancy □)	12(i_1)	0	1/3	1/3	$n_{7(O)} = z - \eta_{10}/2 - \eta_{4(1)}/12 - \eta_{4(2)}/12 - \eta_1/6$
O8	12(i_2)	0	1/6	1/6	$n_{8(O)} = z + \eta_{10}/6 + \eta_7/9 - \eta_{6(1)}/9 + 5\eta_{4(1)}/36 - \eta_{4(2)}/12 - \eta_1/18$
O9	24(l)	1/2	1/3	1/6	$n_{9(O)} = z + \eta_{10}/6 - \eta_7/18 + \eta_{6(1)}/18 - \eta_{4(1)}/36 - \eta_{4(2)}/12 + \eta_1/9$
O10	24(m)	1/6	1/6	1/3	$n_{10(O)} = z + \eta_{10}/6 - \eta_7/18 - \eta_{6(1)}/36 + \eta_{6(2)}/12 - \eta_{4(1)}/36 + \eta_{4(2)}/12 - \eta_1/18$

theoretical model been proposed. The simulation method [127, 128] for the construction of a cubic Ti_5O_5 superstructure appeared only in 2012–2013; its existence was confirmed by electron diffraction data [126, 128].

The unit cell of the cubic (space group $Pm\bar{3}m$) $Ti_5O_5 \equiv Ti_5■O_5□$ ($Ti_{90}■_{18}O_{90}□_{18}$) superstructure is illustrated in Fig. 21. It has translation vectors $\mathbf{a}_{cub} = \langle 300\rangle_{B1}$, $\mathbf{b}_{cub} = \langle 030\rangle_{B1}$, and $\mathbf{c}_{cub} = \langle 003\rangle_{B1}$; accordingly, the reciprocal lattice vectors are $\mathbf{a}_1^* = \langle 0\ 0\ 1/3\rangle$, $\mathbf{a}_2^* = \langle 0\ 1/3\ 0\rangle$, and $\mathbf{a}_3^* = \langle 1/3\ 0\ 0\rangle$. The unit cell contains 18 $Ti_5■O_5□$ formula units; coordinates of atoms and vacancies are listed in Table 19. The disorder–order transition channel involved in the formation of the cubic (space group $Pm\bar{3}m$) Ti_5O_5 superstructure includes all the rays of seven stars: $\{\mathbf{k}_{10}\}$, $\{\mathbf{k}_7\}$, $\{\mathbf{k}_{6(1)}\}$, $\{\mathbf{k}_{6(2)}\}$, $\{\mathbf{k}_{4(1)}\}$, $\{\mathbf{k}_{4(2)}\}$, and $\{\mathbf{k}_1\}$, i.e., a total of 75 superstructure vectors (Table 20).

According to papers [127, 128], the neighboring ■ vacancies in the titanium sublattice of the cubic (space group $Pm\bar{3}m$) Ti_5O_5 superstructure are located within largest distances a_{B1} and $\sqrt{2}\,a_{B1}$ from one another. The distribution function of Ti atoms in the basic fcc lattice found for such an arrangement has the form

$$\begin{aligned} n_{Ti}(x_I, y_I, z_I) &= x + \frac{\eta_{10}}{6}\sum_{j \in \mathbf{k}_{10}} \cos(\mathbf{k}_{10}^{(j)}\mathbf{r}) \\ &- \frac{\eta_7}{18}\sum_{j \in \mathbf{k}_7} \cos(\mathbf{k}_7^{(j)}\mathbf{r}) + \frac{\eta_{6(1)}}{18}\sum_{j \in \mathbf{k}_{6(1)}} \cos(\mathbf{k}_{6(1)}^{(j)}\mathbf{r}) \\ &- \frac{\eta_{6(2)}}{18}\sum_{j \in \mathbf{k}_{6(2)}} \cos(\mathbf{k}_{6(2)}^{(j)}\mathbf{r}) + \frac{\eta_{4(1)}}{18}\sum_{j \in \mathbf{k}_{4(1)}} \cos(\mathbf{k}_{4(1)}^{(j)}\mathbf{r}) \\ &+ \frac{\eta_{4(2)}}{18}\sum_{j \in \mathbf{k}_{4(2)}} \cos(\mathbf{k}_{4(2)}^{(j)}\mathbf{r}) - \frac{\eta_1}{18}\sum_{j \in \mathbf{k}_1} \cos(\mathbf{k}_1^{(j)}\mathbf{r})\,. \end{aligned} \tag{31}$$

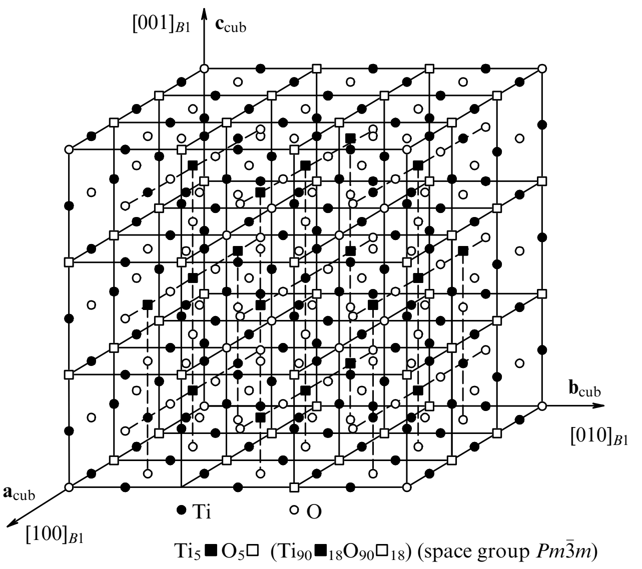

Figure 21. Position of the cubic (space group $Pm\bar{3}m$) unit cell of the $Ti_5■O_5□$ ($Ti_{90}■_{18}O_{90}□_{18}$) superstructure in a basic lattice with the structure $B1$. The vacant sites of the titanium sublattice are in 6(f) and 12(j_1) positions, the vacant sites of the oxygen sublattice are in 6(e) and 12(i_1) positions: (●) titanium (Ti) atoms, (○) oxygen (O) atoms, (■) vacancy in the titanium sublattice, and (□) vacancy in the oxygen sublattice.

In the oxygen sublattice of the cubic (space group $Pm\bar{3}m$) Ti_5O_5 superstructure, the neighboring □ vacancies are also separated by the largest distances a_{B1} and $\sqrt{2}\,a_{B1}$ from one another. The distribution function of O atoms at the sites of the basic oxygen fcc sublattice with these vacant sites has the

Table 20. Disorder–order $Ti_xO_z - Ti_5O_5$ phase transition channel with the formation of the cubic (space group $Pm\bar{3}m$) Ti_5O_5 ($Ti_{90}■_{18}O_{90}□_{18}$) superstructure.

$\{\mathbf{k}_s\}$ star	$\mathbf{k}_s^{(j)}$ rays of $\{\mathbf{k}_s\}$ stars entering transition channel	$\mu^{(s)}$	γ_s	$\varphi_s^{(j)}$ for sublattice	
				Ti	O
$\{\mathbf{k}_{10}\}$	$\mathbf{k}_{10}^{(1)} = (\mathbf{b}_1 + \mathbf{b}_2)/2 = 3\mathbf{a}_1^* = [0\,0\,1]$, $\mathbf{k}_{10}^{(2)}$, $\mathbf{k}_{10}^{(3)}$		$\gamma_{10} = 1/6$	$\varphi_{10}^{(j)} = 0$	$\varphi_{10}^{(j)} = \pi$
$\{\mathbf{k}_7\}$	$\mathbf{k}_7^{(1)} = (\mathbf{b}_1 + \mathbf{b}_3)/2 + \mu_7(\mathbf{b}_1 + \mathbf{b}_2) = 3\mathbf{a}_2^* + \mathbf{a}_1^* = [0\ 1\ 1/3]$, $\mathbf{k}_7^{(2)} = -\mathbf{k}_7^{(1)}$, $\mathbf{k}_7^{(3)}$, $\mathbf{k}_7^{(4)} = -\mathbf{k}_7^{(3)}$, $\mathbf{k}_7^{(5)}$, $\mathbf{k}_7^{(6)} = -\mathbf{k}_7^{(5)}$, $\mathbf{k}_7^{(7)}$, $\mathbf{k}_7^{(8)} = -\mathbf{k}_7^{(7)}$, $\mathbf{k}_7^{(9)}$, $\mathbf{k}_7^{(10)} = -\mathbf{k}_7^{(9)}$, $\mathbf{k}_7^{(11)}$, $\mathbf{k}_7^{(12)} = -\mathbf{k}_7^{(11)}$	$\mu_7 = 1/6$	$\gamma_7 = 1/36$	$\varphi_7^{(j)} = \pi$	$\varphi_7^{(j)} = \pi$
$\{\mathbf{k}_{6(1)}\}$	$\mathbf{k}_{6(1)}^{(1)} = \mu_{6(1)}(\mathbf{b}_1 + \mathbf{b}_2) = \mathbf{a}_1^* = [0\ 0\ 1/3]$, $\mathbf{k}_{6(1)}^{(2)} = -\mathbf{k}_{6(1)}^{(1)}$, $\mathbf{k}_{6(1)}^{(3)}$, $\mathbf{k}_{6(1)}^{(4)} = -\mathbf{k}_{6(1)}^{(3)}$, $\mathbf{k}_{6(1)}^{(5)}$, $\mathbf{k}_{6(1)}^{(6)} = -\mathbf{k}_{6(1)}^{(5)}$	$\mu_{6(1)} = 1/6$	$\gamma_{6(1)} = 1/36$	$\varphi_{6(1)}^{(j)} = 0$	$\varphi_{6(1)}^{(j)} = \pi$
$\{\mathbf{k}_{6(2)}\}$	$\mathbf{k}_{6(2)}^{(1)} = \mu_{6(2)}(\mathbf{b}_1 + \mathbf{b}_2) = 2\mathbf{a}_1^* = [0\ 0\ 2/3]$, $\mathbf{k}_{6(2)}^{(2)} = -\mathbf{k}_{6(2)}^{(1)}$, $\mathbf{k}_{6(2)}^{(3)}$, $\mathbf{k}_{6(2)}^{(4)} = -\mathbf{k}_{6(2)}^{(3)}$, $\mathbf{k}_{6(2)}^{(5)}$, $\mathbf{k}_{6(2)}^{(6)} = -\mathbf{k}_{6(2)}^{(5)}$	$\mu_{6(2)} = 1/3$	$\gamma_{6(2)} = 1/36$	$\varphi_{6(2)}^{(j)} = \pi$	$\varphi_{6(2)}^{(j)} = \pi$
$\{\mathbf{k}_{4(1)}\}$	$\mathbf{k}_{4(1)}^{(1)} = \mu_{4(1)}(\mathbf{b}_1 + \mathbf{b}_2 + 2\mathbf{b}_3) = \mathbf{a}_2^* + \mathbf{a}_3^* = [1/3\ 1/3\ 0]$, $\mathbf{k}_{4(1)}^{(2)} = -\mathbf{k}_{4(1)}^{(1)}$, $\mathbf{k}_{4(1)}^{(3)}$, $\mathbf{k}_{4(1)}^{(4)} = -\mathbf{k}_{4(1)}^{(3)}$, $\mathbf{k}_{4(1)}^{(5)}$, $\mathbf{k}_{4(1)}^{(6)} = -\mathbf{k}_{4(1)}^{(5)}$, $\mathbf{k}_{4(1)}^{(7)}$, $\mathbf{k}_{4(1)}^{(8)} = -\mathbf{k}_{4(1)}^{(7)}$, $\mathbf{k}_{4(1)}^{(9)}$, $\mathbf{k}_{4(1)}^{(10)} = -\mathbf{k}_{4(1)}^{(9)}$, $\mathbf{k}_{4(1)}^{(11)}$, $\mathbf{k}_{4(1)}^{(12)} = -\mathbf{k}_{4(1)}^{(11)}$	$\mu_{4(1)} = 1/6$	$\gamma_{4(1)} = 1/36$	$\varphi_{4(1)}^{(j)} = 0$	$\varphi_{4(1)}^{(j)} = 0$
$\{\mathbf{k}_{4(2)}\}$	$\mathbf{k}_{4(2)}^{(1)} = \mu_{4(2)}(\mathbf{b}_1 + \mathbf{b}_2 + 2\mathbf{b}_3) = 2\mathbf{a}_2^* + 2\mathbf{a}_3^* = [2/3\ 2/3\ 0]$, $\mathbf{k}_{4(2)}^{(2)} = -\mathbf{k}_{4(2)}^{(1)}$, $\mathbf{k}_{4(2)}^{(3)}$, $\mathbf{k}_{4(2)}^{(4)} = -\mathbf{k}_{4(2)}^{(3)}$, $\mathbf{k}_{4(2)}^{(5)}$, $\mathbf{k}_{4(2)}^{(6)} = -\mathbf{k}_{4(2)}^{(5)}$, $\mathbf{k}_{4(2)}^{(7)}$, $\mathbf{k}_{4(2)}^{(8)} = -\mathbf{k}_{4(2)}^{(7)}$, $\mathbf{k}_{4(2)}^{(9)}$, $\mathbf{k}_{4(2)}^{(10)} = -\mathbf{k}_{4(2)}^{(9)}$, $\mathbf{k}_{4(2)}^{(11)}$, $\mathbf{k}_{4(2)}^{(12)} = -\mathbf{k}_{4(2)}^{(11)}$	$\mu_{4(2)} = 1/3$	$\gamma_{4(2)} = 1/36$	$\varphi_{4(2)}^{(j)} = 0$	$\varphi_{4(2)}^{(j)} = 0$
$\{\mathbf{k}_1\}$	$\mathbf{k}_1^{(1)} = \mu_1^{(1)}(\mathbf{b}_1 + \mathbf{b}_3) + \mu_1^{(2)}(\mathbf{b}_2 + \mathbf{b}_3) =$ $[2\mu_1^{(2)}\ 2\mu_1^{(1)}\ 0] = [2/3\ 1/3\ 0]$, $\mathbf{k}_1^{(2)} = -\mathbf{k}_1^{(1)}$, $\mathbf{k}_1^{(3)}$, $\mathbf{k}_1^{(4)} = -\mathbf{k}_1^{(3)}$, $\mathbf{k}_1^{(5)}$, $\mathbf{k}_1^{(6)} = -\mathbf{k}_1^{(5)}$, $\mathbf{k}_1^{(7)}$, $\mathbf{k}_1^{(8)} = -\mathbf{k}_1^{(7)}$, $\mathbf{k}_1^{(9)}$, $\mathbf{k}_1^{(10)} = -\mathbf{k}_1^{(9)}$, $\mathbf{k}_1^{(11)}$, $\mathbf{k}_1^{(12)} = -\mathbf{k}_1^{(11)}$, $\mathbf{k}_1^{(13)}$, $\mathbf{k}_1^{(14)} = -\mathbf{k}_1^{(13)}$, $\mathbf{k}_1^{(15)}$, $\mathbf{k}_1^{(16)} = -\mathbf{k}_1^{(15)}$, $\mathbf{k}_1^{(17)}$, $\mathbf{k}_1^{(18)} = -\mathbf{k}_1^{(17)}$, $\mathbf{k}_1^{(19)}$,	$\mathbf{k}_1^{(20)} = -\mathbf{k}_1^{(19)}$, $\mathbf{k}_1^{(21)}$, $\mathbf{k}_1^{(22)} = -\mathbf{k}_1^{(21)}$, $\mathbf{k}_1^{(23)}$,			

form

$$
\begin{aligned}
n_{\mathrm{O}}(x_{\mathrm{I}}, y_{\mathrm{I}}, z_{\mathrm{I}}) = z &- \frac{\eta_{10}}{6} \sum_{j \in \mathbf{k}_{10}} \cos(\mathbf{k}_{10}^{(j)} \mathbf{r}) \\
&- \frac{\eta_7}{18} \sum_{j \in \mathbf{k}_7} \cos(\mathbf{k}_7^{(j)} \mathbf{r}) - \frac{\eta_{6(1)}}{18} \sum_{j \in \mathbf{k}_{6(1)}} \cos(\mathbf{k}_{6(1)}^{(j)} \mathbf{r}) \\
&- \frac{\eta_{6(2)}}{18} \sum_{j \in \mathbf{k}_{6(2)}} \cos(\mathbf{k}_{6(2)}^{(j)} \mathbf{r}) + \frac{\eta_{4(1)}}{18} \sum_{j \in \mathbf{k}_{4(1)}} \cos(\mathbf{k}_{4(1)}^{(j)} \mathbf{r}) \\
&+ \frac{\eta_{4(2)}}{18} \sum_{j \in \mathbf{k}_{4(2)}} \cos(\mathbf{k}_{4(2)}^{(j)} \mathbf{r}) + \frac{\eta_1}{18} \sum_{j \in \mathbf{k}_1} \cos(\mathbf{k}_1^{(j)} \mathbf{r}) . \qquad (32)
\end{aligned}
$$

Distribution functions (31) and (32) are calculated by formula (3), i.e., from the truncated transition channel; for this reason, sums $\sum_{j \in s} \cos(\mathbf{k}_s^{(j)} \mathbf{r})$ in formulas (31) and (32) are taken only over odd rays of non-Lifshitz stars (for Lifshitz stars $\{\mathbf{k}_{10}\}$, summation is performed over all three rays). The values of parameters γ_s and $\varphi_s^{(j)}$ entering into functions (31) and (32) are given in Table 20. In accordance with Fig. 21, coordinates $(x_{\mathrm{I}}, y_{\mathrm{I}}, z_{\mathrm{I}})$ of the disordered $B1$ structure are related to the coordinates of the cubic (space group $Pm\bar{3}m$) Ti_5O_5 superstructure, presented in Table 19, by the following expressions: $x_{\mathrm{I}} = 3x_{\mathrm{cub}}$, $y_{\mathrm{I}} = 3y_{\mathrm{cub}}$, and $z_{\mathrm{I}} = 3z_{\mathrm{cub}}$.

Distribution functions (31) and (32) take 10 different values (see Table 19) at the sites of the metal sublattice in ordered titanium monoxide. The completely ordered state of titanium monoxide is reached when all long-range order parameters equal 1. In this case, the relative concentration of Ti atoms in the metal sublattice is $x = 5/6$, while that of O atoms in the nonmetal sublattice is $z = 5/6$. The stoichiometric composition of an ideal cubic superstructure can be represented as $Ti_{5/6}O_{5/6}$ ($Ti_{0.83}O_{0.83}$) or T_5O_5 ($Ti_{90}■_{18}O_{90}□_{18}$). In the case of equal long-range order parameters, the distribution functions take only two values each, and every sublattice undergoing ordering breaks up only into two sublattices.

Notice that the mutual arrangement of oxygen vacancies with respect to each other in the ideal fully ordered cubic Ti_5O_5 ($Ti_{90}■_{18}O_{90}□_{18}$) superstructure is exactly the same as that of titanium vacancies (see Fig. 21). Evidently, the titanium vacancy sublattice is displaced by vector $(1/2)\langle 111 \rangle_{Pm\bar{3}m} \equiv (3/2)\langle 111 \rangle_{B1}$ in relation to the oxygen vacancy sublattice.

9.3 Relation between monoclinic and cubic Ti_5O_5 superstructures

In disordered nonstoichiometric titanium monoxide $TiO_{1.0}$ ($Ti_{0.83}O_{0.83}$) with an equal number of vacancies in the titanium and oxygen sublattices, the cubic (space group $Pm\bar{3}m$) ordered $Ti_5■O_5□$ phase may form in addition to the known monoclinic (space group $C2/m$) ordered phase of a similar composition. Are these ordered phases alternatives or is an order–order transition possible between them?

The disordered cubic (space group $Fm\bar{3}m$) phase of titanium monoxide TiO_y ($\mathrm{Ti}_x\mathrm{O}_z$) has the point group $m\bar{3}m$ that includes all 48 symmetry elements, h_1-h_{48}, of the total symmetry group of the cube. The point symmetry groups of monoclinic (space group $C2/m$) and cubic (space group $Pm\bar{3}m$) $\mathrm{Ti}_5\mathrm{O}_5$ superstructures include 4 (h_1, h_4, h_{25}, h_{28}) and 48 (h_1-h_{48}) symmetry elements, respectively [1, 2, 30, 31]; they make up subgroups of the point group of the basic disordered cubic (space group $Fm\bar{3}m$) TiO_y ($\mathrm{Ti}_x\mathrm{O}_z$) phase. Therefore, a transition from disordered monoxide to any of these superstructures is a disorder–order phase transformation.

The monoclinic (space group $C2/m$) $\mathrm{Ti}_5\mathrm{O}_5$ superstructure forms via the transition channel involving rays of the Lifshitz $\{\mathbf{k}_{10}\}$ star and two non-Lifshitz $\{\mathbf{k}_4\}$ and $\{\mathbf{k}_1\}$ stars to which three long-range order parameters correspond. The cubic (space group $Pm\bar{3}m$) $\mathrm{Ti}_5\mathrm{O}_5$ superstructure forms via the transition channel involving rays of Lifshitz $\{\mathbf{k}_{10}\}$ star and six non-Lifshitz $\{\mathbf{k}_7\}$, $\{\mathbf{k}_{6(1)}\}$, $\{\mathbf{k}_{6(2)}\}$, $\{\mathbf{k}_{4(1)}\}$, $\{\mathbf{k}_{4(2)}\}$, and $\{\mathbf{k}_1\}$ stars (see Table 20). Under symmetry distortion through a few stars, only critical order parameters corresponding to non-Lifshitz stars should be regarded for the assessment of the type of phase transitions. The number of critical order parameters for monoclinic and cubic $\mathrm{Ti}_5\mathrm{O}_5$ superstructures is greater than 1; therefore, $\mathrm{Ti}_x\mathrm{O}_z \to \mathrm{Ti}_5\mathrm{O}_5$ phase transitions do not satisfy the Landau group-theoretical criterion for second-order phase transitions and are realized through a first-order transition mechanism. The disorder–order transition of the first kind for monoclinic (space group $C2/m$) $\mathrm{Ti}_5\mathrm{O}_5$ superstructures is confirmed experimentally by the change in period a_{B1} of the basic crystalline lattice in titanium monoxide during ordering [120].

As regards phase transformations between $\mathrm{Ti}_5\mathrm{O}_5$ superstructures, the ratio among h_i elements indicates that the monoclinic (space group $C2/m$) superstructure is a subgroup of the cubic (space group $Pm\bar{3}m$) superstructure in terms of symmetry, because its point group is a subgroup of the point group of the cubic $\mathrm{Ti}_5\mathrm{O}_5$ superstructure. This inference is also confirmed by a change in the transition channel that involves the rays of seven stars, $\{\mathbf{k}_{10}\}$, $\{\mathbf{k}_7\}$, $\{\mathbf{k}_{6(1)}\}$, $\{\mathbf{k}_{6(2)}\}$, $\{\mathbf{k}_{4(1)}\}$, $\{\mathbf{k}_{4(2)}\}$, and $\{\mathbf{k}_1\}$, for the cubic $\mathrm{Ti}_5\mathrm{O}_5$ superstructure, and the rays of only three stars, $\{\mathbf{k}_{10}\}$, $\{\mathbf{k}_4\}$, and $\{\mathbf{k}_1\}$, for the monoclinic superstructure. This means that the transition between cubic and monoclinic $\mathrm{Ti}_5\mathrm{O}_5$ phases is the order–order cubic (space group $Pm\bar{3}m$) $\mathrm{Ti}_5\mathrm{O}_5$ phase → monoclinic (space group $C2/m$) $\mathrm{Ti}_5\mathrm{O}_5$ phase transformation accompanied by a 12-fold reduction in rotational symmetry. The cubic (space group $Pm\bar{3}m$) $\mathrm{Ti}_5\mathrm{O}_5$ superstructure is a high-temperature phase with respect to the monoclinic superstructure.

The above results suggest successive realization of disorder–order and order–order cubic (space group $Fm\bar{3}m$) disordered monoxide TiO_y ($\mathrm{Ti}_x\mathrm{O}_z$) → cubic (space group $Pm\bar{3}m$) $\mathrm{Ti}_5\mathrm{O}_5$ superstructure → monoclinic (space group $C2/m$) $\mathrm{Ti}_5\mathrm{O}_5$ superstructure transitions in the homogeneity interval of nonstoichiometric cubic titanium monoxide with decreasing temperature.

9.4 Rhombic $\mathrm{Ti}_3\mathrm{O}_2$ and $\mathrm{Ti}_2\mathrm{O}_3$ superstructures

The authors of Refs [116, 124, 125] observed the appearance of an orthorhombic superstructure with the space group $Immm$ or $I222$ in the $\mathrm{TiO}_{0.7}-\mathrm{TiO}_{0.9}$ region. The orthorhombic M_3X_2 ($M_3X_2\square = M_{2t}X_{2t-1}$, where $t = 1.5$) superstructure described in Section 4.2 has a stoichiometric composition closest to the lower boundary of the homogeneity interval of cubic titanium monoxide $\mathrm{TiO}_{0.70} \equiv \mathrm{Ti}_{0.97}\mathrm{O}_{0.68}$. The maximum value of the long-range order parameter is known to depend on the composition of the compound undergoing ordering [1, 2, 5, 6]. In $M_3X_2\square$ ($t = 1.5$) type orthorhombic ordering of titanium monoxide $\mathrm{TiO}_y = \mathrm{Ti}_x\mathrm{O}_z$ with $z/x \equiv y < 1$, the maximum long-range order parameter in the oxygen sublattice is given by

$$\eta_4^{(\mathrm{O})\max}(z) = 2t(1-z) \equiv 3(1-z) \quad \text{at} \quad t = 1.5\,. \qquad (33)$$

This means that the maximum value of the long-range order parameter in the ordered phase is less than 1 even at the lower boundary of the homogeneity interval of titanium monoxide $\mathrm{TiO}_{0.70} \equiv \mathrm{Ti}_{0.97}\mathrm{O}_{0.68}$ ($y = 0.70$, $z = 0.68$). The orthorhombic (space group $Immm$) $\mathrm{Ti}_3\mathrm{O}_2$ (M_3X_2) superstructure forms via the transition channel presented in Table 5 and has the unit cell depicted in Fig. 7; it is described by the distribution function

$$n_{\mathrm{O}}(x_{\mathrm{I}}, y_{\mathrm{I}}, z_{\mathrm{I}}) = z - \frac{2\eta_4^{(\mathrm{O})}}{3}\cos\left[\frac{4\pi(x_{\mathrm{I}} + y_{\mathrm{I}})}{3}\right]. \qquad (34)$$

Translation vectors of this unit cell and coordinates of atoms and vacancies are listed in Table 6. Distribution function (34) at the sites of the oxygen sublattice assumes two values: $n_{1(\mathrm{O})} = z - 2\eta_4^{(\mathrm{O})}/3$ in positions $2(a)$, and $n_{2(\mathrm{O})} = z + \eta_4^{(\mathrm{O})}/3$ in positions $4(g)$. Evidently, $n_{2(\mathrm{O})}$ for $1 > z > (2t-1)/2t$ always equals 1, and $n_{1(\mathrm{O})} \geqslant 3z - 2$ is always smaller than unity, which means that in the ordered orthorhombic phase of monoxide TiO_y ($y < 1$), the oxygen atoms occupy all $4(g)$ positions, whereas $2(a)$ positions are vacant with a probability of $P = 1 - n_1$, i.e., some of them are occupied by O atoms with probability n_1.

The ordered orthorhombic (space group $Immm$) $\mathrm{Ti}_3\mathrm{O}_2\square$ phase should be distinguished from the hexagonal (space group $P6/mmm$) $\mathrm{TiO}_{0.5}$ (or $\mathrm{Ti}_3\mathrm{O}_2$) phase, which is not a superstructure of cubic monoxide TiO_y. The stoichiometric $\mathrm{Ti}_3\mathrm{O}_2\square$ composition of this superstructure does not enter the homogeneity interval of cubic titanium monoxide and therefore cannot be realized. Only the partly ordered orthorhombic $\mathrm{Ti}_3\mathrm{O}_2\square$ phase forms.

According to Hilti [117], the orthorhombic phase of the nominal $\mathrm{TiO}_{1.20}$ composition is produced from the disordered cubic TiO_y phase with the basic structure $B1$ in the $\mathrm{TiO}_{1.00}-\mathrm{TiO}_{1.20}$ region and belongs to the space groups $Immm$, $Imm2$, or $I222$. The superstructure proposed in Ref. [177] has the same symmetry and Bravais cell as the orthorhombic M_3X_2 superstructure described in Section 4.2, although its Ti atoms and $\blacksquare$ vacancies of the titanium sublattice are ordered, whereas the nonmetal fcc sublattice is totally occupied by oxygen atoms. Thus, the ordered orthorhombic phase proposed in Ref. [177] can be represented as an $M_2\blacksquare X_3$ superstructure inverse with respect to $M_3X_2\square$. Indeed, it was shown in work [122] that ordering of titanium monoxide TiO_y for $y < 1.0$ and $y > 1.0$ can be described via $\mathrm{Ti}_3\mathrm{O}_2\square$ and $\mathrm{Ti}_2\blacksquare\mathrm{O}_3$ superstructures characterized by rhombic symmetry and an ordered arrangement of O atoms and oxygen vacancies $\square$ (for $y < 1.0$) or Ti atoms and titanium vacancies $\blacksquare$ (for $y > 1.0$).

The orthorhombic (space group $Immm$) $\mathrm{Ti}_2\blacksquare\mathrm{O}_3$ ($\mathrm{Ti}_{2t-1}\blacksquare\mathrm{O}_{2t}$, where $t = 1.5$) superstructure forms via the disorder–order transition channel involving $\mathbf{k}_4^{(1)}$ and $\mathbf{k}_4^{(2)} = -\mathbf{k}_4^{(1)}$ rays of the non-Lifshitz $\{\mathbf{k}_4\}$ star with parameter $\mu_4 = 1/3$. The unit cell of the ordered orthorhombic

Table 21. Orthorhombic $Ti_2■O_3$ superstructure and tetragonal $Ti_4■O_5$ superstructure of disordered monoxide Ti_xO_z ($y \equiv z/x > 1$) with the basic $B1$ structure.

Symmetry	Space group	Translation vectors of unit cell	V *	Atom	Position and multiplicity	Atomic coordinates in ideal ordered structure			Values of distribution functions $n_{Ti}(x_I, y_I, z_I)$ and $n_O(x_I, y_I, z_I)$
						x/a_{rh}	y/b_{rh}	z/c_{rh}	
Ortho-rhombic	No. 71 *Immm* (D_{2h}^{25})	$\mathbf{a}_{rh} = \frac{1}{2}\langle 1\bar{1}0\rangle_{B1}$, $\mathbf{b}_{rh} = \frac{3}{2}\langle 110\rangle_{B1}$, $\mathbf{c}_{rh} = \langle 001\rangle_{B1}$	$3a_{B1}^3/2$	Ti1 (vacancy)	$2(c)$	1/2	1/2	0	$n_{1(Ti)} = x - 2\eta_4^{(Ti)}/3$
				Ti2	$4(h)$	0	2/3	1/2	$n_{2(Ti)} = y + \eta_4^{(Ti)}/3$
				O1	$2(a)$	0	0	0	$n_O = z$
				O2	$4(g)$	0	1/3	0	$n_O = z$
						x/a_t	y/b_t	z/c_t	
Tetragonal	No. 87 $I4/m$ (C_{4h}^5)	$\mathbf{a}_t = \frac{1}{2}\langle 310\rangle_{B1}$, $\mathbf{b}_t = \frac{1}{2}\langle \bar{1}30\rangle_{B1}$, $\mathbf{c}_t = \langle 001\rangle_{B1}$	$5a_{B1}^3/2$	Ti1 (vacancy)	$2(a)$	0	0	0	$n_{1(Ti)} = x - 4\eta_1^{(Ti)}/5$
				Ti2	$8(h)$	2/5	1/5	0	$n_{2(Ti)} = x + \eta_1^{(Ti)}/5$
				O1	$2(b)$	0	0	1/2	$n_O = z$
				O2	$8(h)$	1/10	3/10	0	$n_O = z$

* The volume of the unit cell of a superstructure expressed through parameter a_{B1} of the unit cell of the basic disordered structure of type $B1$.

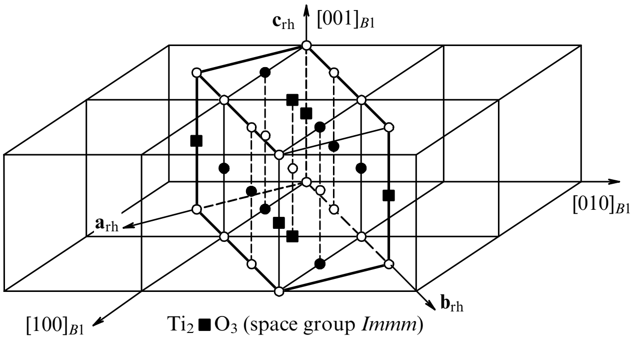

Figure 22. Position of the orthorhombic (space group *Immm*) unit cell of $Ti_2■O_3$ monoxide superstructure $TiO_y \equiv Ti_xO_z$ ($y \equiv z/x > 1$) in the lattice with the basic $B1$ structure: (○) oxygen atom, (●) titanium atom, and (■) vacancy in metal sublattice (titanium vacancy).

(space group *Immm*) $Ti_2■O_3$ phase of monoxide TiO_y with $y > 1$ (Fig. 22) is inverse with regard to the unit cell of the rhombic M_3X_2 ($Ti_3O_2□$) superstructure (see Fig. 7) and can be obtained by substituting nonmetal sublattice sites for metal sublattice ones. Translation vectors and coordinates of atoms and vacancies in the unit cell of the $Ti_2■O_3$ phase are presented in Table 21. The distribution function of Ti atoms over the sites of the titanium sublattice in the orthorhombic $Ti_2■O_3$ superstructure of monoxide Ti_xO_z has the form

$$n_{Ti}(x_I, y_I, z_I) = x - \frac{2\eta_4^{(Ti)}}{3} \cos\left[\frac{4\pi(x_I + y_I)}{3}\right]. \qquad (35)$$

During the ordering in the metal sublattice of titanium monoxide Ti_xO_z, in which $1 > x > (2t-1)/2t$ and $y \equiv z/x > 1$, the maximum value of the long-range order parameter is equal to

$$\eta_4^{(Ti)\,max}(x) = 2t(1-x) \equiv 3(1-x) \quad \text{at} \quad t = 1.5\,. \qquad (36)$$

At the upper boundary of the TiO_y ($y \approx 1.28$, $x \approx 0.77$) monoxide homogeneity interval, the maximum value of the long-range order parameter $\eta_4^{(Ti)}$ in the ordered Ti_2O_3 phase does not exceed 0.70. Distribution function (36) at the sites of the metal sublattice takes two values: $n_{1(Ti)}$ in $2(c)$ positions, and $n_{2(Ti)}$ in $4(h)$ positions (see Table 21). In the case of a maximum value of long-range order parameter and $1 > x > (2t-1)/2t$, $n_{2(Ti)}$ always equals 1 and $x \geqslant n_{1(Ti)} \geqslant 3x - 2$ is always smaller than unity. This means that the titanium atoms occupy all $4(h)$ positions in the ordered rhombic phase of monoxide TiO_y ($y > 1$), whereas $2(c)$ positions are vacant with a probability of $P = 1 - n_{1(Ti)}$.

The $Ti_2■O_3$ superstructure should be distinguished from the trigonal Ti_2O_3 phase which is not the ordered phase of titanium monoxide TiO_y.

9.5 Tetragonal Ti_4O_5 superstructure

The unit cell of the tetragonal (space group $I4/m$) $Ti_4■O_5$ superstructure of monoxide $TiO_y \equiv Ti_xO_z$ with $y \equiv z/x > 1$ is shown in Fig. 23. Such an ordered phase was examined in Ref. [125]. Translation vectors and coordinates of atoms and vacancies in the unit cell of this phase are presented in Table 21. The tetragonal (space group $I4/m$) Ti_4O_5 superstructure forms via the disorder–order transition channel involving four rays: $\mathbf{k}_1^{(1)}$, $\mathbf{k}_1^{(2)} = -\mathbf{k}_1^{(1)}$, $\mathbf{k}_1^{(13)}$, and

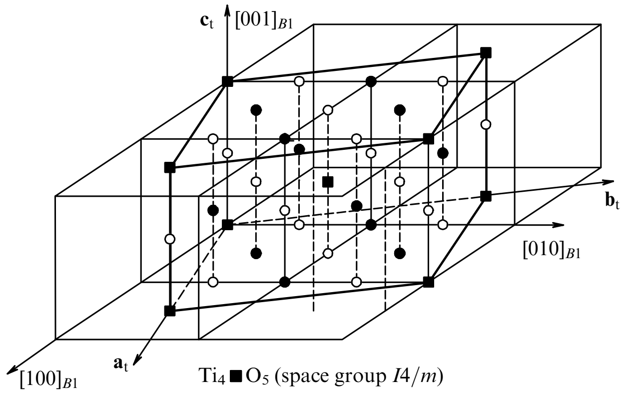

Figure 23. Position of the tetragonal (space group $I4/m$) unit cell of $Ti_4■O_5$ superstructure of the $TiO_y \equiv Ti_xO_z$ ($y \equiv z/x > 1$) monoxide in a lattice with the basic $B1$ structure: (○) oxygen atom, (●) titanium atom, and (■) vacancy in metal sublattice (titanium vacancy).

$\mathbf{k}_1^{(14)} = -\mathbf{k}_1^{(13)}$ of the non-Lifshitz $\{\mathbf{k}_1\}$ star with parameters $\mu_1^{(1)} = 2/5$ and $\mu_1^{(2)} = 1/5$.

The distribution function of Ti atoms over the sites of the titanium sublattice in the tetragonal $Ti_4\blacksquare O_5$ ($Ti_{2t-1}\blacksquare O_{2t}$, where $t = 2.5$) superstructure of the Ti_xO_z monoxide has the form

$$n_{\mathrm{Ti}}(x_\mathrm{I}, y_\mathrm{I}, z_\mathrm{I}) = x - \frac{2\eta_1^{(\mathrm{Ti})}}{5}\left\{\cos\left[\frac{4\pi(x_\mathrm{I} + 2y_\mathrm{I})}{5}\right] + \cos\left[\frac{4\pi(2x_\mathrm{I} - y_\mathrm{I})}{5}\right]\right\}. \qquad (37)$$

Referring to Fig. 23, coordinates $(x_\mathrm{I}, y_\mathrm{I}, z_\mathrm{I})$ of the disordered cubic $B1$ structure are related to the coordinates of the tetragonal (space group $I4/m$) Ti_4O_5 superstructure, presented in Table 21, by the following expressions: $x_\mathrm{I} = 3x_\mathrm{t}/2 - y_\mathrm{t}/2$, $y_\mathrm{I} = x_\mathrm{t}/2 + 3y_\mathrm{t}/2$, and $z_\mathrm{I} = z_\mathrm{t}$. At all sites of the metal sublattice, function (37) takes two values (see Table 21).

9.6 Tetragonal $V_{52}O_{64}$ superstructure

A peculiar structural feature of the ordered $V_{52}O_{64}$ phase is that four of the 52 vanadium atoms occupy tetrahedral interstices of the basic cubic lattice. This property is extrinsic to nonstoichiometric MX_y compounds with the $B1$ structure, where metal M atoms populate $4(a)$ positions with coordinates (000), and nonmetal X atoms occupy $4(b)$ positions with coordinates (1/2 1/2 1/2). Positions $4(b)$ and $4(a)$ are octahedrally surrounded by the sites of metal and nonmetal sublattices, respectively. The tetrahedral interstices, i.e., crystallographic $8(c)$ positions with coordinates (1/4 1/4 1/4), in disordered nonstoichiometric compounds with the $B1$ structure are always vacant. In all known superstructures of nonstoichiometric compounds with the $B1$ structure, both the atoms and the vacancies are redistributed only over the $4(b)$ or $4(a)$ positions of the basic disordered lattice. The structure of the $V_{52}O_{64}$ phase is such that V atoms are distributed during ordering over two different sublattices, namely over the sites of the basic nonmetal fcc sublattice and over some of the sites of the cubic sublattice formed by tetrahedral interstices. The crystalline structure of disordered nonstoichiometric vanadium monoxide was studied with reference to peculiarities of the $V_{52}O_{64}$ superstructure in Refs [135, 142]. It was shown that the disordered VO_y monoxide has a cubic (space group $Fm\bar{3}m$) structure of the type $D0_3$ differing from the generally accepted $B1$ structure, making ordering in monoxide VO_y fundamentally different from that in titanium monoxide $Ti_{0.83}O_{0.83}$, in which two atomic species (Ti and O) are ordered in two equitype basic fcc sublattices.

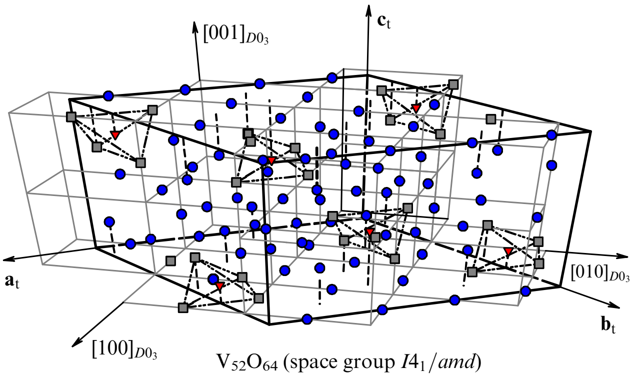

Figure 24. (Color online.) Position of the tetragonal (space group $I4_1/amd$) unit cell of an ideal $V_{52}O_{64}$ ($V_{52}\blacksquare_{12}O_{64}$) superstructure in the basic cubic lattice with the $D0_3$ structure: (●) vanadium (V) atoms in octahedral positions, (▼) vanadium (V) atoms filling tetrahedral interstices of the basic disordered lattice, and (■) vacant sites of the metal sublattice. Oxygen atoms are not shown.

The position of the unit cell in the ideal tetragonal (space group $I4_1/amd$) $V_{52}O_{64}$ superstructure in its cubic lattice with the $D0_3$ structure is shown in Fig. 24. Translation vectors and coordinates of atoms and vacancies for this cell are presented in Table 22. The $V_{52}O_{64}$ superstructure forms via the disorder–order transition channel involving $\mathbf{k}_{10}^{(2)}$ and $\mathbf{k}_{10}^{(3)}$ rays of the Lifshitz $\{\mathbf{k}_{10}\}$ star, four rays $\mathbf{k}_4^{(1)}$, $\mathbf{k}_4^{(2)} = -\mathbf{k}_4^{(1)}$, $\mathbf{k}_4^{(3)}$, $\mathbf{k}_4^{(4)} = -\mathbf{k}_4^{(3)}$ of the 12-ray $\{\mathbf{k}_4\}$ star with parameter $\mu_4 = 1/4$, eight rays $\mathbf{k}_3^{(1)}$, $\mathbf{k}_3^{(2)} = -\mathbf{k}_3^{(1)}$, $\mathbf{k}_3^{(3)}$, $\mathbf{k}_3^{(4)} = -\mathbf{k}_3^{(3)}$, $\mathbf{k}_3^{(5)}$, $\mathbf{k}_3^{(6)} = -\mathbf{k}_3^{(5)}$, $\mathbf{k}_3^{(7)}$, and $\mathbf{k}_3^{(8)} = -\mathbf{k}_3^{(7)}$ of the 24-ray $\{\mathbf{k}_3\}$ star with parameter $\mu_3 = 1/8$, and eight rays $\mathbf{k}_2^{(1)} = \mu_1(\mathbf{b}_1 + \mathbf{b}_2) + \mu_2\mathbf{b}_3$, $\mathbf{k}_2^{(2)} = -\mathbf{k}_2^{(1)}$, $\mathbf{k}_2^{(3)}$, $\mathbf{k}_2^{(4)} = -\mathbf{k}_2^{(3)}$, $\mathbf{k}_2^{(5)}$, $\mathbf{k}_2^{(6)} = -\mathbf{k}_2^{(5)}$, $\mathbf{k}_2^{(7)}$, and $\mathbf{k}_2^{(8)} = -\mathbf{k}_2^{(7)}$ of the 24-ray $\{\mathbf{k}_2\}$ star with parameters $\mu_2 = 1/4$ and $\mu_1 = 3/8$.

During the formation of the $V_{52}O_{64}$ superstructure, vanadium atoms undergo redistribution over two Ising

Table 22. Ideal tetragonal [space group No. 141 — $I4_1/amd\,(D_{4h}^{19})$] $V_{52}O_{64}$ ($V_{52}\blacksquare_{12}O_{64}$) superstructure: $Z = 1$, $V = 16a_{B1}^3$, $\mathbf{a}_\mathrm{t} = \langle 2\bar{2}0\rangle_{B1}$, $\mathbf{b}_\mathrm{t} = \langle 220\rangle_{B1}$, and $\mathbf{c}_\mathrm{t} = \langle 002\rangle_{B1}$.

Atom	Position and multiplicity	Atomic coordinates in ideal ordered structure			Values of distribution functions $n_{\mathrm{V}(1)}(x_\mathrm{I}, y_\mathrm{I}, z_\mathrm{I})$ and $n_{\mathrm{V}(2)}(x_\mathrm{I}, y_\mathrm{I}, z_\mathrm{I})$ of vanadium atoms
		x/a_t	y/b_t	z/c_t	
V1 (vacancy)	$16(h)$	0	5/8	1/4	$n_{1(\mathrm{V}(2))} = x - \eta_{10}/16 - \eta_4/4 - \eta_3/4 - \eta_2/4$
V2	$16(h)$	0	1/8	1/4	$n_{2(\mathrm{V}(2))} = x - \eta_{10}/16 - \eta_4/4 + \eta_3/4 + \eta_2/4$
V3	$16(f)$	1/8	0	0	$n_{3(\mathrm{V}(2))} = x - \eta_{10}/16 + \eta_4/4 + \eta_3/4 - \eta_2/4$
V4	$16(f)$	5/8	0	0	$n_{4(\mathrm{V}(2))} = x - \eta_{10}/16 + \eta_4/4 - \eta_3/4 + \eta_2/4$
V5	$4(a)$*	0	3/4	1/8	$n_{1(\mathrm{V}(1))} = \eta_{10}$
O1	$16(h)$	0	1/8	1/2	
O2	$16(h)$	0	7/8	0	
O3	$32(i)$	1/8	0	1/4	

* Tetrahedral interstice — position $8(c)$ of the basic disordered $D0_3$ structure.

lattices. Let us find the distribution function $n_V^{(1)}$ for V atoms in the Ising lattice formed by four of the 128 tetrahedral (c) sites of the basic cubic $D0_3$ structure: it is represented by four sites in position (a) of the tetragonal $V_{52}O_{64}$ structure (see Table 22 and Fig. 24). The distribution of V atoms over this lattice is governed by the rays of the $\{\mathbf{k}_{10}\}$ star. In the disordered state, V atoms do not occupy tetrahedral sites, i.e., $x = 0$. Therefore, the distribution function for V atoms over the Ising lattice formed by four tetrahedral sites of the basic $D0_3$ structure is given by

$$n_{V(1)}(x_I, y_I, z_I) = -\frac{\eta_{10}}{2}\left[\sin(2\pi x_I) + \sin(2\pi y_I)\right] \qquad (38)$$

and takes a single value $n_{1(V(1))} = \eta_{10}$ at the 4(a) sites of the $V_{52}O_{64}$ superstructure.

The distribution function for V atoms in the second Ising lattice formed by octahedral (a) sites of the basic $D0_3$ structure is related to the rays of three stars $\{\mathbf{k}_4\}$, $\{\mathbf{k}_3\}$, and $\{\mathbf{k}_2\}$. This lattice of the $V_{52}O_{64}$ superstructure contains 64 sites located in four 16-fold positions (f) and (h) (see Table 22). When the $V_{52}O_{64}$ superstructure forms in oxide V_xO_z (VO_y), some of the V atoms pass from the second Ising lattice to the first one; due to this, the order parameter η_{10} is also present in the distribution function of V atoms over the second Ising lattice. In the end, the first lattice contains $4\eta_{10}$ vanadium atoms, whereas their number in the second lattice decreases from $64x$ to $64x - 4\eta_{10}$. The relative number of sites in the second lattice occupied by V atoms decreases from x to $(x - \eta_{10}/16)$. In accordance with this fact and the transition channel peculiarities, the distribution function $n_{V(2)}(\mathbf{r})$ for V atoms in the second Ising lattice has the form

$$\begin{aligned}
n_{V(2)}(x_I, y_I, z_I) &= x - \frac{\eta_{10}}{16} \\
&+ \frac{\eta_4}{4}\Big\{\sin\left[\pi(x_I + y_I)\right] - \cos\left[\pi(x_I - y_I)\right]\Big\} \\
&- \frac{\eta_3}{8}\Bigg\{\sqrt{2}\sin\left[\frac{\pi(x_I + 3y_I + 2z_I)}{2}\right] \\
&+ \cos\left[\frac{\pi(x_I - 3y_I - 2z_I)}{2}\right] - \sin\left[\frac{\pi(x_I - 3y_I - 2z_I)}{2}\right] \\
&- \cos\left[\frac{\pi(-x_I + 3y_I - 2z_I)}{2}\right] - \sin\left[\frac{\pi(-x_I + 3y_I - 2z_I)}{2}\right] \\
&- \sqrt{2}\sin\left[\frac{\pi(-x_I - 3y_I + 2z_I)}{2}\right]\Bigg\} \\
&- \frac{\eta_2}{8}\Bigg\{\cos\left[\frac{\pi(x_I + y_I + 2z_I)}{2}\right] + \sin\left[\frac{\pi(x_I + y_I + 2z_I)}{2}\right] \\
&- \sqrt{2}\cos\left[\frac{\pi(x_I - y_I - 2z_I)}{2}\right] \\
&- \sqrt{2}\cos\left[\frac{\pi(-x_I + y_I - 2z_I)}{2}\right] \\
&- \cos\left[\frac{\pi(-x_I - y_I + 2z_I)}{2}\right] + \sin\left[\frac{\pi(-x_I - y_I + 2z_I)}{2}\right]\Bigg\}
\end{aligned} \qquad (39)$$

and depends on four long-range order parameters η_{10}, η_4, η_3, and η_2. It follows from Fig. 24 that coordinates (x_I, y_I, z_I) of the disordered cubic $D0_3$ structure are related to the coordinates of the tetragonal (space group $I4_1/amd$) $V_{52}O_{64}$ superstructure, listed in Table 22, by the following expressions: $x_I = 2x_t + 2y_t - 3/4$, $y_I = -2x_t + 2y_t + 5/4$, and $z_I = 2z_t$.

In an ideal ordered phase with order parameters $\eta_4 = \eta_3 = \eta_2 = 1$, the quantity $x - \eta_{10}/16 = 3/4$; therefore, the fraction of sites occupied by V atoms in two sublattices undergoing ordering equals $x = 13/16$ at $\eta_{10} = 1$. In other words, the relative stoichiometric concentration of V atoms in the totally ordered tetragonal phase is $x_{st} = 13/16$. Distribution function (39) of V atoms at the sites of the ordered metal sublattice in the tetragonal $V_{52}O_{64}$ superstructure with an arbitrary degree of order takes 4 different values: $n_{1(V(2))}$, $n_{2(V(2))}$, $n_{3(V(2))}$, and $n_{4(V(2))}$ (see Table 22). These values in 16(h) and 16(f) positions of the metal sublattice depend on all four long-range order parameters η_{10}, η_4, η_3, and η_2. At the same time, the $n_{1(V(1))}$ value of distribution function (38) in tetrahedral 4(a) positions depends on parameter η_{10} alone (see Table 22).

Symmetry distortion over a few irreducible representations and the presence of rays of non-Lifshitz stars in the transition channel suggest that the VO_y (space group $Fm\bar{3}m$) → $V_{52}O_{64}$ (space group $I4_1/amd$) phase transition does not fulfill the Landau group-theoretical criterion for second-order phase transitions and is realized through the first-order transition mechanism.

The point symmetry group $4/mmm$ (D_{4h}) of the tetragonal $V_{52}O_{64}$ superstructure includes 16 symmetry elements, $h_1 - h_4$, $h_{13} - h_{16}$, $h_{25} - h_{28}$, $h_{37} - h_{40}$, from the 48 elements, $h_1 - h_{48}$, making up the $m\bar{3}m$ (O_h) point group of the basic disordered cubic VO_y phase; hence, the rotational symmetry reduction reaches 3. Translational symmetry reduction equals the ratio between the unit cell volumes of ordered and disordered phases and amounts to 16 in our case. Therefore, the overall symmetry reduction in the disordered cubic monoxide (space group $Fm\bar{3}m$) VO_y → ordered tetragonal (space group $I4_1/amd$) $V_{52}O_{64}$ phase transition is $N = 48$.

9.7 Monoclinic $V_{14}O_6$ superstructure

The monoclinic (space group $C2/m$) $V_{14}O_6$ superstructure is produced during ordering of an oxygen solid solution in vanadium β-V(O). The solid β-V(O) solution has a body-centered tetragonal (bct) lattice with the $I4/mmm$ space group. The bct lattice with periods a and c possesses a reciprocal lattice with structural vectors $\mathbf{b}_1 = \langle 0\ \pi/a\ \pi/c\rangle$, $\mathbf{b}_2 = \langle \pi/a\ 0\ \pi/c\rangle$, and $\mathbf{b}_3 = \langle \pi/a\ \pi/a\ 0\rangle$ [30, 31]. The position of the unit cell of an ideal $V_{14}O_6$ superstructure in the basic tetragonal lattice is illustrated in Fig. 25. Translation vectors and the coordinates of atoms and vacancies for this cell are presented in Table 23.

The $V_{14}O_6$ superstructure forms via the disorder–order transition channel involving two rays of each of the three 8-ray non-Lifshitz $\{\mathbf{k}_{1-1}\}$, $\{\mathbf{k}_{1-2}\}$, and $\{\mathbf{k}_{1-3}\}$ stars of the $\{\mathbf{k}_1\}$ type. The vector-representative for the $\{\mathbf{k}_1\}$ star of the reciprocal bct lattice has the form $\mathbf{k}_1^{(1)} = \nu\mathbf{b}_2 + \mu(\mathbf{b}_3 - \mathbf{b}_1)$. The stars to which superstructure vectors belong differ only in the ray length, i.e., the numerical values of parameters ν and μ. The $\{\mathbf{k}_{1-1}\}$ star has parameters $\nu_1 = 2/7$ and $\mu_1 = -1/7$; for the $\{\mathbf{k}_{1-2}\}$ star $\nu_2 = 1/7$ and $\mu_2 = 3/7$, and for the $\{\mathbf{k}_{1-3}\}$ star $\nu_3 = 4/7$ and $\mu_3 = -2/7$. The transition channel involves two $\mathbf{k}_{1-1}^{(1)} = 2\mathbf{b}_2/7 - (\mathbf{b}_3 - \mathbf{b}_1)/7 = [1/7\ 0\ 3/7]$ and $\mathbf{k}_{1-1}^{(2)} = -\mathbf{k}_{1-1}^{(1)}$ rays of the $\{\mathbf{k}_{1-1}\}$ star, two $\mathbf{k}_{1-2}^{(1)} =$

Table 23. Monoclinic [space group No. 12 — $C2/m$ (C^3_{2h})] $V_{14}O_6$ superstructure; $Z = 1$, $\mathbf{a}_m = \langle 30\bar{1}\rangle_{bct}$, $\mathbf{b}_m = \langle 010\rangle_{bct}$, and $\mathbf{c}_m = \langle 102\rangle_{bct}$.

Atom	Position and multiplicity	Atomic coordinates in ideal ordered structure			Values of distribution function $n_O(x_I, y_I, z_I)$* of oxygen atoms
		x/a_m	y/b_m	z/c_m	
O1	2(a)	0	0	0	$n_{1(O)} = y + \gamma^{(1)}_{1-1}\eta_{1-1} + \gamma^{(1)}_{1-2}\eta_{1-2} + \gamma^{(1)}_{1-3}\eta_{1-3}$
O2	4(i)	2/7	0	1/7	$n_{2(O)} = y + \cos(2\pi/7)\gamma^{(1)}_{1-1}\eta_{1-1} - \cos(\pi/7)\gamma^{(1)}_{1-2}\eta_{1-2} - \cos(3\pi/7)\gamma^{(1)}_{1-3}\eta_{1-3}$
O3 (vacancy)	4(i)	6/7	0	3/7	$n_{3(O)} = y - \cos(\pi/7)\gamma^{(1)}_{1-1}\eta_{1-1} - \cos(3\pi/7)\gamma^{(1)}_{1-2}\eta_{1-2} + \cos(2\pi/7)\gamma^{(1)}_{1-3}\eta_{1-3}$
O4 (vacancy)	4(i)	4/7	0	2/7	$n_{4(O)} = y - \eta_{1-1}/7 - \eta_{1-2}/7 - \eta_{1-3}/7$
V1	2(d)	0	1/2	1/2	
V2	4(i)	9/14	0	1/14	
V3	4(i)	11/14	0	9/14	
V4	4(i)	13/14	0	3/14	

* $\gamma^{(1)}_{1-1} = 1/[7\cos(3\pi/7)]$, $\gamma^{(1)}_{1-2} = -1/[7\cos(2\pi/7)]$, $\gamma^{(1)}_{1-3} = 1/[7\cos(\pi/7)]$.

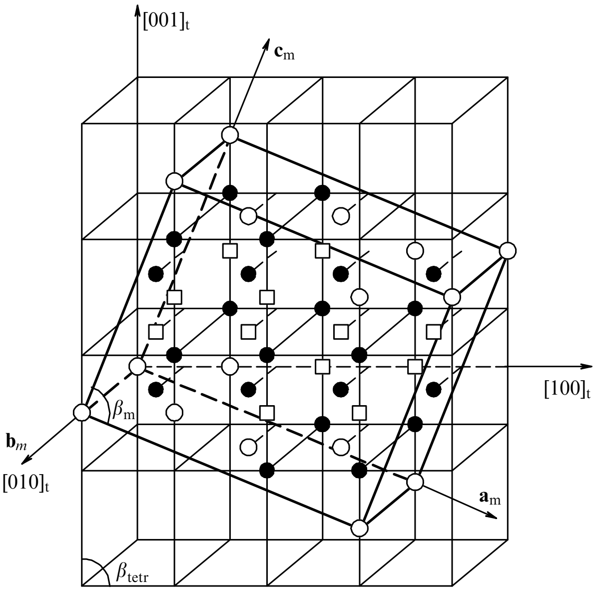

Figure 25. Position of the monoclinic (space group $C2/m$) unit cell of the $V_{14}O_6$ superstructure in the body-centered tetragonal lattice: (●) vanadium (V) atom, (○) oxygen (O) atom, and (□) vacancy in oxygen sublattice.

$\mathbf{b}_2/7 + 3(\mathbf{b}_3 - \mathbf{b}_1)/7 = [4/7\ 0\ -2/7]$ and $\mathbf{k}^{(2)}_{1-2} = -\mathbf{k}^{(1)}_{1-2}$ rays of the $\{\mathbf{k}_{1-2}\}$ star, and two $\mathbf{k}^{(1)}_{1-3} = 4\mathbf{b}_2/7 - 2(\mathbf{b}_3 - \mathbf{b}_1)/7 = [2/7\ 0\ 6/7]$ and $\mathbf{k}^{(2)}_{1-3} = -\mathbf{k}^{(1)}_{1-3}$ rays of the $\{\mathbf{k}_{1-3}\}$ star. The simultaneous presence of the rays of several non-Lifshitz stars in the transition channel unambiguously suggests the first kind of the β-V(O) (space group $I4/mmm$) → γ-phase of $V_{14}O_6$ (space group $C2/m$) phase transformation under consideration.

The distribution function of oxygen atoms in the monoclinic (space group $C2/m$) $V_{14}O_6$ superstructure with any degree of order has the form

$$n_O(x_I, y_I, z_I) = y + \frac{\eta_{1-1}}{7\cos(3\pi/7)}\cos\left[\frac{2\pi(x_I + 3z_I)}{7}\right] - \frac{\eta_{1-2}}{7\cos(2\pi/7)}\cos\left[\frac{2\pi(4x_I - 2z_I)}{7}\right] + \frac{\eta_{1-3}}{7\cos(\pi/7)}\cos\left[\frac{2\pi(2x_I + 6z_I)}{7}\right]. \tag{40}$$

Referring to Fig. 25, coordinates (x_I, y_I, z_I) of a basic disordered body-centered structure are related by expressions $x_I = 3x_m + z_m$, $y_I = y_m$, and $z_I = -x_m + 2z_m$ to the coordinates of the monoclinic (space group $C2/m$) $V_{14}O_6$ superstructure, presented in Table 23. Given arbitrary values of the long-range order parameters, distribution function (40) takes 4 different values (see Table 23).

The point symmetry group $2/m$ (C_{2h}) of the monoclinic $V_{14}O_6$ superstructure includes 4 symmetry elements h_1, h_4, h_{25}, and h_{28}, while the point group $4/mmm$ (D_{4h}) of the basic tetragonal disordered β-phase of V(O) consists of 16 elements: $h_1 - h_4$, $h_{13} - h_{16}$, $h_{25} - h_{28}$, and $h_{37} - h_{40}$ [30, 31]; hence, rotational symmetry reduction equals 4. The unit cell volume increases by a factor of 7 during transition from the disordered β-phase to monoclinic $V_{14}O_6$ suboxide; therefore, the translational symmetry reduction reaches 7, while the overall symmetry reduction in the β-V(O) (space group $I4/mmm$) → γ-phase of $V_{14}O_6$ (space group $C2/m$) transformation amounts to 28.

10. Conclusion

The most distinctive feature of strongly nonstoichiometric compounds is the high concentration of structural vacancies that can vary from zero to a few dozen atomic percent at the lower boundary of the homogeneity interval. The high vacancy concentration is a prerequisite for disorder or order in the distribution of atoms and vacancies in the structure of nonstoichiometric compounds. Deviations from the statistical (disordered) distribution of atoms and vacancies affect their crystalline structure, as is apparent from the appearance of short- or long-range orders. The former characterizes only the radial distribution of the atoms, i.e., fluctuations of the atomic concentrations in different coordination spheres. The long-range order includes both radial and angular distributions and permits determining the atom of which kind is located in one site or another of the crystal lattice.

The present review gives evidence that atom–vacancy ordering in strongly nonstoichiometric interstitial compounds is a widespread phenomenon, even though superstructures of many nonstoichiometric compounds have not yet been identified.

Superstructures of nonstoichiometric compounds are more diverse and frequently more complicated than those of solid substitution solutions (alloys). Indeed, ordering in nonstoichiometric compounds, e.g., cubic titanium and vanadium monoxides, may simultaneously occur in several sublattices of a basic disordered structure.

Changes in the properties of strongly nonstoichiometric compounds as a result of ordering are similar in magnitude to those in the compositions within the homogeneity interval of an ordered phase. Thus, variation in the composition of strongly nonstoichiometric compounds and redistribution of atoms and vacancies in their crystal lattices are two equitable ways to modify the characteristics of these compounds, creating an additional motivation to study superstructures of nonstoichiometric compounds.

This study was supported by the RFBR projects 13-03-00077a.

References

1. Gusev A I, Rempel A A, Magerl A J *Disorder and Order in Strongly Nonstoichiometric Compounds: Transition Metal Carbides, Nitrides, and Oxides* (Berlin: Springer, 2001)
2. Gusev A I *Nestekhiometriya, Besporyadok, Blizhnii i Dal'nii Poryadok v Tverdom Tele* (Nonstoichiometry, Disorder, Short- and Long-Range Orders in a Solid) (Moscow: Fizmatlit, 2007)
3. Gusev A I, Rempel A A *Phys. Status Solidi A* **163** 273 (1997)
4. Gusev A I, Rempel A A, in *Materials Science of Carbides, Nitrides, and Borides* (NATO Science Ser. Partnership Sub-Ser. 3, High Technology, Vol. 68, Eds Y G Gogotsi, R A Andrievski) (Dordrecht: Kluwer Acad. Publ., 1999) p. 47
5. Gusev A I *Phys. Usp.* **43** 1 (2000); *Usp. Fiz. Nauk* **170** 3 (2000)
6. Gusev A I, Rempel A A *Nestekhiometriya, Besporyadok i Poryadok v Tverdom Tele* (Nonstoichiometry, Disorder and Order in a Solid) (Ekaterinburg: UrO RAN, Institut Khimii Tverdogo Tela, 2001)
7. Rabenau A (Ed.) *Problems of Nonstoichiometry* (Amsterdam: North-Holland, 1970)
8. Richter J B *Anfangsgründen der Stöchiometrie oder Messkunst chemischer Elemente* Bd. 1, 2 (Breslau: J.F. Korn dem Aeltern 1792, 1794)
9. Kurnakov N S *Izbrannye Trudy* (Selected Works) Vols 1–3 (Moscow: Izd. AN SSSR, 1960–1963)
10. Parthé E, Yvon K *Acta Cryst. B* **26** 153 (1970)
11. Gusev A I, Rempel A A *Termodinamika Strukturnykh Vakansii v Nestekhiometricheskikh Fazakh Vnedreniya* (Thermodynamics of Structural Vacancies in Nonstoichiometric Interstitial Phases) (Sverdlovsk: UNTs AN SSSR, 1987)
12. Gusev A I, Rempel A A *Strukturnye Fazovye Perekhody v Nestekhiometricheskikh Soedineniyakh* (Structural Phase Transitions in Nonstoichiometric Compounds) (Moscow: Nauka, 1988)
13. Gusev A I *Fizicheskaya Khimiya Nestekhiometricheskikh Tugoplavkikh Soedinenii* (Physical Chemistry of Nonstoichiometric Refractory Compounds) (Moscow: Nauka, 1991)
14. Rempel A A *Effekty Uporyadocheniya v Nestekhiometricheskikh Soedineniyakh Vnedreniya* (Ordering Effects in Nonstoichiometric Interstitial Compounds) (Ekaterinburg: Nauka, 1992)
15. Gusev A I, Rempel A A *Phys. Status Solidi B* **131** 43 (1985)
16. Gusev A I, Rempel A A *Phys. Status Solidi B* **140** 335 (1987)
17. Gusev A I *Philos. Mag. B* **60** 307 (1989)
18. Novotnyi G, Benezovskii F, in *Metallovedenie: Struktura i Svoistva Stalei i Splavov. Metallidy. Novye Metody Issledovaniya. Materialy Simpoziuma po Metallurgii i Metallovedeniyu, Posvyashchennogo 100-letiyu Otkrytiya D.K. Chernovym Polimorfizma Zheleza (14–18 Maya 1968 g.)* (Metal Science: The Structure and Properties of Steels and Alloys, Metalloids, New Research Methods. Proc. of the Symp. on Metallurgy and Metallography, Dedicated to the 100th Anniversary of the Opening by D K Chernov of Iron Polymorphism (14–18 May 1968)) (Ed. N V Ageev) (Moscow: Nauka, 1971) p. 315
19. De Novion C H, Maurice V *J. Physique Colloq.* **38** C7-211 (1977)
20. Khaenko B V *Poroshkovaya Metallurgiya* (1) 71 (1978)
21. Khaenko B V *Izv. Akad. Nauk SSSR. Neorgan. Mater.* **15** 1952 (1979)
22. De Novion C H, Landesman J P *Pure Appl. Chem.* **57** 1391 (1985)
23. De Novion C H et al., in *The Physics and Chemistry of Carbides, Nitrides, and Borides* (NATO ASI Ser. Ser. E, No. 185, Ed. R Freer) (Dordrecht: Kluwer Acad. Publ., 1990) p. 329
24. Lipatnikov V N, Gusev A I *Uporyadochenie v Karbidakh Titana i Vanadiya* (Ordering in Titanium and Vanadium Carbides) (Ekaterinburg: UrO RAN. Institut Khimii Tverdogo Tela, 2000)
25. Gusev A I *Phys. Status Solidi B* **163** 17 (1991)
26. Gusev A I, Rempel A A *Phys. Status Solidi A* **135** 15 (1993)
27. Rempel' A A *Phys. Usp.* **39** 31 (1996); *Usp. Fiz. Nauk* **166** 33 (1996)
28. Gusev A I *Russ. Chem. Rev.* **71** 439 (2002); *Usp. Khim.* **71** 507 (2002)
29. Lipatnikov V N *Russ. Chem. Rev.* **74** 697 (2005); *Usp. Khim.* **74** 768 (2005)
30. Kovalev O V *Neprivodimye Predstavleniya Prostranstvennykh Grupp* (Irreducible Representations of the Space Groups) (Kiev: Izd. AN UkrSSR, 1961)
31. Kovalev O V *Irreducible Representations of the Space Groups* (New York: Gordon and Breach, 1965); Translated from Russian: *Neprivodimye i Indutsirovannye Predstavleniya i Kopredstavleniya Fedorovskikh Grupp* (Moscow: Nauka, 1986)
32. Gusev A I, Rempel' A A *Sov. Phys. Solid State* **26** 2178 (1984); *Fiz. Tverd. Tela* **26** 3622 (1984)
33. Gusev A I, Rempel A A *Phys. Status Solidi A* **93** 71 (1986)
34. Gusev A I, Rempel A A *J. Phys. C Solid State Phys.* **20** 5011 (1987)
35. Naish V E, Syromyatnikov V N *Sov. Phys. Crystallogr.* **21** 627 (1976); *Kristallogr.* **21** 1085 (1976)
36. Khachaturyan A G *Teoriya Fazovykh Prevrashchenii i Struktura Tverdykh Rastvorov* (The Theory of Phase Transformations and the Structure of Solid Solutions) (Moscow: Nauka, 1974)
37. Lipatnikov V N, Zueva L V, Gusev A I, Kottar A *Phys. Solid State* **40** 1211 (1998); *Fiz. Tverd. Tela* **40** 1332 (1998)
38. Goretzki H *Phys. Status Solidi B* **20** K141 (1967)
39. Karimov I et al. *Izv. Akad. Nauk UzSSR. Ser. Fiz.-Mat. Nauk* (4) 81 (1979)
40. Arbuzov M P, Golub S Ya, Khaenko B V *Izv. Akad. Nauk SSSR Neorgan. Mater.* **13** 1779 (1977)
41. Christensen A N, Alamo A, Landesman J P *Acta Cryst. C* **41** 1009 (1985)
42. Delmas C et al. *Int. J. Inorg. Mater.* **1** 11 (1999)
43. Peres J P, Weill F, Delmas C *Solid State Ionics* **116** 19 (1999)
44. Arroyo y de Dompablo M E, Ceder G *J. Power Sources* **119–121** 654 (2003)
45. Arai H et al. *Solid State Ionics* **80** 261 (1995)
46. Pickering I J et al. *Solid State Ionics* **53–56** 405 (1992)
47. Reimers J N, Li W, Dahn J R *Phys. Rev. B* **47** 8486 (1993)
48. Gusev A I *JETP Lett.* **79** 148 (2004); *Pis'ma Zh. Eksp. Teor. Fiz.* **79** 183 (2004)
49. Peres J P, Demourgues A, Delmas C *Solid State Ionics* **111** 135 (1998)
50. Gusev A I *JETP Lett.* **91** 119 (2010); *Pis'ma Zh. Eksp. Teor. Fiz.* **91** 130 (2010)
51. Gusev A I *Phys. Solid State* **52** 1935 (2010); *Fiz. Tverd. Tela* **52** 1804 (2010)
52. Landau L D, Lifshitz E M *Statistical Physics* Vol. 1 (Oxford: Pergamon Press, 1980); Translated from Russian: *Statisticheskaya Fizika* Pt. 1 (Moscow: Nauka, 1976)
53. Gusev A I *Sov. Phys. Solid State* **32** 1595 (1990); *Fiz. Tverd. Tela* **32** 2752 (1990)
54. Gusev A I, Lipatnikov V N *JETP Lett.* **82** 287 (2005); *Pis'ma Zh. Eksp. Teor. Fiz.* **82** 320 (2005)
55. Lipatnikov V N, Gusev A I *Phys. Solid State* **48** 1634 (2006); *Fiz. Tverd. Tela* **48** 1546 (2006)
56. Gusev A I, Kurlov A S, Lipatnikov V N *J. Solid State Chem.* **180** 3234 (2007)
57. Markhasev B I et al. *Izv. Akad. Nauk SSSR Neorgan. Mater.* **19** 1997 (1983)
58. Markhasev B I et al. *Izv. Akad. Nauk SSSR Neorgan. Mater.* **18** 2001 (1982)
59. Markhasev B I et al. *Izv. Akad. Nauk SSSR Neorgan. Mater.* **20** 1652 (1984)
60. Gusev A I, Rempel A A, Lipatnikov V N *J. Phys. Condens. Matter* **8** 8277 (1996)
61. Rempel' A A, Lipatnikov V N, Gusev A I *Sov. Phys. Dokl.* **35** 103 (1990); *Dokl. Akad. Nauk SSSR* **310** 878 (1990)
62. Gusev A I, Rempel' A A, Lipatnikov V N *Sov. Phys. Solid State* **33** 1295 (1991); *Fiz. Tverd. Tela* **33** 2298 (1991)
63. Gusev A I *JETP* **109** 417 (2009); *Zh. Eksp. Teor. Fiz.* **136** 486 (2009)

64. Gusev A I, Kurlov A S, in *Niobium: Chemical Properties, Applications and Environmental Effects* (Eds M Segers, T Peeters) (New York: Nova Science Publ., 2013) p. 61
65. Venables J D, Kahn D, Lye R G *Philos. Mag.* **18** 177 (1968)
66. Venables J D, Lye R G *Philos. Mag.* **19** 565 (1969)
67. Kahn D, Lye R G *Bull. Am. Phys. Soc.* **14** 332 (1969)
68. Karimov I et al. *Dokl. Akad. Nauk UzSSR Ser. Fiz.-Mat. Nauk* (2) 32 (1976)
69. Karimov I et al. *Izv. Akad. Nauk UzSSR Ser. Fiz.-Mat. Nauk* (4) 87 (1978)
70. Cenzual K et al. *Acta Cryst. B* **47** 433 (1991)
71. Vainshtein B K *Sovremennaya Kristallografiya* (Modern Crystallography) Vol. 1 *Simmetriya Kristallov. Metody Strukturnoi Kristallografii* (Crystal Symmetry. Methods of Structural Crystallography) (Moscow: Nauka, 1979) p. 182
72. Lipatnikov V N et al. *J. Alloys Compounds* **261** 192 (1997)
73. Kesri R, Hamar-Thibault S *Acta Metallurg.* **36** 149 (1988)
74. Berger T "Phase transformations in interstitial Pd-B alloys", PhD Thesis (Stuttgart: Univ. Stuttgart, 2005); http://hdl.handle.net/11858/00-001M-0000-0010-26B9-A
75. Berger T G et al. *Z. Kristallogr.* **221** 450 (2006)
76. Gusev A I *JETP* **113** 96 (2011); *Zh. Eksp. Teor. Fiz.* **140** 112 (2011)
77. Gusev A I *Phys. Solid State* **53** 1664 (2011); *Fiz. Tverd. Tela* **53** 1582 (2011)
78. Billingham J, Bell P S, Lewis M H *Philos. Mag.* **25** 661 (1972)
79. Billingham J, Bell P S, Lewis M H *Acta Cryst. A* **28** 602 (1972)
80. Hiraga K *Philos. Mag.* **27** 1301 (1973)
81. Karimov I et al. *Izv. Akad. Nauk UzSSR Ser. Fiz.-Mat. Nauk* (4) 74 (1976)
82. Rempel' A A, Gusev A I *Uporyadochenie v Nestekhiometricheskom Monokarbide Niobiya* (Ordering in Nonstoichiometric Niobium Carbide) (Ekaterinburg: Ural'skii Nauchnyi Tsentr AN SSSR, Institut Khimii, 1983)
83. Rempel' A A, Gusev A I, Zubkov V A, Shveikin G P *Sov. Phys. Dokl.* **29** 257 (1984); *Dokl. Akad. Nauk SSSR* **275** 883 (1984)
84. Rempel' A A, Gusev A I *Sov. Phys. Crystallogr.* **30** 648 (1985); *Kristallogr.* **30** 1112 (1985)
85. Rempel A A, Gusev A I, Belyaev M Yu *J. Phys. C Solid State Phys.* **20** 5655 (1987)
86. Khaenko B V, Sivak O P *Kristallogr.* **35** 1110 (1990)
87. De Novion C H, Lorenzelli N, Costa P *C.R. Acad. Sci. B* **263** 775 (1966)
88. Alyamovskii S I et al. *Russ. J. Inorgan. Chem.* **13** 895 (1968); *Zh. Neorgan. Khim.* **13** 895 (1968)
89. Henfrey A W, Fender B E F *Acta Cryst. B* **26** 1882 (1970)
90. Athanassiadis T, Lorenzelli N, de Novion C H *Ann. Chim. France* **12** 129 (1987)
91. Rafaja D et al. *J. Alloys Compounds* **269** 60 (1998)
92. Lipatnikov V N, Gusev A I, Ettmayer P, Lengauer W *J. Phys. Condens. Matter* **11** 163 (1999)
93. Kurlov A S, Gusev A I *Tungsten Carbides: Structure, Properties and Application in Hardmetals* (Cham: Springer, 2013)
94. Kurlov A S, Gusev A I *Russ. Chem. Rev.* **75** 617 (2006); *Usp. Khim.* **75** 687 (2006)
95. Rudy E, Windisch S *J. Am. Ceram. Soc.* **50** 272 (1967)
96. Butorina L N, Pinsker Z G *Sov. Phys. Crystallogr.* **5** 560 (1960); *Kristallogr.* **5** 585 (1960)
97. Morton N et al. *J. Less Common Met.* **29** 423 (1972)
98. Yvon K, Nowotny H, Benesovsky F *Monatsch. Chem.* **99** 726 (1968)
99. Harsta A, Rundqvist S, Thomas J O *Acta Chem. Scand. A* **32** 891 (1978)
100. Gusev A I, Kurlov A S *JETP Lett.* **85** 34 (2007); *Pis'ma Zh. Eksp. Teor. Fiz.* **85** 40 (2007)
101. Lönnberg B, Lundström T, Tellgren R *J. Less Common Met.* **120** 239 (1986)
102. Dubois J et al. *Acta Metallurg.* **36** 1891 (1988)
103. Epicier T et al. *Acta Metallurg.* **36** 1903 (1988)
104. Epicier T et al. *C.R. Acad. Sci. II* **297** 215 (1983)
105. Kublii V Z, Velikanova T Ya, Khaenko B V *Metallofiz. Noveish. Tekhnol.* **21** (9) 26 (1999)
106. Kublii V Z, Velikanova T Ya *Poroshkovaya Metallurgiya* (11 – 12) 101 (2004)
107. Kurlov A S, Gusev A I *Dokl. Phys.* **52** 656 (2007); *Dokl. Ross. Akad. Nauk* **417** 616 (2007)
108. Kurlov A S, Gusev A I *JETP* **105** 710 (2007); *Zh. Eksp. Teor. Fiz.* **132** 812 (2007)
109. Kurlov A S, Gusev A I *Phys. Rev. B* **76** 174115 (2007)
110. Telegus V S, Gladyshevskii E I, Kripyakevich P I *Kristallogr.* **12** 936 (1967)
111. Telegus V S, Kuz'ma Yu B, Marko M A *Poroshkovaya Metallurgiya* (11) 56 (1971)
112. Nozik Yu Z, Lipin Yu V, Kuvaldin B V *Izv. Akad. Nauk Latv. SSR Ser. Fiz.-Tekh. Nauk* (6) 30 (1968)
113. Kublii V Z at al. *Poroshkovaya Metallurgiya* (3 – 4) 46 (2000)
114. Suetin D V et al. *Phys. Solid State* **50** 1420 (2008); *Fiz. Tverd. Tela* **50** 1366 (2008)
115. Andersson S et al. *Acta Chem. Scand.* **11** 1641 (1957)
116. Watanabe D et al. *Nature* **210** 934 (1966)
117. Hilti E *Naturwissenschaften* **55** 130 (1968)
118. Hilti E, Laves F *Naturwissenschaften* **55** 131 (1968)
119. Terauchi H, Cohen J B, Reed T B *Acta Cryst. A* **34** 556 (1978)
120. Valeeva A A, Rempel' A A, Gusev A I *JETP Lett.* **71** 460 (2000); *Pis'ma Zh. Eksp. Teor. Fiz.* **71** 675 (2000)
121. Valeeva A A, Rempel A A, Gusev A I *Inorg. Mater.* **37** 603 (2001); *Neorgan. Mater.* **37** 716 (2001)
122. Gusev A I *JETP Lett.* **74** 91 (2001); *Pis'ma Zh. Eksp. Teor. Fiz.* **74** 96 (2001)
123. Valeeva A A, Tang G, Gusev A I, Rempel A A *JETP Lett.* **77** 25 (2003); *Pis'ma Zh. Eksp. Teor. Fiz.* **77** 28 (2003)
124. Watanabé D et al. *Acta Cryst.* **23** 307 (1967)
125. Watanabé D et al., in *The Chemistry of Extended Defects in Non-Metallic Solids* (Eds L Eyring, M O'Keeffe) (Amsterdam: North-Holland, 1970) p. 238
126. Gusev A I, Valeeva A A *JETP Lett.* **96** 364 (2012); *Pis'ma Zh. Eksp. Teor. Fiz.* **96** 400 (2012)
127. Gusev A I *J. Solid State Chem.* **199** 181 (2013)
128. Gusev A I *JETP* **117** 293 (2013); *Zh. Eksp. Teor. Fiz.* **144** 340 (2013)
129. Westman S, Nordmark C *Acta Chem. Scand.* **14** 465 (1960)
130. Andersson B, Gjonnes J *Acta Chem. Scand.* **24** 2250 (1970)
131. Bell P S, Lewis M H *Phys. Status Solidi A* **7** 431 (1971)
132. Andersson B, Gjønnes J, Taftø J *Acta Cryst. A* **30** 216 (1974)
133. Gusev A I, Davydov D A *JETP Lett.* **88** 111 (2008); *Pis'ma Zh. Eksp. Teor. Fiz.* **88** 119 (2008)
134. Davydov D A, Gusev A I *JETP* **108** 267 (2009); *Zh. Eksp. Teor. Fiz.* **135** 301 (2009)
135. Gusev A I, Davydov D A, Valeeva A A *J. Alloys Compounds* **509** 1364 (2011)
136. Cambini M, Pellergini G, Amelinckx S *Mater. Res. Bull.* **6** 791 (1971)
137. Hiraga K, Hirabayashi M *J. Solid State Chem.* **14** 219 (1975)
138. Galkin L N, Vavilova V V, Fykin L E *Izv. Akad. Nauk SSSR Neorgan. Mater.* **13** 1839 (1977)
139. Arbuzov M P, Bugaichuk N T, Khaenko B V *Dokl. Akad. Nauk UkrSSR A* (4) 307 (1979)
140. Gusev A I, Davydov D A *JETP Lett.* **86** 657 (2007); *Pis'ma Zh. Eksp. Teor. Fiz.* **86** 746 (2007)
141. Davydov D A, Gusev A I *Phys. Solid State* **51** 156 (2009); *Fiz. Tverd. Tela* **51** 147 (2009)
142. Davydov D A, Gusev A I *JETP Lett.* **91** 286 (2010); *Pis'ma Zh. Eksp. Teor. Fiz.* **91** 306 (2010)